CPTR 73
SEPTEMBER 2001

SOLID PROPELLANT TEST MOTOR SCALING

R.S. Fry

CHEMICAL PROPULSION INFORMATION AGENCY

• THE JOHNS HOPKINS UNIVERSITY •
• WHITING SCHOOL OF ENGINEERING • COLUMBIA, MARYLAND 21044-3204 •

REPORT DOCUMENTATION PAGE

Form Approved
OMB No. 0704-0188

1. AGENCY USE ONLY *(Leave Blank)*	2. REPORT DATE	3. REPORT TYPE AND DATES COVERED
	July 2001	Technical Report, 2001

4. TITLE AND SUBTITLE

Solid Propellant Test Motor Scaling

5. FUNDING NUMBERS

C:SP0700-97-D-4004

6. AUTHOR(S)

Fry, Ronald S.

7. PERFORMING ORGANIZATION NAME(S) AND ADDRESS(ES)

The Johns Hopkins University
Chemical Propulsion Information Agency
10630 Little Patuxent Parkway, Suite 202
Columbia, MD 21044-3204

8. PERFORMING ORGANIZATION REPORT NUMBER

CPTR 73

9. SPONSORING/MONITORING AGENCY NAME (S) AND ADDRESS(ES)

DTIC - AI
8725 John J. Kingman Road
Suite 0944
Ft. Belvoir, VA 22060-6218

Naval Air Warfare Center Weapons Division
Code 477000D
China Lake, CA 93555-6100

10. SPONSORING/MONITORING AGENCY REPORT NUMBER

11. SUPPLEMENTARY NOTES

Hardcopies available from CPIA only. Reproduction is not authorized except by specific permission from CPIA. CPIA's DTIC-assigned source code is 423900.

12a. DISTRIBUTION/AVAILABILITY STATEMENT

Approved for public release; distribution is unlimited.

12b. DISTRIBUTION CODE

13. ABSTRACT *(Maximum 200 words)*

Current burning rate measurement test techniques and subscale test hardware used within the NATO community are reviewed and recommendations are made to support improved scaling and prediction of internal ballistics of a full-scale solid propellant motor.

The NATO Research and Technology Organization (RTO), Advanced Vehicle Technology (AVT), Working Group (WG) 016 (formerly AGARD/PEP Working Group #27) undertook to evaluate methods used within the NATO propulsion community to measure burning rate in solid propellant rocket systems. The purpose was to identify similarities and differences among the member nations. The WG 016 sought to contribute to improvements in the burning rate tools by addressing issues that have remained unresolved in the solid propulsion industry for over 40 years:

(1) Better understanding of burning rate, $r_b(p,T_o)$, data from various facilities to ease the comparison of propellants from various manufacturers and to improve international exchanges and cooperation.
(2) Improved measurement accuracy and reliability to allow a decrease in the number of tests (and associated time and cost) and improved control of manufacturing and quality assurance and the assessment of aging.

AVT WG 016 activities have identified that manufacturer burning rate data may not easily be compared without accounting for industry-wide differences in subscale devices, test methods and scaling analysis methods. The WG recommends the NATO propulsion community review these findings as a means of advancing their own burning rate measurement and analysis methods.

14. SUBJECT TERMS

Burning rate	Firing tests (motor)	Rocket motor	Test methods
Combustion	Igniters	Rocket propellant grain	Burning rate scaling
Combustion chambers	Instrumentation	Solid propellants	Subscale motors
Composite propellants	Measurement	Solid rocket propellants	CPIA Collection

15. NUMBER OF PAGES

103

16. PRICE CODE

17. SECURITY CLASSIFICATION OF REPORT	18. SECURITY CLASSIFICATION OF THIS PAGE	19. SECURITY CLASSIFICATION OF ABSTRACT	20. LIMITATION OF ABSTRACT
UNCLASSIFIED	UNCLASSIFIED	UNCLASSIFIED	UA

CPTR 73
SEPTEMBER 2001

SOLID PROPELLANT TEST MOTOR SCALING

R.S. Fry

CHEMICAL PROPULSION INFORMATION AGENCY

• THE JOHNS HOPKINS UNIVERSITY •
• WHITING SCHOOL OF ENGINEERING • COLUMBIA, MARYLAND 21044-3204 •

CPIA is a DISA/DTIC-sponsored DoD Information Analysis Center operating under contract SPO700-97-D-4004.

The Chemical Propulsion Information Agency (CPIA) is a DoD Information Analysis Center operated by The Johns Hopkins University, Whiting School of Engineering, under Defense Supply Center Columbus (DSCC) contract SPO700-97-D-4004. The applicable DoD Instruction is 3200.12-R-2, "Centers for Analysis of Scientific and Technical Information." The CPIA's mailing address is The Johns Hopkins University, Chemical Propulsion Information Agency, Attn: Security Office, 10630 Little Patuxent Parkway, Suite 202, Columbia, Maryland, 21044-3204. The CPIA also provides technical and administrative support to the Joint Army-Navy-NASA-Air Force (JANNAF) Interagency Propulsion Committee.

The Government Administrative Manager for CPIA is the Defense Technical Information Center (DTIC), Code DTIC-AI, 8725 John J. Kingman Road, Suite 0944, Ft. Belvoir, VA 22060-6218. The Government Technical Manager (Contracting Officer's Technical Representative) is Mr. Stuart Blashill, Naval Air Warfare Center Weapons Division, Code 477000D, China Lake, CA 93555-6100.

PREFACE

This issue of the Chemical Propulsion Technology Reviews (CPTR 73) continues CPIA's recurrent series of technical summaries and status reports on topics pertaining to missile, space, and gun propulsion technology. The general aim is to collect, analyze, and discuss technology advancements in a language understood by a broad range of propulsion technologists.

The results reported upon here are a part of the overall technical approach of:

(1) Surveying the NATO solid propulsion community for subscale and non-intrusive test methods, analysis, and scaling methods, and

(2) Analyzing "simulated" and "real" motor pressure-time data using multiple thickness/time and mass conservation burning rate analysis methods taken from the survey.

This CPTR reviews recommendations on current burning rate measurement test techniques and subscale test hardware for accurate scaling and prediction of internal ballistics of a full-scale solid propellant motor. Trends in observed differences in calculated burning rate for the different analysis methods were evaluated with a goal of making recommendations on preferred analysis methods. Detailed recommendations on current burning rate measurement test techniques and subscale test hardware for accurate prediction of internal ballistics of a full-scale solid propellant motor are reported in JHU/CPTR 74, "Solid Propellant Subscale Burning Rate Test Techniques and Hardware for U.S. and Selected NATO Facilities," July 2001. These results, including surveys of analysis methods and results of the round robins are reviewed in a companion JHU/CPIA CPTR 75, "Solid Propellant Subscale Burning Rate Analysis Methods for U.S. and Selected NATO Facilities," October 2001. A complete report of the NATO RTO AVT WG 016 activities is available, and companion JHU/CPIA CPTR's summarizing other aspects of this work including non-intrusive burning rate measurement methods, and performance scaling, and the entire work are to be published in CY2002. The metric system of units is employed in this report except where industry convention dictates otherwise.

The author wishes to express his appreciation to Professor L.T. De Luca, Dipartimento di Energetica, Politecnico di Milan, Italy and Mr. T. Whitehouse, British Aerospace Defence / Royal Ordnance Defence Rocket Motors, United Kingdom for their contributions to portions of this document.

CPIA solicits comments on the CPTR effort, including suggestions on topics for future issues. For technical comments or suggestions contact Mr. Tom Moore, CPIA Technical Services Supervisor, at 410-992-9951, ext 207, or Mr. Ronald Fry at 410-992-9951, ext. 206. Individuals employed by organizations that subscribe to CPIA services may request personal copies of this document by contacting CPIA at 410-992-7300, cpia@jhu.edu, or http://www.cpia.jhu.edu.

ABSTRACT

Current burning rate measurement test techniques and subscale test hardware used within the NATO community are reviewed and recommendations are made to support improved scaling and prediction of internal ballistics of a full-scale solid propellant motor.

The NATO Research and Technology Organization (RTO), Advanced Vehicle Technology (AVT), Working Group (WG) 016 (formerly AGARD/PEP Working Group #27) undertook to evaluate methods used within the NATO propulsion community to measure burning rate in solid propellant rocket systems. The purpose was to identify similarities and differences among the member nations. The WG 016 sought to contribute to improvements in the burning rate tools by addressing issues that have remained unresolved in the solid propulsion industry for over 40 years:

(1) Better understanding of burning rate, $r_b(p,T_o)$, data from various facilities to ease the comparison of propellants from various manufacturers and to improve international exchanges and cooperation.

(2) Improved measurement accuracy and reliability to allow a decrease in the number of tests (and associated time and cost) and improved control of manufacturing and quality assurance and the assessment of aging.

AVT WG 016 activities have identified that manufacturer burning rate data may not easily be compared without accounting for industry-wide differences in subscale devices, test methods and scaling analysis methods. The WG recommends the NATO propulsion community review these findings as a means of advancing their own burning rate measurement and analysis methods.

CONTENTS

NOMENCLATURE

a	pressure coefficient of ballistic steady burning rate, nondimemsional
A_b	area of the burning surface, cm^2
A_p	area of the grain port cross-section, cm^2
A_t	area of the nozzle throat, cm^2
CCP	circular center perforated grain
EB	end burner grain
g_0	standard acceleration gravity at sea level, 9.807 m/s^2
K	ratio of burning surface area A_b to nozzle throat area A_t, nondim.
L^*	ratio of the combustor cavity volume to nozzle throat area, m
m	mass burning rate, g/cm^2s
n	pressure exponent of ballistic steady burning rate, nondimemsional
p	pressure, MPa
p_c	combustion chamber, pressure, MPa
r_b	burning rate, cm/s
r_{MB}	mass balance burning rate, cm/s
r_{TOT}	thickness/time burning rate, cm/s
$\Re$	universal gas constant, 1.987 cal/mole, K
SCP	star center perforated grain
t	time, s
t_b	burning time, s
T	temperature, K
T_0	initial propellant temperature, K
T_c	combustion chamber gas temperature, K
T_{ref}	reference temperature (298 K)
V_c	combustion chamber free volume, cm^3
w_b	web thickness, mm

Greek Symbols

k	burned gas specific heat ratio
M	average molecular mass, g/mole
π_K	temperature sensitivity of steady chamber pressure, K^{-1}
ρ_c	combustion chamber gas density, g/cm^3
ρ_p	propellant density, g/cm^3
σ_p	temperature sensitivity of steady burning rate, K^{-1}

Subscripts

amb	ambient
avg	average
b	burning
c	chamber
max	maximum

LIST OF FIGURES

LIST OF TABLES

1.0 INTRODUCTION

The rocket motor designer must have a good understanding of the variation of propellant burning rate with both pressure and temperature in order to produce an efficient design and minimize design iterations during development. It is well known that the burning rate deduced from test firings of full-scale motors sometimes differs from that measured in strand burner or subscale motor work. This difference is typically only a few percent but this may be sufficient to cause motor performance to lie outside the required limits and so force a change in propellant formulation, motor grain design or nozzle throat diameter with associated cost and schedule penalties. Difficulties may also arise when burning rate data for a given propellant formulation is passed across national boundaries as in technology exchange programs or even when passed from company to company within the same country. If the size and type of device used to generate the baseline data is not fully taken into account then the data cannot be correctly interpreted and errors due to scale-up may result.

1.1 Historical Background on Burning Rate Scaling

Effects of propellant ingredients on burning rate and other propellant properties are generally established using laboratory and subscale devices. On the other hand, motor size effects as well as associated processing and testing differences on propellant properties (in particular burning rate) have been historically difficult to define. The burning rate prediction of the first full-scale motor has generally been based exclusively on past experience. Analysts expect the ratio of the new full-scale motor to subscale motor burning rate, referred to as the burning rate scale factor, to be the same as that experience on earlier motor programs. Hence, engineering practice evolved the use of an empirical scale, or multiplying factor, because of an inability to understand and account for the controlling physics.

Accurate prediction of internal ballistics for the first full-scale solid propellant motor of a new design becomes increasingly important as motor size increases. The addition of ballistic verification tests to the motor development program is costly and can impact schedule. Evaluating mission burning time sensitivity, and the use of near flightweight hardware on the first full-scale test require internal ballistics that are close to design values.

Historically, it has been observed that propellant burning rates vary with motor size and are usually higher in motors than in ballistic test devices. Large motor burning rates are typically higher than the rates observed in small motors, for both double base and composite propellants. The industry wants to accurately predict scale factor at reasonable cost so as to eliminate some motor static tests. This is particularly desirable for large motors because of the high cost involved in a single test.

1.2 Objectives and Approach

This chapter discusses the differences in burning rate apparent when scaling up from a subscale burning rate measurement device or small motor to a larger motor. The fundamental factors influencing scaling of burning rate are reviewed. Historical approaches for correlating subscale and full-scale motor burning rate are reviewed. Survey results from the participants of the AVT Working Group 16 are presented to illustrate a historical basis for accounting for scale effects. The discussion proceeds through a revelation of how the factors influencing scaling of burning rate are accounted for differently by the scale factors from different countries and facilities. Conclusions are drawn from these revelations and recommendations are made for future applications.

1.2.1 NATO/RTO AVT Working Group Formation

The NATO Research and Technology Organization (RTO), Advanced Vehicle Technology (AVT), Working Group (WG) 016 (formerly AGARD/PEP Working Group #27) undertook to evaluate methods used within the NATO propulsion community to measure burning rate in solid propellant rocket systems. This report summarizes the objectives, approach, findings, and recommendations relative to test

techniques and hardware used by the surveyed countries and facilities. A complete report of the NATO RTO AVT WG 016 activities is available[1], The WG was formed in 1996, consisting of representatives from 6 of the 15 member nations of NATO, with inputs accepted from 4 other member nations and a couple non-member nations. The WG conducted its activity from October 1997 to March 2001. The justification and relevance of this task to the Solid Rocket Industry includes the importance of solid propulsion to tactical and strategic rockets, missiles and space launch systems; the influence solid propellant burning rate has on performance; and the influence burning rate testing has on program costs.[2, 3]

1.2.2 Justification for Studying Solid Propellant Burning Rate

Solid Rocket propulsion remains the major propulsion concept for the tactical and strategic missiles, and for many first stage launch systems. Among the parameters controlling the solid rocket motor operation, burning rate plays a very important role. The burning rate determines, with the burning area, the combustion processes, the mass flow rate, and therefore directly controls the pressure and thrust of the motor. Burning rate is a characteristic of the propellant that can be measured independently, at least for the more usual combustion regimes.

Accuracy of solid rocket thrust-time prediction has become increasingly more important in solid rocket design. One of the most significant variables in this prediction is the propellant burning rate. Accuracy of this value depends on empirical methods for calculating burning rate from subscale motor tests and for correlating this rate with predictions derived from full-scale motor tests. Thrust is very sensitive to the reference propellant burning rate. A variation in propellant burning rate of ±1%, for example, will result in a thrust variation of 1.5 – 2%. The methods of determining burning rate must be reliable and correlations dependable to predict thrust to an accuracy of ±3% using the Solid Performance Program (SPP).

Burning rate measurement is an important and significant activity in the solid propellant industry is devoted to, first during the development of a new propellant, then during the manufacturing (quality control), or for the service life (aging). All the countries with a tradition in the development and manufacturing of solid propellants are equipped with facilities for the burning rate measurement. These facilities are being continuously improved to increase the accuracy and reliability of the burning rate data.

The NATO RTO AVT WG 016 sought to contribute to improvements in the burning rate tools to provide for a:

- Better understanding of burning rate, $r_b(p,T_o)$, data from various facilities to ease the comparison of propellants from various manufacturers and to improve international exchanges and cooperation.
- Improved measurement accuracy and reliability to allow a decrease in the number of tests (and associated time and cost) and improved control of manufacturing and quality assurance and the assessment of aging.

1.2.3 Objectives and Scope of the Work

The working group has reviewed and compared methods for measuring steady-state burning rate of solid rocket propellant through current subscale motor practices with an emphasis on data analysis methods and non-intrusive techniques. The overall focus of the working group was approximately 70% small motors, 25% non-intrusive diagnostics and 5% other methods including strand burners. After three years of technical interchange meetings, the AVT WG 016 (formerly AGARD/PEP Working Group #27), whose charter was "Evaluation of Methods for Solid Propellant Burning Rate Measurements" completed its last meeting in Ottawa, Canada on 18-23 October 1999. Six NATO countries were actively participating, with a few others providing technical support. This report is the product of the six AVT WG 016 Meetings conducted between October 1996 and October 1999, supplemented with collaboration by WG members between the meetings and throughout CY2000-2001 during preparation of the final report. Specific objectives of WG 016 relevant to this report are to:

a) Review the small-scale motors used by the various NATO countries and the problems encountered.

b) Compare measurement methods and evaluate the differences
c) Produce an Advisory Report to the NATO community with the following features:
    1) Provide information suitable as training for entry-level person and reference for the expert.
    2) Collect, analyze and condense information into a language understandable to a wide range of technologists and managers.

1.2.4 Technical Approach

1.2.4.1 General Summary

WG activity included analyses, presentations, and discussions in support of completing a final RTO AVT advisory report. Topics addressed in this report by chapter include (1) introduction to the problem, justification for the WG and definition of the technical approach, (2) direct measurement techniques and hardware, (3) conclusions and recommendations.

The basic technical approach used to address the overall and specific objectives cited above has involved

a) Surveying the NATO solid propulsion community for subscale and non-intrusive test methods, analysis, and scaling methods, and
b) Analyzing "simulated" and "real" motor pressure-time data using multiple thickness/time and mass conservation burning rate analysis methods taken from the survey.

Time-consuming survey and analysis support was solicited from a wide range of facilities within the NATO solid propulsion community during the course of this effort. Four separate Analysis Round Robins were conducted with solicitations for support made to NATO propulsion industry contributors. The influence of various burning behaviors was examined in these round robins, such as progressive or regressive burning, constant and random bore offset variations, constant and random L* variations, and different rate equations. Trends in observed differences in calculated burning rate for the different analysis methods were evaluated for these cases with a WG goal of making recommendations on preferred analysis methods. Detailed recommendations on current burning rate measurement test techniques and subscale test hardware for accurate prediction of internal ballistics of a full-scale solid propellant motor are reported in JHU/CPTR 74.[4] Results of the surveys on analysis methods and results of the round robins are reviewed in a companion JHU/CPIA CPTR 75.[5] A complete report of the NATO RTO AVT WG 016 activities is available[1], and companion JHU/CPIA CPTR's summarizing other aspects including the entire work are to be published in CY2002.

1.2.4.2 WG 016 as a Catalyst for Change

Analysis Round Robins were used in analyzing "simulated" and "real" motor pressure-time data for the purposes of involving the participants in the data analysis, review and discussion, and conclusion process. The WG considered this critical if either voluntary change was to be expected as an outcome of this study, or if resistance to changed procurement specifications was to be forestalled. One concern was, if the participants were not intimately involved in this process and were only acquainted with the finished comparisons/conclusions, that inertia and conservatism would likely dominate any subsequent actions. Steps to involve the participants in this process take time. Clearly participation and peer review was integral to activities as members of this WG. Peer review of the comparisons and the resulting conclusions was sought outside this WG on a selected basis throughout the period of this effort. Continuing efforts in this regard will be beneficial to understanding the merits of, or for taking further action on any conclusions drawn from this study.

1.2.5 NATO RTO AVT Working Group 016 Membership and Participants

Dr. P. Kuentzmann of ONERA, France, initiated the WG in 1997 under the former AGARD Propulsion and Energetics Panel (PEP), now the Applied Vehicle Technology (AVT) panel of the Research and

Technology Organization (RTO), a Working Group 016 with the charter of "Evaluation of Methods for Solid Propellant Burning Rate Measurements." His early vision as advocate for this effort is appreciated.

The primary AVT Working Group 016 membership included:

Table 1.0 NATO RTO AVT WG 016 Membership		
Mr. Ronald Fry (Co-Chairman)	JHU/CPIA	U.S.
Dr. Robert Frederick	Univ Alabama in Huntsville	U.S.
Mr. Rene Couturier (Co- Chairman)	SNPE	France
Mr. Dominique Ribereau	SNPE	France
Mr. Jean-Paul Reynard	ONERA	France
Mr. Jean-Claude Traineau	ONERA	France
Dr. Hans-Ludwig Besser	Bayern-Chemie	Germany
Dr. Rudiger Strecker	Bayern-Chemie	Germany
Prof. Luigi DeLuca	Politecnico di Milano	Italy
Dr. Guy M.H.J.L. Gadiot	TNO PML	Netherlands
Mr. Tony Whitehouse	Royal Ordinance	UK

The WG016 members most gratefully acknowledge the significant contributions of Mr. Richard Hessler, independent consultant to the WG016 from the U.S. Additionally, the WG members are sincerely grateful to the NATO international propulsion community (facilities and their representatives) for their contributions included in this report. Over 50 contributors participated from over 35 companies, universities and agencies. These contributions included information on test hardware, analysis and scaling methods, and support for multiple analysis round robins of simulated and real motor data. A complete list is provided in Appendix A.

2.0 BURNING RATE FUNDAMENTALS

2.1 Burning Rate Physics and Features

Knowing burning rates of solid propellants, whether steady or unsteady, under a variety of operating conditions is of critical importance both for applications (due to their sensible influence on performances and cost of propulsive devices) and fundamental reasons (understanding of combustion processes). Furthermore, since no available theory/model is capable of predicting burning rates with accuracies within 1% and including the effects of rate modifiers, they must be measured experimentally. However, while experiments measuring steady burning rates are reasonably robust, those measuring unsteady values are fragile and still a matter of research. Since a variety of experimental hardware and procedures are in use today, even for the common steady-state operations, the need arises to understand and perhaps standardize the different approaches developed among the NATO countries.

2.1.1 Burning Rate Physics[6]

2.1.1.1 Background

Energetic materials in general are capable of a dual reacting regime:

- Supersonic regime: a combustion wave preceded by a strong shock wave brings about a detonation wave, propagating at a speed on the order of several km/s and limited by the total thermochemical energy content of the reacting material;
- Subsonic regime: a combustion wave brings about a deflagration wave, propagating at a speed on the order of cm/s and limited by heat and/or mass diffusion.

For a more detailed background, which lies outside the scope of this writing, the interested reader may wish to consult.[7,8,9,10] Here it is enough to remark that deflagration is the common operating mode for the vast majority of engineering applications. Thus, only subsonic combustion waves (or deflagration waves) are considered in this report.

Whether steady or unsteady, deflagration waves in energetic solid materials in general consist of an initial condensed phase and a final phase, and in most cases essentially gaseous reaction products. The interface between the condensed phase and gas phase is called the *burning surface*. The propagation rate of this interface is called *burning rate*; physically, this can also be seen as the regression rate of the condensed phase.

For many studies it is convenient to define, more precisely, a *linear* burning rate (or deflagration rate) as the web thickness burned per unit time in the direction perpendicular to the burning surface.[9]

2.1.1.2 Internal Ballistics

Design and operation of solid rocket motors strongly depend on the combustion features of the propellant charge (burning rate, burning surface, and grain geometry) and their evolution in time. *Internal ballistics* is the applied science devoted to these problems.

Burning Rate

In general, burning rates depend on:

- Nature of energetic material (basic ingredients and their mixture ratio);
- Details of chemical composition (catalysts, modifiers, additives, etc. usually present in small or fractional percentages);
- Physical effects (particle size distribution, presence of wires or staples, etc.);
- Details of manufacturing process and other miscellaneous factors (see Sections 2.2 and 3.0);
- Operating conditions (pressure, initial temperature, natural and/or external radiation, heat losses, gas flow parallel to the burning surface, acceleration, etc.);
- Mode of operation (steady vs. unsteady).

This report is primarily concerned with the measurement of steady burn rates, implying a steady set of operating conditions and equilibrium combustion.

For propulsive applications, the influences of pressure (typically, in a range from 1-30 MPa) and initial temperature (typically, in a range from 219-344 K for air-launched missile motors) on burning rate are of paramount importance. Natural radiation is important for heavily metallized compositions (15-20% metal addition), while external radiation still is a matter of laboratory experiments; heat losses are important only under special circumstances. High velocity gas flowing parallel to the burning surface can seriously increase the local burning rate (causing the so-called *erosive burning* phenomenon), due to increased heat transfer from the adjacent turbulent boundary layer, especially in the aft-end portion of the motor cavity. Motor acceleration larger than 10 g_0, whether longitudinal or lateral or due to spinning motion, directed into the burning surface and within an angle of 60 to 90 degrees with respect to it, perceivably increases burning rates. Other peculiar ballistic effects, due to details of manufacturing process, may be important for motor operations but are sensibly dependent on the actual configuration. Detailed comments are discussed in later sections of this report, with further reading in References.[9,11,12]

Notwithstanding impressive progress, combustion theory is not yet capable of predicting steady or unsteady rates with sufficient accuracy for routine use in motor predictions. Thus, propulsion designers and engineers require experimental measurements.

Burning Surface

The burning surface of solid energetic materials regresses in a direction essentially perpendicular to itself. In other words, solid propellants are considered to burn by parallel layers and the grain "tends to retain its original configuration until the web has burned through" (Robert's law, 1839); for details.[13,7] Notice that this law, originally proposed for homogeneous compositions, can be extended to the modern

heterogeneous compositions if the propellant heterogeneity is limited to a "sufficiently small scale." [7] The actual burning surface and its evolution in time depend on the initial grain geometry and overall combustion processes.

Grain Geometry

The initial grain geometry of a solid propellant strictly depends on the propulsive mission. See Figure 1.0 [9] for a variety of shapes commonly employed. The following nomenclature is currently used:[9]

- Grain configuration: the designed shape of the initial burning surfaces of a grain in a motor.
- End-burning grain: the propellant grain is a solid cylinder ideally burning, like a cigarette, only in the axial direction.
- Cylindrical grain: a propellant grain in which the internal cross section is constant along the axis regardless of perforation shape.
- Perforation: the central cavity port or flow passage of a propellant grain.
- Inhibitor: a layer or coating of slow- or non-burning material covering parts of the grain's propellant surface to prevent burning.
- Restricted surface: a grain surface restricted from burning by the bonding of an inhibitor layer.
- Sliver: unburned propellant remaining (or lost because ejected through the nozzle) at the time of web burnout.

Motor Pressure

Let us assume uniform pressure and burning rate throughout the combustion chamber of a solid propellant rocket motor filled with a perfect gas burned mixture. All properties are considered constant. Transient mass conservation[14] requires

$$m_g = m_d + \frac{d(\rho_c V_c)}{dt} \tag{1}$$

where the mass production of gas due to combustion is

$$m_g = \rho_p A_b r_b$$

the mass flow rate exiting the nozzle is

$$m_d = \frac{p_c A_t}{C_D} = p_c A_t c^*$$

and the mass accumulation rate in the combustion chamber is

$$\frac{d(\rho_c V_c)}{dt} = \rho_c \frac{dV_c}{dt} + V_c \frac{d\rho_c}{dt} = \rho_c A_b r_b + V_c \frac{1}{\Gamma^2 c^{*2}} \frac{dp_c}{dt}$$

where c*

$$c^* = \frac{1}{\Gamma}\sqrt{\frac{\Re}{M} T_c}$$

is the characteristic velocity

By substitution in the mass conservation equation, one finds the transient equation of the internal ballistics

$$\frac{dp_c}{dt} = \frac{\Gamma^2 c^{*2}}{V_c}\left(\rho_p - \rho_c\right) A_b r_b - \frac{\Gamma^2 c^*}{V_c} A_t p_c \tag{2}$$

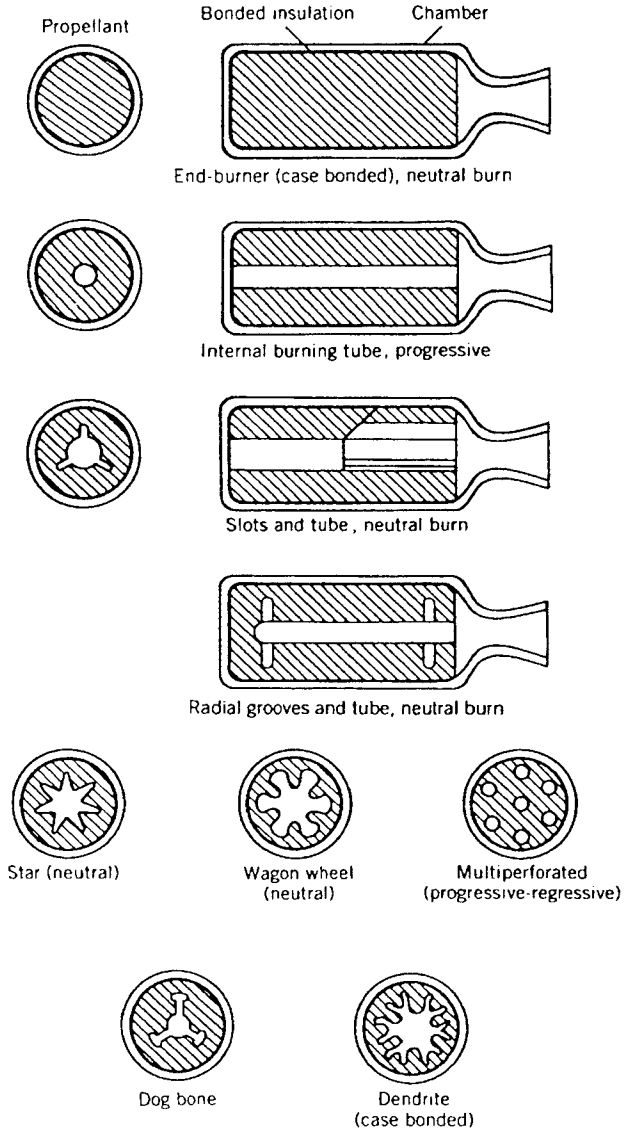

Figure 1. Simplified Diagrams of Several Grain Configurations.[9]

Under steady operations, one obtains the equilibrium pressure of the rocket motor combustion chamber

$$\bar{p}_c = \left(\frac{A_b}{A_t} a_b \rho_p c^* \right)^{\frac{1}{1-n}} \tag{3}$$

where the steady burning rate has been taken as $\bar{r}_b = a_b \bar{p}_c^{\,n}$

and $\rho_p >> \rho_c$.

2.1.2 Burning Rate Features

Under any circumstances, ideal one-dimensional steady-state combustion waves, if not impossible, are at least very rare. It is important to realize that, besides the main factors summarized in Section 2.1.1, a variety of details conspire against the establishment of an ideal combustion wave. Even for simple strand burners these factors can include size of the sample, lateral surface inhibitor, ignition, and nature and flow rate of the ambient gas, radiative environment, and other factors. Under actual motor operating conditions, further effects worsen the situation even for the simple end-burner configuration. These additional factors include grain processing details, aging, mechanical stresses, contacts with walls, interfaces with inhibitors, migration of various propellant ingredients, rate of polymerization, and propellant state of cure for composite propellants.[12] The high strain grain surface near the bond line of large end-burning grains, for example, encourages the burning surface to become conical from its initially planar shape, as shown in Figure 2.0.[9] In larger end-burning grains (above approximately 0.5 m diameter) the burning surface does not remain perpendicular to the axis, but gradually increases and assumes a conical shape. The burning rate at the bond line is larger than in the center. The lines in the grain indicate successive burning surface contours. Thus in most cases, including small motors for ballistic evaluation, one-dimensional steady-state combustion wave is only an ideal picture. The factors influencing non-ideal burning are reviewed in more detail in later sections relative to the issue of burning rate scaling. Only the general classes of non-ideal burning are reviewed in this section.

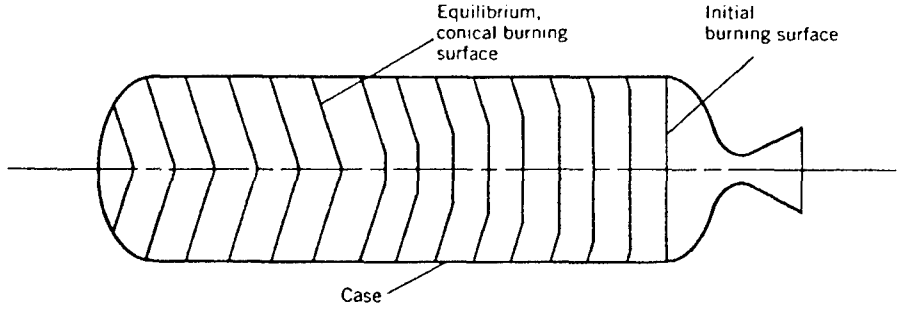

Figure 2. Burning Surface Does Not Remain Perpendicular to the Axis in Larger End-Burning Grains.[9]

2.1.2.1 Quasi-Steady Burning

For heterogeneous compositions, the combustion wave is by definition the result of local 3-D and unsteady effects depending on the initial loading fractions and particle size distributions of solid ingredients. On a microscale, unsteady effects are due to the arrival of different ingredients at the burning

surface and changes of local thermophysical properties of each ingredient. Even for homogeneous compositions (double-base and triple-base solid propellants), different chemical reactions of the ingredients produce unsteady effects due to changes of chemical reaction rates and possible accumulation of carbonaceous residues on scattered sites of the burning surface. In general, the ideal uniform burning surface is rare to achieve due to foam, bubbles, hot spots, material dispersion, etc. occurring for a variety of reasons.[15] Thus, steady-state combustion processes have to be seen more properly as *quasi-steady* in time, and measurements of linear burning rates must be taken over distances much *larger* than the corresponding thermal wave thickness (as well as the distance required to establish).

2.1.2.2 Mean Steady Burning / Neutral

In general, steady burning rates have to be seen as a mean value occurring over an appropriate time span. In particular, ignition and extinction transients have always to be excluded from the measurement procedure; but in general this is systematically done only in strand burners and ultrasound burners or other specialized rigs. Under these circumstances, a reacting propellant often shows a mean burning rate that is constant in time. With reference to a motor, the combustion process is said to be *neutral* if chamber pressure or thrust behavior are maintained constant in time; but for neutral burn rate, pressure only is required to keep constant in time. Note that (slowly varying) excursions within a typical but arbitrary fraction of 15% of the average value are accepted.[9] Under actual operating conditions, however, peculiar motor effects may affect burning rates yielding unwanted consequences (see later sections). For example, hump effects for cast composite propellants manifest an excess burning rate of 3-7% at about halfway through the web.[11] Thus, neutral burning is a very convenient configuration but not easy to obtain. Most small motors for ballistic evaluation are meant to be neutral.

2.1.2.3 Transient Burning / Non-Neutral

Under transient conditions, burning rate may differ greatly from the equilibrium or steady rate. The degree of the effect depends on instantaneous operating conditions and their time rates of change, past history, and propellant type (primarily through thermophysical properties). In most applications, pressure cannot be held precisely constant. In motors, transient burning commonly contributes to a pressure peak at the beginning of operation, and may also cause extinction of remaining slivers during the depressurization at the end of operation. Through the middle portion of operation, the pressure may also vary with time because of the grain configuration, nozzle size changes or manufacturing variables, such as the hump effect above. In general, a reacting propellant features a burning rate variable in time.

With reference to a motor, the combustion process is said to be non-neutral. In particular, *progressive* or *regressive* processes are defined if chamber pressure (or thrust) is overall increasing or decreasing in time (causing excursions wider than 15% of the average value[9]). The following definitions illustrated in Figure 3.0 [9], although arbitrary, are commonly accepted:

- Neutral burning: motor burning time during which thrust or chamber pressure remain approximately constant, typically within a corridor of ± 15%;
- Progressive burning: motor burning time during which thrust or chamber pressure increase (beyond the ± 15% corridor);
- Regressive burning: motor burning time during which thrust, chamber pressure, and burning surface area decrease (beyond the ± 15% corridor).

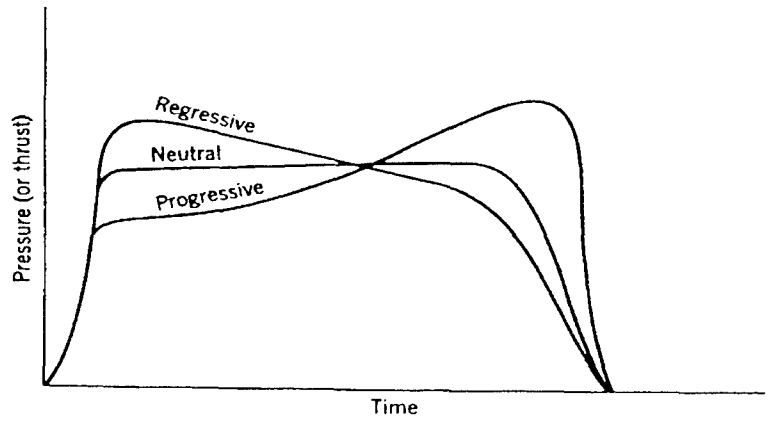

Figure 3. Classification of Grains According to Pressure-Time Characteristics[9]

Even the simplest burners experience dynamic burning effects, at least during the ignition transient, caused by the abrupt hot gas production. For well-designed burners, the associated rapid pressure change is a minor feature. But even if the pressure transient is avoided, the thermal transient still needs to be dealt with. In strand burners, this is accomplished by allowing the strand to burn some distance after ignition before starting the measurement period; likewise, the measurement period is stopped some distance from the strand end to avoid extinction transient. Also in the so-called non-intrusive burners (ultrasound, microwave, laser recoil, and x-ray) in which "instantaneous" (or very short-term averaged) burning rate measurements are obtained, both the starting and ending transients can be avoided. However, in motors the transients are essentially unavoidable, and are necessarily included in the data analysis because the only length known is the total thickness. In principle under no circumstances, including neutral burning, measurements should be taken during transient operations (ignition and extinction). But should diagnostic techniques capable of direct measurements of burning rates (e.g., ultrasound) be available, high-frequency measurements during transient operations can provide a corresponding time-resolved burning rate history.

2.2 Burning Rate Laws

2.2.1. Empirical Burning Rate Laws

Under steady conditions and for a given initial temperature, the Vieille or de Saint Robert law[16,9] is empirically used to describe the burning rate dependence on pressure

$$\bar{r}_b = a_b \bar{p}^n \tag{4}$$

where the two parameters (a_b and n) are constants experimentally defined over some limited measurement range. Figure 4.0 compares various burning rate pressure relationships.

Propellants showing a region of markedly reduced or zero pressure exponent are known as "plateau" propellants (for example double base propellants with small amounts of lead compounds). Propellants showing small negative values of n over short pressure ranges are called "mesa" propellants. Often it is possible to represent burning rate as a series of straight segments, with different a_b and n for various pressure ranges. To establish a_b and n for one range of pressure and initial temperature, it is industrial practice to use 7 runs (3 at the nominal pressure, 2 at the higher and 2 at lower pressure) at normal initial temperature and 5 runs each at expected temperature extremes.

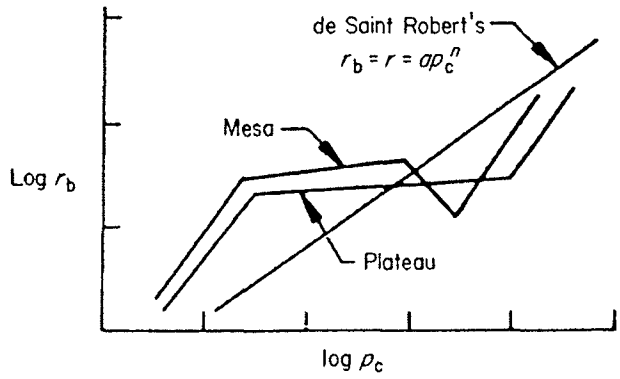

Figure 4. Various Burning Rate versus Pressure Relationships[14]

For years, the industry standard technique to acquire these data has been based on the so-called Crawford bomb.[17] The particular form with n =1

$$\bar{r}_b = a_b \bar{p} \tag{5}$$

has been used in the past to represent steady burning rates of simple single base (nitrocellulose) gun propellants with some accuracy.[10] An alternative form borrowed from artillery and called Muraour law[16]

$$\bar{r}_b = b_b + a_b \bar{p} \tag{6}$$

describes[10] the behavior of many double base propellants for pressures above 200 atm as well or better than Eq. (4) and also provides[7] good estimates of the *constants* b_b and a_b.[7] Basically it yields results similar to Eq. (4) for the pressure interval of interest in rocket propulsion. Another alternative form[16]

$$\bar{r}_b = b_b + a_b \bar{p}^n \tag{7}$$

gives accurate results for many double base propellants over a wide pressure range, but it differs little from both Eq. (4) and Eq. (6) and is anyway inadequate for most rocket propellants.[10] The classical Granular Diffusion Flame (GDF) theory, developed by Summerfield and coworkers [18, 19, 20] can be applied to AP-based composite propellants burning at moderate pressures (0.2-0.8 MPa[7]) leading to the standard expression

$$\frac{\bar{p}}{\bar{r}_b} = a + b \cdot \bar{p}^{-2/3} \tag{8}$$

where the constants *a* and *b* respectively measure the importance of chemical kinetics and mass diffusion in the gas phase.[21,22] For lack of better knowledge, the use of Eq. (4) is recommended.

As an alternative for some particular compositions, the *"normal"* ballistic law (first proposed by Zeldovich[23,24] in 1942 and much used in the Russian literature[25, 26] can be implemented. This burning rate law, of exponential form, under steady conditions is usually written as

$$\bar{m}_{Ze}(\bar{T}_s) = M_s \exp\left(-\frac{E_{Ze}}{\Re \bar{T}_s}\right) \tag{9}$$

where $\bar{m}_{Ze} = \rho_c \bar{r}_{b,Ze}$ is the steady surface mass burning rate and the pre-exponential factor M_s is the (asymptotic) maximum mass burning rate. The relationship of Eq. (9) was experimentally shown to hold as an "universal" law for particular compositions, over a wide range of pressure and initial

temperature, by taking proper values of the relevant constants: for all known[26] double-base propellants (DBP) and nitrocellulose (NC) the activation temperature $E_{Ze}/\Re$ =5000 K and the pre-exponential factor M_s=1.8 10^3 g/cm^{2}s.[26] In this report, for convenience, the steady burning rate of Eq. (9) is called the *normal or Zeldovich burning rate* law.

2.2.2 Pressure and Temperature Sensitivity

If $\bar{r}_b$ is the steady linear burning rate, the commonly accepted definition (see Figure 2.4) for the steady burning rate pressure sensitivity is

$$n \equiv \left(\frac{\partial \ln \bar{r}_b}{\partial \ln \bar{p}} \right)_{To} = \frac{\bar{p}}{\bar{r}} \left(\frac{\partial \bar{r}_b}{\partial \bar{p}} \right)_{To} \tag{10}$$

while for the steady burning rate temperature sensitivity[9]

$$\sigma_p \equiv \left(\frac{\partial ln \bar{r}_b}{\partial T_0} \right)_{\bar{p}} = \frac{1}{\bar{r}_b} \left(\frac{\partial \bar{r}_b}{\partial T_0} \right)_{\bar{p}} \tag{11}$$

Practically, over the appropriate *pressure and initial temperature* intervals, the familiar empirical steady relationships[9] are used

$$\bar{r}_{b,Vi} = a_b(T_{ref}) \cdot \bar{p} \cdot \exp\left[\sigma_p (T_0 - T_{ref})\right] \tag{12}$$

being

$$a_b(T_0) = a_b(T_{ref}) \cdot \exp\left[\sigma_p (T_0 - T_{ref})\right] \tag{13}$$

where T_{ref} is the reference ambient temperature, T_0 is the actual initial or ambient temperature, n and σ_p are constants over some limited operating range. In this report, for convenience, the steady burning rate of Eq. (12), obtained from experiments, is called the generalized power burning rate law also referred to as *Vieille (or Saint Robert) burning rate* law. The steady burning rate laws of Eq. (12) and Eq. (4) are convenient widely used over the appropriate range of operating conditions. Notice that Eq. (12) implies the simplifying assumption that $n=n(p)$ while $a_b=a_b(T_0)$, as often observed due to the limited range of industrial burn rate testing. But this is not necessarily true in general. However, if the assumption is kept, then

$$\sigma_p \equiv \left(\frac{\partial \ln \bar{r}_b}{\partial T_0} \right)_{\bar{p}} = \frac{1}{a_b} \left(\frac{\partial a_b}{\partial T_0} \right)_{\bar{p}} \tag{14}$$

For motor operation, the commonly accepted definition for temperature sensitivity is

$$\pi_K \equiv \left(\frac{\partial ln \bar{p}}{\partial T_0} \right)_K = \frac{1}{\bar{p}} \left(\frac{\partial \bar{p}}{\partial T_0} \right)_K \tag{15}$$

from which over some limited operating range

$$\bar{p}(T_0) = \bar{p}(T_{ref}) \cdot exp\left[\pi_K (T_0 - T_{ref})\right] \tag{16}$$

Moreover, combination of Eq. (12) and Eq. (16) yields

$$\pi_K = \frac{\sigma_p}{1-n} \tag{17}$$

valid if the relevant parameters are constant and small, i.e. $\sigma_p(T_0-T_{ref})<<1$ and $\pi_K(T_0-T_{ref})<<1$, as often observed. As matter of fact, typical values fall in the range $\sigma_p \approx 0.001$ to 0.01 K^{-1} and $\pi_K \approx 0.0005$ to 0.01 K^{-1}; double-base propellants usually feature larger values than composite propellants and ammonium nitrate based compositions are more sensitive than ammonium perchlorate ones. Specific values are reported in References.[7, 9, 12, 8,22, 27, 28, 29]

2.2.3. Analytical Burning Rate Models

Two different viewpoints have been taken to develop analytical models of steady burning rate.[7] Propellant chemists try to understand ballistic properties from a detailed knowledge of chemical kinetics mechanisms, while neglecting other less important physical processes. This approach has proved useful mainly for homogeneous compositions. Aerothermochemists have emphasized the importance of fluid mechanics and heat transfer while idealizing the role of chemistry to a few basic steps. These two different but complementary approaches are explained by examining the complexity of the underlying phenomena.

Still today the basic picture of DB burning (Figure 5.0) is that originally proposed by Rice[30] and Parr.[31] The burning process can be seen as one-dimensional, but several zones can be distinguished where chemistry plays a dominant role. In the gas-phase a fizz-zone (strong thermal gradient), dark-zone (vanishing thermal gradient, flame temperature around 1500 K, intermediate products), and luminous zone (strong thermal gradient, final flame temperature, final products) are identified. In the condensed-phase a rate controlled concentrated surface decomposition is assumed [30] or, more likely, a distributed foam zone involving exothermic processes and partial gasification of the solid propellant.[58] For increasing pressure, the overall flame thickness decreases. However, for pressures below 0.15 MPa the luminous zone cannot take place for kinetic reasons and the final temperature is that of the dark-zone.

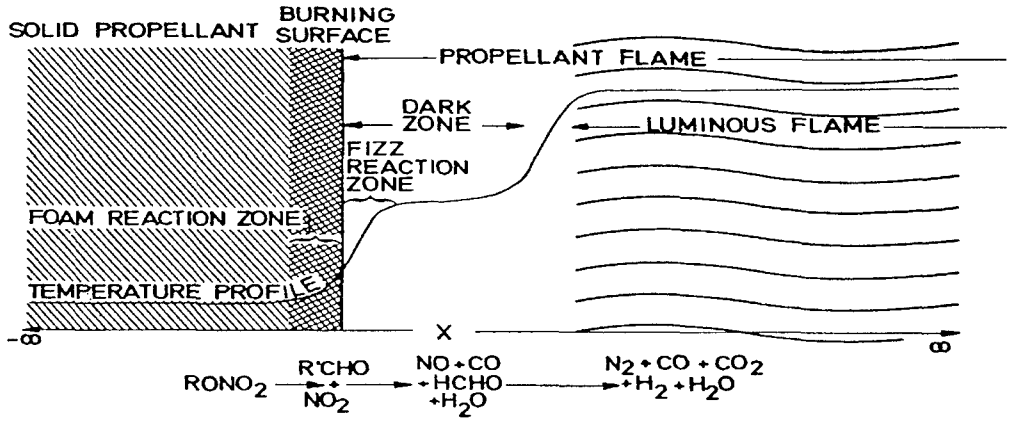

Figure 5. Basic One-Dimensional View of Double Base Propellant Burning [30,31]

Several models were proposed for heterogeneous compositions as well, but rarely based on first principles due to the intrinsically 3D and unsteady nature of the associated burning processes. The GDF two-stage flame model by Summerfield and coworkers [18, 19, 20] (Figure 6.0) and the BDP [32] multiple flame model (Figure 7.0) are prominent examples. In the GDF model the burning surface includes dissociative sublimation of NH_4ClO_4 into NH_3+$HClO_4$ over the oxidizer surface and endothermic zero-order pyrolysis of the solid fuel. A double flame structure is then portrayed in the gas-phase: a primary premixed monopropellant flame (between NH_3 and $HClO_4$ provided by the oxidizer dissociation) followed by a final

diffusion flame between gaseous fuel pockets and the oxidizing atmosphere of the premixed flame products. The premixed flame is seen as very thin as compared to the diffusion flame; for pressures below approximately 0.1 MPa the gaseous premixed flame collapses to the burning surface. Thus, the resulting flame structure is seen as one-stage for most operating conditions (from 0.1 to 10 MPa). In the BDP model, the premixed monopropellant flame (between NH_3 and $HClO_4$) over the oxidizer surface takes place simultaneously to a primary diffusion flame confined at the edges of the oxidizer crystal. The main or final diffusion flame subsequently follows both flames between fuel and oxidizer intermediate products.

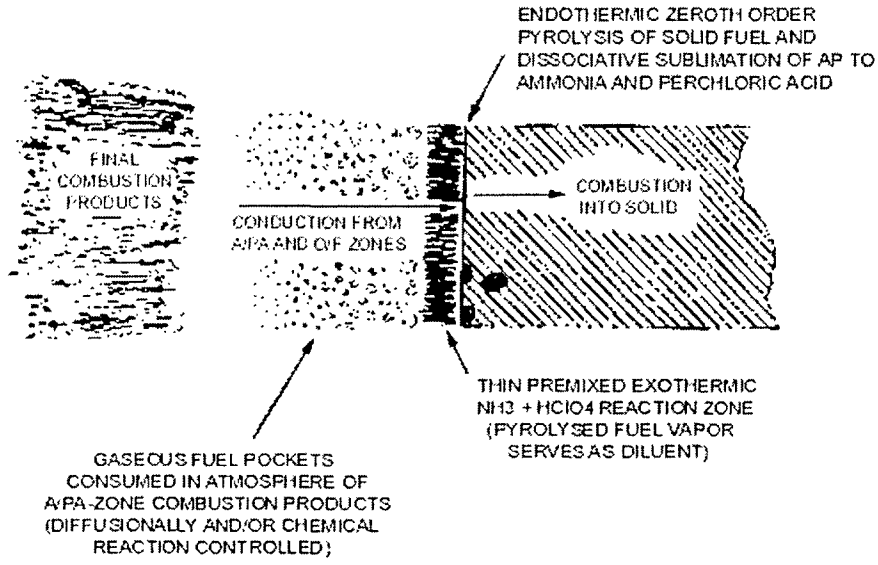

Figure 6. Schematic of Granular Diffusion Flame (GDF) Two-Stage Flame Structure for AP-based Composite Solid Propellants[18, 19, 20]

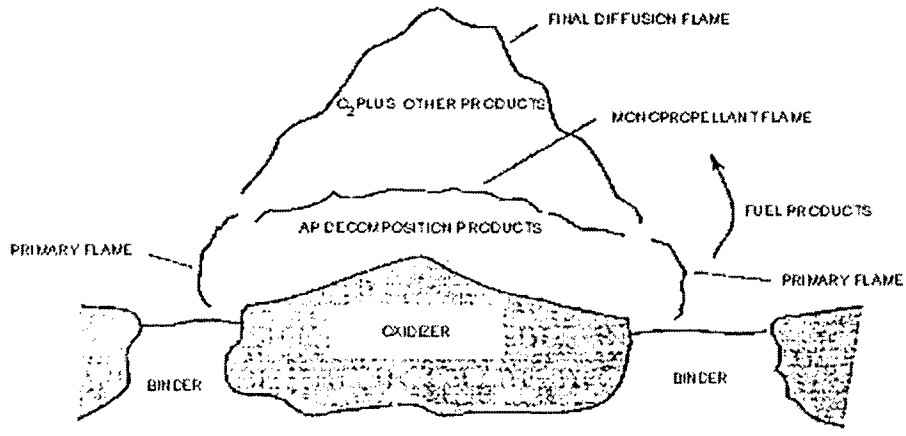

Figure 7. Schematic of Beckstead-Derr-Price (BDP) Multiple Flame Structure of AP-based Propellants[32]

2.3 Combustion Stability

Propellant and/or combustor stability problems may be encountered during any experimental burn rate testing. Both are anomalies to be avoided.

2.3.1 Intrinsic Stability of Propellants

This matter concerns the capability of a reacting solid propellant to recover its initial value of burning rate when perturbed. It is also known as *intrinsic stability* because it is strictly dependent on the nature of the burning solid propellant and operating conditions (typically, but not exclusively, pressure and initial temperature). Following the pioneering work by Zeldovich[23] in 1942, two main approaches, known as Zeldovich-Novozhilov (ZN) method and Flame Modeling (FM) method, have emerged to study intrinsic stability of solid propellants. Both share the basic assumptions of Quasi-Steady gas phase, Homogeneous condensed phase, and One-Dimensional propellant strand (QSHOD framework). Within this framework and for pressure perturbations only, linear stability analyses were first presented by Denison and Baum [33] in 1961 for premixed flames and Novozhilov [34, 25, 35] in 1965 by the ZN method. Both works, in the linear approximation of the problem, relaxed the assumption of constant surface temperature until then used. The linear stability boundary so deduced is the *same*; this boundary was shown later to hold true even under nonlinear conditions.[36] Just on the stability boundary a reacting solid propellant is expected to reveal self-sustained oscillations of the burning rate. The combustion behavior beyond this stability boundary still is a matter of speculation, but likely self-sustained oscillatory burning are observed until no steady solution whatsoever is allowed.[37]

2.3.2 Burning Stability of Motors

Catastrophic, high frequency combustion instability became relatively uncommon with the advent of aluminized propellants in the late 1950's. As a result, related research and development dwindled. However, compelling need for reduced visibility or opacity of rocket exhaust has dictated elimination of significant concentrations of aluminum from many tactical rocket propellants. The instability problem has reemerged at great cost to many motor development programs.

Burning stability concerns the capability of the combustor to recover its initial configuration when perturbed. There are many ways of classifying instabilities, but usually the frequency of the oscillation clearly reveals their source. The instability of concern to the one interested in measuring the burning rate of a propellant and motor configuration arises from coupling of the rate-determining combustion processes with acoustic oscillation modes of the combustion chamber. A rocket motor with a simple center-perforated grain of reasonably high length-to-diameter ratio acts acoustically as a closed cylinder. The simple acoustic modes of such a cylinder are illustrated in Figure 8.0. [38]

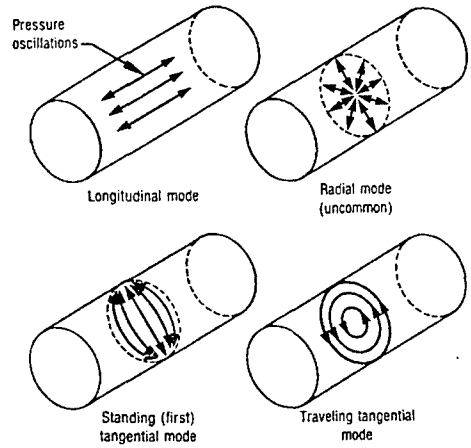

Figure 8. Acoustic Oscillation Modes in a Rigid, Closed Cylindrical Cavity[38]

Burning instabilities manifest as high frequency oscillations of the relevant motor variables (burning rate, pressure, temperature, etc.) superimposed on the corresponding average values, accompanied by corresponding vibrations of the motor case. Pressure histories of heavywall test motors containing an unstable, reduced smoke propellant (i.e., non-aluminized HTPB/AP) often reveal pressure excursions far more than sufficient to rupture a flight weight motor case. Note that in actual industrial practice combustion pressure excursions are not considered serious if below some limiting value (5%[9] or 2.5%[39]). These fluctuations are always undesirable; even though catastrophic failures are not necessarily observed, failure of the mission often still can occur. In general, vibrations are set up and transmitted to the whole propulsive system and vehicle, including payloads. Performances are modified due to shifting of the average chamber pressure, burning time is modified, and mechanical and/or thermal failures may occur. Typically, bulk mode instability occurs in the low frequency range (up to 150 Hz), axial mode instability for combustor cavity lengths between 0.3 and 5 m occurs in a larger frequency range (100 to 2,000 Hz), transverse mode instability for combustor diameter between 0.01 and 1 m occurs in an even larger frequency range (500 to 50,000 Hz).[40]

Bulk mode instability throughout the combustor is associated with low values of L^*, typical of early burning in space motors where high mass fraction and low combustion pressure (below 20 atm) are usually met. It is a nonsteady mode of operation of rocket motors, involving growing low frequency oscillations possibly leading to a succession of quenching and reignition (also known as *chuffing* mode) without ever reaching a steady-state operation regime. This peculiar mode of operation is not common, it may last for the entire mission or naturally disappear in time due to growing values of L^*.[41]

The high frequency range, whether axial or transversal, is much more common and usually associated with combustion details. "When oscillatory behavior occurs ... the oscillations would be more correctly attributed to instability of the entire *combustor*. The phenomenon results from a very complex interaction of the combustion, the combustor flowfield, and the combustor cavity walls." [41] Burning instabilities take place when perturbations excite any of the many acoustic oscillation modes of the chamber cavity. This problem is strongly dependent on the details of the fluid dynamics (interaction of oscillations with the mean flow, vorticity, viscosity, flow turning, multiphase flow, etc.) and 3D geometry of the combustion chamber (acoustics) as well as their interactions with the burning solid propellant. The balance of the various contributions (amplifying or damping) is currently assessed by means of a linear analysis; but some nonlinear aspects are also discussed in literature.[42] Although much progress has been made, this problem is far from being understood in its generality. Further comments can be found in References[40, 41, 21, 11]; some practical stability problems are also discussed in References.[21, 43]

2.4 Burning Rate Measurement Methods

2.4.1 Test Devices

Early descriptions of burning rate measurement methods were given in a previous AGARD publication by Young [44] and several classical textbooks [7, 10, 16, 45]; more recent descriptions are reported elsewhere.[9,12, 21] In general the burning rates obtained by different techniques are not the same; even using identical specimens and the same technique at different facilities, the measured burning rates are different due to a variety of details not fully controllable or controlled. A host of methods, ranging from reduced scale rocket motors to the simple strand burner, is today implemented to measure steady burning rates. In general, small scale motors are preferred to evaluate the burning rate of actual rocket motors (ballistic evaluation), while strand burners are used for quick assessment tests or quality control of large propellant production; other methods are mainly used for special purposes (interrupted burning, high pressure combustion, etc.).

The experimental results from the various methods used today are in general accurate to within ± 2-3% both for small motors and strand burners[12], but accuracy less than of 1% is sought for actual rocket motor design.[15] In most cases, strand burners reveal burning rates below the values of small motors, which in turn fall below full-scale motors. Nitramines seem to be a notable exception by scaling somewhat higher

than full-scale motors.[46] Therefore, it is not only important to understand and standardize the technical procedures implemented by different users, but also to estimate the scale factor with respect to the full size engine if the burning rate value under the actual motor operating conditions is desired. In general, motor burning rate increases with the motor size[12]; other possible differences between data collected in motors and strands (changes in slopes or plateaus) are discussed in later sections.

2.4.1.1 Subscale Motors

While the development of gun propellants relies on precise control of the manufacturing procedure and chemical compositions, this is impossible[45] for rocket propellants due to the much more complex chemical composition and dependence on parameters difficult to control (particle size, minor additions of catalytic ingredients, etc.). Thus, the most satisfactory method to evaluate steady burning rates is to fire a certain number of rockets loaded with the actual propellant under test. For practical reasons, reduced cost, and improved safety, different rocket motors of reduced size (typically, 2 to 6 inches - or about 5 to 15 cm - diameter) were specifically developed for ballistic evaluation purposes at many facilities. These reduced scale rocket motors are usually made with heavy case and fitted with nozzles of different sizes to provide a number of convenient operating pressures (see Eq. 18).

Typically, small ballistic evaluation motors are radial burners providing a neutral pressure trace in time (within ± 10%), a sharp tail-off, port area / throat area ratio $A_p/A_t > 6$ and grain length / diameter ratio ≤ 2 to minimize erosive burning, short burning duration (2-10 s) to minimize heat losses and nozzle erosion, small grain web thickness to minimize thermal shrinkage, conical nozzle geometry with 15° ± 0.5° half angle of divergence and no flow separation. The motor nozzle size, A_t, is estimated[12] from the burning rate r_b established from initial strand burner rate measurements based on the mass conservation equation

$$A_t = \frac{A_b r_b \rho_p}{C_D p_c} \tag{18}$$

In some cases, non-neutral pressure traces in time are used to reduce the number of tests, but the determination of the pressure exponent n is less accurate. In the industrial practice, over a pressure range for which a and n remain constant (see Eq. 4), a minimum of seven motors at the nominal operating initial temperature and five at the expected initial temperature extremes are fired.[27]

Tests with small motors provide better correlation with full-scale motor burning rates, but are considerably more time- and money-consuming than tests in strand burners. Tests in small motors are normally performed only after the neighborhood of the final propellant formulation is reached, in order to obtain a more accurate full-scale motor rate prediction and determine the temperature sensitivity of the motor combustion pressure π_K.

Many specific configurations of subscale motors are used in different countries. The term micromotors or the acronyms BEM for ballistic evaluation motors, BTM for batch test motors, BCM for batch check motors, SSTM for subscale test motors and others are randomly found in the literature to identify this specific but loosely defined class of motors. In this report, only the broad expression "subscale motors" is used. Although several suitable motor designs may be implemented, the most common configuration is a neutral burning grain providing a relatively constant combustion pressure p_c. Detailed recommendations on current burning rate measurement test techniques and subscale test hardware for accurate prediction of internal ballistics of a full-scale solid propellant motor are reported in JHU/CPIA CPTR 74[4]. Trends in observed differences in calculated burning rate for the different analysis methods were also evaluated with a goal of making recommendations on preferred analysis methods. These results, including surveys of analysis methods and results of the round robins are reviewed in a companion JHU/CPIA CPTR 75[5], and References [1,25]. Further modifications, or complementary tools, of this basic setup are briefly described below.

2.4.1.2 Vented Vessels

In the simplest version, vented vessels are actual rocket motors abruptly extinguished by sudden release of pressure by blowing off the nozzle or by water injection. More sophisticated designs were also

developed in which sticks, or slabs, of propellant are burnt and are quenched with water after about half the sample has been consumed. The pressure of operation is controlled by a much larger tubular charge of some faster burning standard propellant. By measurement of the burning time and the dimensions of the propellant sample before and after firing, the rate of burning can be determined directly.[44] This method to obtain burning rates, which is laborious, is no longer practiced. But the technique of vented vessels is used still today for other purposes, such as interrupted burning to examine the conditions of the propellant charge during combustion.[10]

2.4.1.3 Closed Vessels

Several closed vessel configurations are currently available to obtain the burning rate of the propellant from experimental pressure records in time. One option is to burn a small propellant sample in a large closed vessel filled with inert gas, producing a small pressure increase. The burning time is obtained as the time span between the onset and decay of the pressure rise. Another option is to increase the mass of the propellant sample up to a loading density of 0.3 g/cm^3, producing a very large pressure increase and pressurization rate from which the burning rate is deduced. This is not a direct measurement and the overall approach is a laborious process requiring a number of assumptions, but the method is used still today for very high pressure combustion (gun propellants).[7, 10, 15, 47]

An alternative technique to assess performances of gun propellants in particular is to measure the so-called heat of explosion in some type of calorimeter. This is a sensitive and quick method, derived from chemistry, capable of detecting any important changes or gross error in chemical composition. But it is useful in rocket propulsion only if, for the given propellant, the rate of burning is directly related to the heat of explosion,[44] which is not commonly the case.

2.4.1.4 Strand Burners

For about 50 years, the industry standard apparatus for routine measurements of linear burning rates has been the so-called Crawford bomb proposed in 1947.[17] This method, very quick, simple, and economic, is particularly suitable for exploring new propellant compositions or performing quality control of established compositions. Strands of propellant having circular or square cross section, 3 to 6 mm in diameter or side, are employed. The overall strand length usually ranges anywhere from some 10 mm to about 150 mm. These are supported in a suitable holder and inserted into a closed vessel, typically pressurized with nitrogen. The strands are coated with an inhibitor to prevent side burning. In the original configuration, two small holes are drilled, about 5 inches (about 127 mm) apart, along the diameter. Fuse wires are passed through each hole and connected to terminals. The strand is ignited at the top by a hot wire, and the time taken for burning to pass from the first to the second fuse wire is accurately measured. It is usual to take several measurements at each pressure.[13] The burning surface should remain planar and normal to the strand axis.

Over the years, several modifications of this basic setup for solid strands have been proposed. In the most common modification, the whole apparatus can be placed in a thermally controlled environment capable of producing the desired initial temperature range. In another version, called *window strand burner*, the burner is equipped with optical windows allowing optical recording of the burning processes (still photography, movie camera, video camera, etc. both in the visible and infrared ranges).[48] At Thiokol/Huntsville, a bomb holding three strands was used.[46] All configurations are easy and quick to operate, use a minor amount of propellant, and require little instrumentation. Thus, the strand burner method is widely used.

A further modification was developed at Aerojet Solid Propulsion Company (and occasionally used also at other locations), where the additional option of testing liquid strands of the uncured propellant instead of the familiar cured propellant solid strands is implemented. Burn rates of liquid strands are used in propellant manufacturing as controls for acceptance of the uncured propellant before casting into the motor. The liquid strands are obtained by casting the uncured propellant into a proper vessel (6.4 mm diameter paper cup or plastic tube or 6.4 x 6.4 x 139.7 mm rounded solid strip) coated with an inert lacquer; see sketch in Figure 9.[12] The measured burning rate differs with respect to both the solid strands

and motor, but values can be correlated, as discussed more fully in later sections. The strand burning rate relationshoip is developed along with other control parameters during propellant development as illustrated in Figure 10. Once the strand burning rate has been established with its tolerance limits, the motor burning rate can be predicted. Challenges and successes in this correlation are reviewed in Section 6.0. A representative comparison of liquid and solid strand data is given in Figure 11. The liquid strand burn rate is of importance once the propellant reaches a production level. The solid strand burn rate is confined mainly to the development stage, where the composition versus burn rate is being established.[12]

An updated description and discussion of various strand burners is given in Reference [21]; further useful comments are reported in References [7, 7, 9, 10, 22].

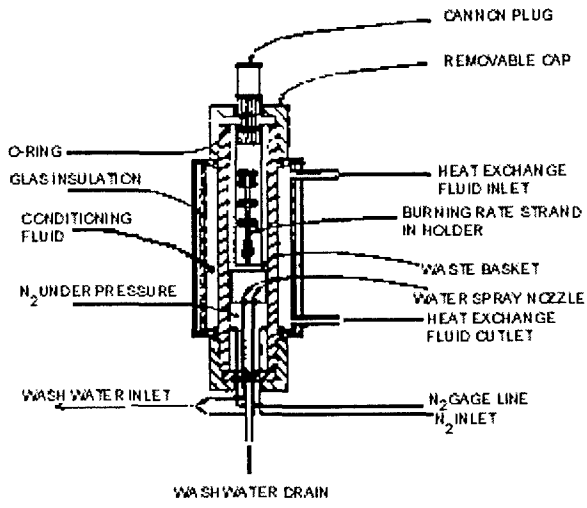

Figure 9. Modern Crawford Bomb (Solid or Liquid Strands)[12]

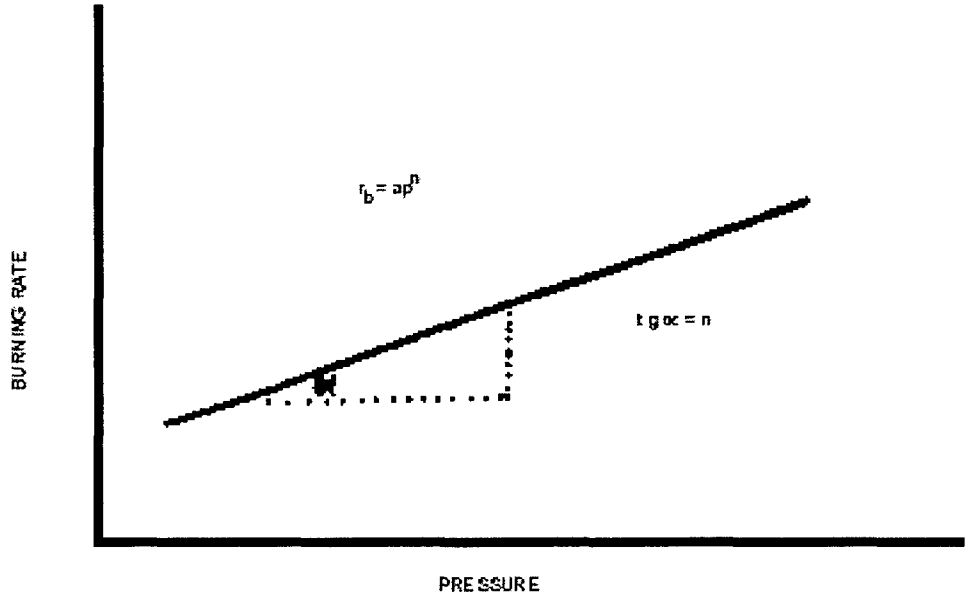

Figure 10. Traditional Power Law Burning Rate Behavior[12]

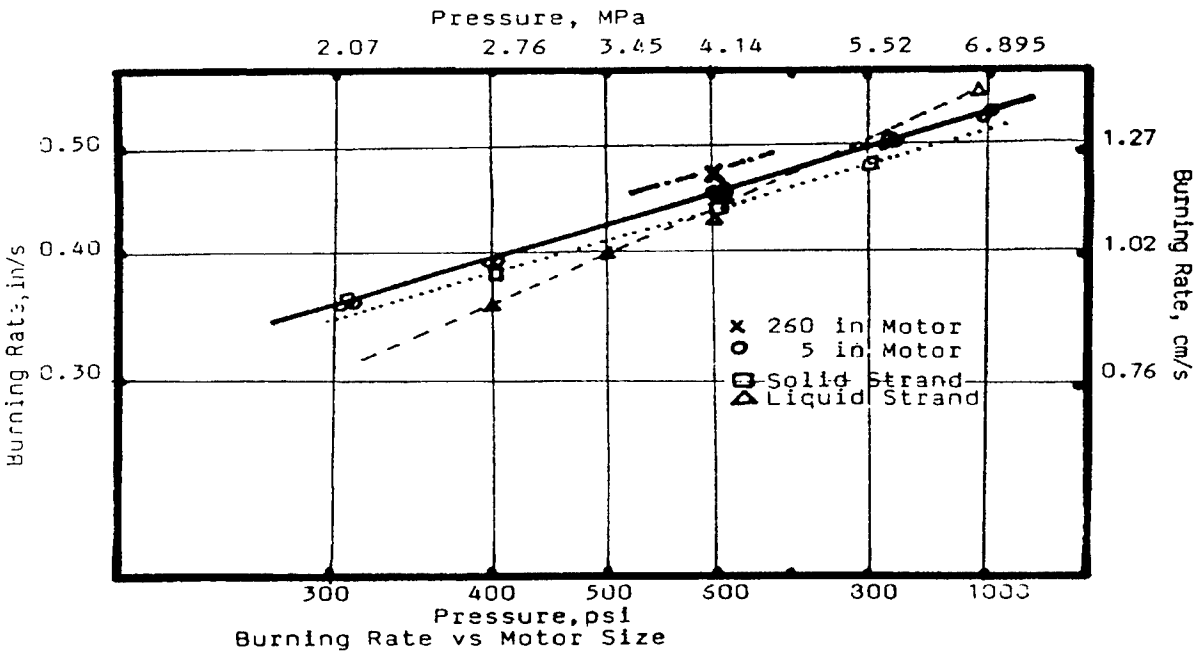

Figure 11. Behavior of Solid and Liquid Strand Burning Rate Relative to Motor Size[12]

2.4.2. Non-Intrusive Methods

Several diagnostic techniques are used to deduce burning rates. The well-known fuse wire technique set up for strand burners[17] allows only discrete measurements and under steady state burning. It is an intrusive method and thus suitable only for operating conditions far from the intrinsic stability boundaries. Other diagnostic techniques, notably non-intrusive and continuous in time, are needed for motors.

Non-intrusive methods were developed with the aim of measuring burning rates while minimizing disturbance of the combustion processes independently of the experimental apparatus. Several techniques are available with a different features and degree of maturity: film or video recording[49], X-rays[50], microwaves[51], ultrasonic[52], acoustic emissions[53], radiation recoil (typically, but not necessarily by a laser source[54]), plasma capacitance.[55] The X-rays technique, while applicable to any burning apparatus, is recommended for full-scale motors. Film or video recording, radiation recoil, and acoustic emissions techniques are more suitable for strand burners. Microwaves and ultrasonic techniques are suitable for both small-scale motors and strand burners. Radiation recoil and acoustic emission techniques do not detect the burning surface position and thus provide an indirect measurement; all other techniques are direct. Several of these techniques (in particular microwaves and ultrasonic) are also apt to measure transient burning rates; in addition, the acoustic emission technique is apt[56] to provide information as to the burning rate nonuniformity (due to localized and intermittent burning rate variations).[1]

2.5 Burning Rate Measurements in Subscale Motors

When testing motors, the burning rate measurement is actually deduced from the observed pressure-time or thrust-time history. Thus, following Hessler [57], it is convenient to recognize from start that appropriate definitions are required for burning rate in motors.

2.5.1 Burning Rate Definitions

Two basic classes of empirical burning rate definitions are in use for motor applications. These two families of fundamentally different burning rate determination each have their advantages and disadvantages. One definition is based on propellant thickness and the burning time and is referred to as the thickness/time (TOT) method, and the second is based on the conservation of mass in the ballistic test motor and is accordingly termed mass conservation or mass balance (MB) method.

The conventional burning rate definition is the fundamental TOT rate, r_{TOT}

$$r_{TOT} = \bar{r}_b = \frac{web\ \ thickness}{burning\ \ time} = \frac{w_b}{t_b} \tag{16}$$

requiring the appropriate but elusive value of thickness besides that of the related time. Real world effects such as non-uniform web and non-instantaneous burnout make accurate measurements of burning rate difficult. In attempting to correct for these factors, an alternative definition evolved based on some approximation of the mass conservation equations, rather than the fundamental ratio of Eq. 16 was in use already around 1960.[58]

Mass balance methods evaluate the steady burning rate r_{MB}, indirectly, from the balance between mass flow input from the burning propellant and output through the nozzle throat. Burning is assumed to occur throughout motor operation, implicitly accounting for non-instantaneous burnout. Mass conservation should include gas storage in the combustion chamber due to density change and/or volume change; accordingly, several versions of this approach exist. The mass balance rate, mass conservation neglecting corrections, features less data scattering than the thickness/time rate, because it partially corrects for non-instantaneous burnout.[58]

Neglecting gas storage in the combustion chamber due to density change and/or volume change, an (average) mass balance rate r_{MB} is written See Figure 12 for notation definitions) as

$$r_{MB} = \frac{W_A - W_G}{t_E - t_B}\frac{\int_B^E p_c dt}{\int_A^G p_c dt} = \frac{W_{avg}}{t_b}\frac{\int_B^E p_c dt}{\int_A^G p_c dt} \tag{17}$$

Several variations of Eqn. 17 are used, involving primarily corrections for the neglect of mass storage.

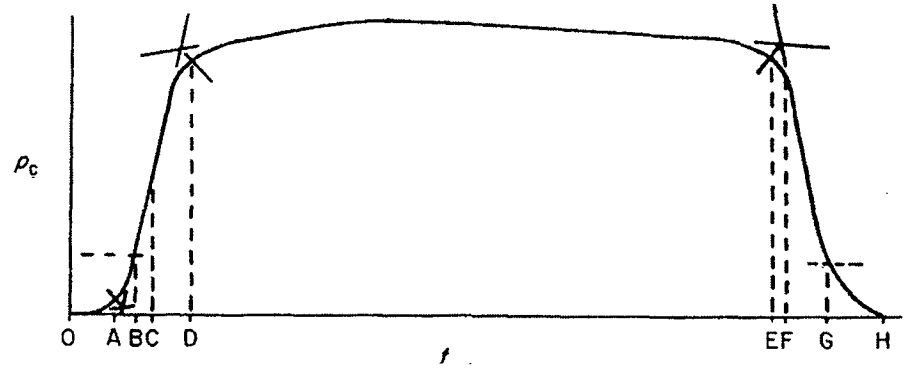

Figure 12. Various Burning Time Definitions[59]

Many r_{TOT} procedures do not explicitly account for non-instantaneous burnout. In fact, r_{TOT} procedures typically define end of burning as the knee of the curve (web burnout), when the experimental pressure trace begins to fall rapidly near the end of motor operation. However, specific choices of time points may make the correction implicitly. Procedures that define end of burning near 50% pressure implicitly assume burning continuation and thus partially avoid non-instantaneous burnout error, but not as well as an r_{MB} definition that actually uses the integral ratio. Due to transient operations, these r_{TOT} procedures tend to behave essentially like r_{MB} procedures. While use of 50% pressure time points for start of burning only has small effect on burning rate, the choice of 50% or more for end of burn during pressure decay can be a source of higher rate bias. A drawback of a 50-50 definition is that the time-averaged pressure differs much more from the rate-averaged pressure because the ending points are much lower down the tailoff curve than for an equilibrium or web-knee definition. More bias in burning rate is introduced, as the rate-averaged pressure is seldom used.

r_{MB} methods yield rates that are systematically low by a mass storage error. In turn, mass storage error also introduces a systematic nonlinearity in measured $r_b(p)$. Procedures essentially behaving like r_{MB} are likewise low by a mass storage error and generate similar nonlinearities. r_{TOT} methods, with instantaneous burnout, avoid the mass storage error yielding negligible nonlinear errors but high bias due to non-instantaneous burnout. Comparisons between MB and TOT analysis methods are more fully discussed in JHU/CPIA CPTR 75.[5]

3.0 FUNDAMENTAL FACTORS INFLUENCING SCALING OF BURNING RATE

Some of the underlying reasons for the differences observed in burning rate between large scale motors, subscale motors, strands and non-intrusive methods become apparent by considering the factors influencing propellant burning rate. Section 2.0 reviewed burning rate physics and mathematical models for burning rate description. This section discusses Intrinsic and Global Parameters and their influence on the correlation of burning rate between motor scales.

3.1 Intrinsic Parameters

Intrinsic parameters are evident from a consideration of burning rate physics and models of burning rate mechanisms, and can be studied independently in the laboratory. Such parameters may be dependent on the type of propellant in question. For instance double base plateau propellants will have a lesser dependency on pressure than composite propellants. Intrinsic parameters influencing scaling include pressure, temperature, propellant mechanical properties, cross-flow velocity and radiation. The latter two parameters may be studied independently in the laboratory. However, since they are so closely tied to the motor design and operations conditions, they will be discussed in the next section relative to the Global Parameters.

3.1.1 Pressure

For composite propellants burning rate is generally proportional to the pressure acting at the burning front raised to a value less than 1, typically 0.2 to 0.7(see Sections 2.1.1 and 2.2.2). Double base propellants may in some cases have a pressure exponent of zero in which case burning rate is independent of pressure (plateau effect) or may have a negative exponent (mesa effect), see Figure 4.

3.1.2 Temperature

Propellant burning rate generally increases with temperature. The relation between burning rate and temperature is quantified by the measured temperature sensitivity of burning rate, σ_p, and the effect of temperature on pressure sensitivity,π_k, (see Eqns. 7 – 14). These coefficients may themselves be a function of temperature for a given propellant, see Sections 2.1.1 and 2.2.2.

3.1.3 Propellant Mechanical Properties

Consistent ballistic performance of a case-bonded solid rocket motor within the envelope of a given design specification is contingent upon maintaining predictable response and structural integrity of the grain and its interfaces throughout the motor duty cycle. In order to predict the response of viscoelastic materials to applied stress, it is necessary to know the elastic and viscous parameters of the material as a function of time, rate and temperature. These characteristics may be determined in the laboratory. In principle these parameters may all be combined into a generalized stress-strain law such that the strain (stress) may be calculated or deduced for an applied stress (strain) as a function of these parameters. Propellant stress-strain responses to different mechanical loading conditions associated with different motor scales can contribute to variations in apparent burning rate.

3.2 Global Parameters

Global parameters are derived from a consideration of the engineering design of the motor and its operating environment. Modern large diameter SRM's may have a number of demanding performance specifications imposed. Factors that typically contribute to modeling complexity of these motors include:[60]

1. High length to diameter ratio (L/D > 9)
2. Large axial pressure drop ((P > 100 psid at ignition)
3. Potential for erosive burning (Mach No.>0.4 in aft end at ignition)
4. Uncertainty in rheology (hump) response for new propellant and manufacturing process
5. Complex ignition process due to high L/D
6. Demanding customer specifications on trace shape reproducibility (±3%)

Global parameters influencing scaling may be divided into principal and contributing factors.

3.2.1 Principal Parameters

The real motor internal geometry at actual firing conditions is the most significant factor in correlating subscale and full-scale motor performance. Principal parameters that contribute to differences in real motor internal geometry with scale include internal ballistic/structural/CFD flowfield-grain interaction, deformed grain structural response, erosive burning response, and 2-D spatial burning rate variations due to propellant rheology effects.

3.2.1.1 Internal Flowfield Model

A good internal flowfield model is essential for meeting the design challenges summarized above and understanding the operation of modern complex solid rocket motors. Safety and economy place unusually stringent demands on the accuracy of ballistic models, and require application of state-of-the-art modeling technology to achieve the required confidence in the first motor prediction. A combination of 1-D, 2-D and 3-D methods is required to accurately predicting nozzle mass flow rate, overall thrust-time, case/nozzle component loads, and grain structural loads. The following principal parameters are integral elements for improving accuracy and reducing motor development uncertainty.

3.2.1.2 Real Solid Propellant Grain Geometry at Test Firing – Grain Deformation Effects

Grain deformation is one of the most significant factors influencing the correlation between subscale and full-scale motor performance. This parameter includes the combined influence of both the grain and case design. Grain design may influence burning rate behavior in a number of ways. The geometric configuration of the grain dictates the gas flow and pressure distribution within the rocket motor and hence can modify the burning rate. The grain design may influence the extent of erosive burning for radially burning grains. For cast case-bonded grains the grain configuration controls the stress state of the propellant, which can modify burning rate, as previously discussed.

Small motors designed for burning rate measurements often have specific grain configuration features as discussed above. For radial burners the cross sectional loading density is usually low relative to an operational motor and the grain is shaped to give a neutral burn. In contrast, motors designed for a mission application have moderate to high cross sectional loading densities and may have grains shaped to give a specific thrust time profile. This produces higher cross flow velocities and enhanced variations in static and total pressure distributions over the burning surface. The gas cross flow conditions may even be sufficient to promote erosive burning, discussed further in the next section, which is generally not present in the small scale burning rate measurement motors. Case design may indirectly affect burning rate by dilation allowing the grain to take up a tensile stress state. The motor design characteristics recommended in JHU/CPIA CPTR 74[4], are established to minimize the effects of scale. [61]

Considerations of motor residence time contribute to conditions during the test firing. Residence time is defined here as the time interval for combustion products to leave the surface of the burning propellant and pass through the throat section of the nozzle. In small motors and motors having low values of grain port to throat area ratio the residence time may become short enough to prevent full reaction of the combustion products and in this way modify the energy feedback into the burning surface and so affect burning rate. Aluminized composite propellants are particularly affected by short residence times, as the molten aluminum droplets given off from the propellant surface may not burn completely before they leave the motor.

Propellant mechanical behavior during firing contributes to differences between subscale and full-scale motor conditions. For example, the grain configuration derived from a preliminary composite solid rocket motor design may be deformed due to thermal shrinkage, pressure curing, firing position, and firing pressure. The effects of the resultant strain on grain burning area versus web thickness behavior are illustrated below in Figures 13, 14, and 15 for three different grain configurations[62], cylindrical, star and dendrite. Refer to Figure 1 for illustrations of these grain configurations.

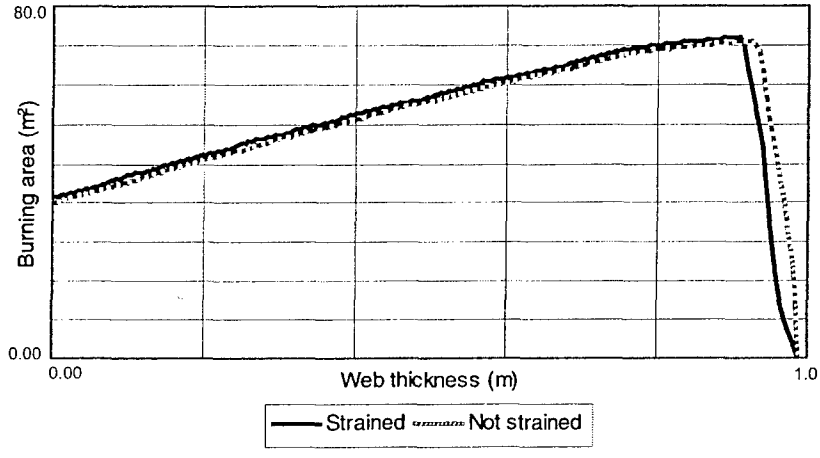

Figure 13. Effect of Strain on the Burning Area versus Web for a Cylindrical Grain[62]

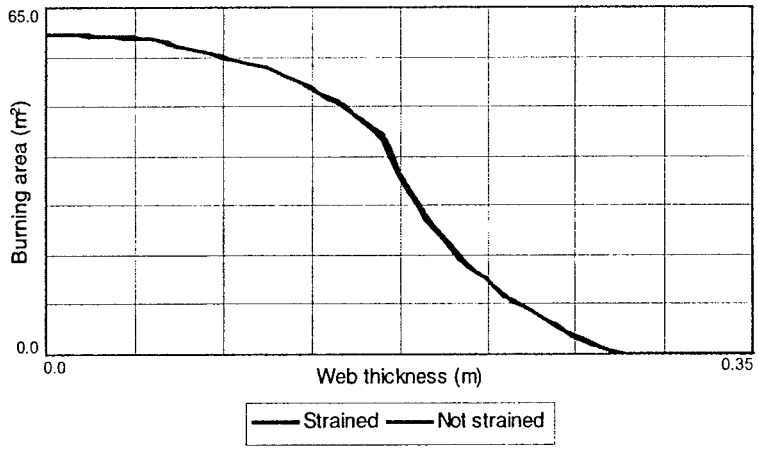

Figure 14. Effect of Strain on the Burning Area versus Web for a Star Grain[62]

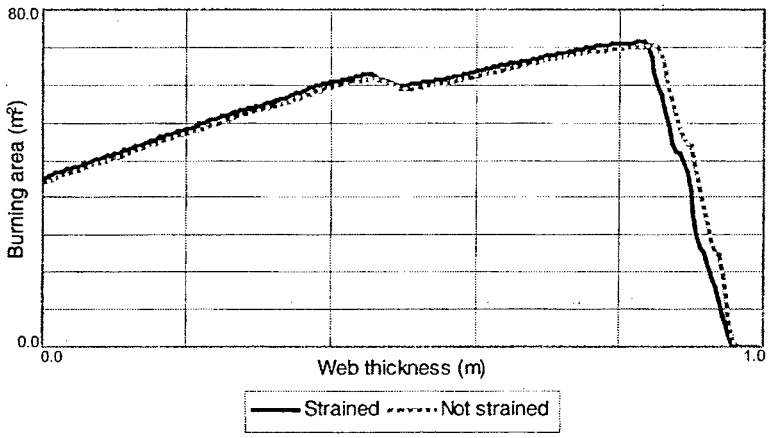

Figure 15. Effect of Strain on the Burning Area versus Web for a Dendrite Grain[62]

The real grain geometry may be predicted with the help of structural analysis to account for:

Thermal shrinkage:	ΔT curing (accounts for grain curing under pressure)
Firing Orientation:	Grain deformation due to firing orientation.
Pressure effects:	Easy to calculate for a constant pressure firing, but much more difficult for non-constant pressure firing.

Figure 16 illustrates the combined effect of these grain deformation factors on surface area versus burn distance for each segment of the US Shuttle RSRM as well as the overall motor.

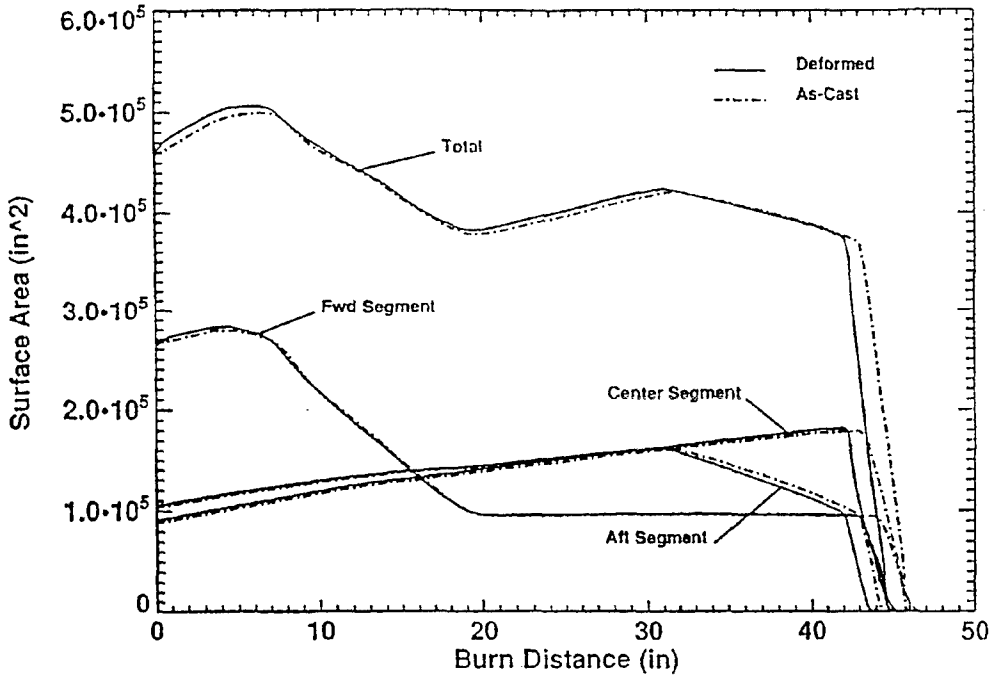

Figure 16. Grain Deformation Effects on Shuttle RSRM Surface Area versus Burn Distance[60]

Generally, the grain deformation reduces the effective web thickness producing a reduction in average scale factor. Thus, accounting for the real grain geometry has the effect of reducing the dispersion in average scale factor. Real solid grain geometry is estimated to contribute as much as 30% of the scale factor observed in large motors. The exact value depends on the details of the grain design, case design and type of manufacturing process.

Cosstephens[63] developed a simplified analytical method enabling the efficient coupling between the internal flowfield of a solid rocket motor and its propellant response. The approach takes advantage of the strong one-dimensional character of large aspect ratio motor flowfields where static pressure is nearly constant across the bore. The results rival the best 2-D calculations when compared to subscale test data in a fraction of the computational time.

3.2.1.3 Erosive Burning Effects – Cross-Flow Velocity

Increasing the cross velocity of combustion products flowing over the propellant surface may modify the energy transport mechanisms governing burning rate. This phenomenon is generally known as erosive burning and results in a dramatic increase in burning rate once a 'threshold' condition is reached. Strand[64] indicates this threshold condition, where the burning rate levels off at its non-erosive value, has been correlated by relating the critical crossflow Reynolds No., Re_c, to the reduced surface transpiration (burning rate) Reynolds No., Re_s. Thus, the measured magnitude of erosive burning rate augmentation was correlated by the amount that the driving parameter (mass flux or Reynolds No.) exceeds the threshold value for erosive augmentation at the given test condition. However, the data exhibits a motor size effect, with the magnitude of burning rate augmentation decreasing with increasing motor size (scale). Figure 17 illustrates motor test results for a typical 5-inch X 10-inch segmented motor test showing the higher than predicted pressure caused by the erosive burning rate augmentation. Also shown in this figure is a larger BATES motor used to evaluate scale effects of erosive burning. Figure 18 illustrates a distinct size scaling effect between the 12-inch diameter BATES and the 5-inch diameter motors.

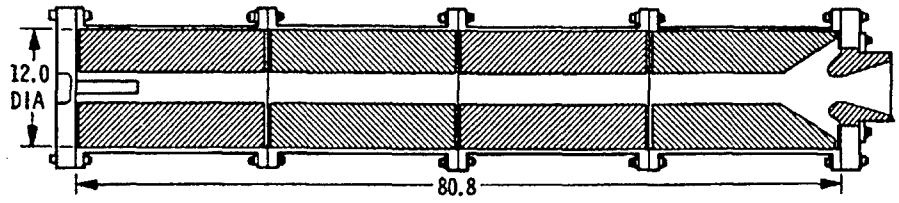

BATES Erosive Burning Test Motor

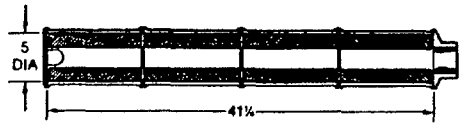

Subscale Batch-Check Test Motor
5-inch D x 10-inch L segments

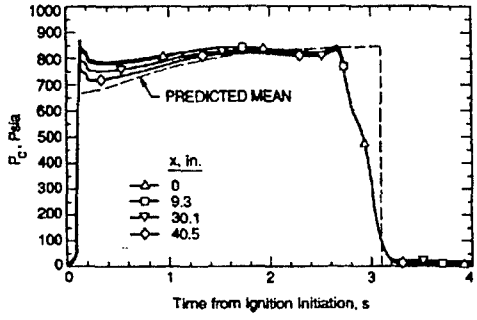

Measured vs Predicted Mean (No Erosion)
P- t Behavior for 5-inch Subscale Motor

Figure 17. Cross Flow Velocity Effect[64]

Strand found the BATES and 5x10 data of Figure 17 could provide the required motor size scaling by empirically correlating r/r_0 with $\{Re_c / Re_{c,th} / R^{0.5}\}^{0.8}$. Many of the simplified erosive burning models do not show scale effects, while the more sophisticated models do.[64] Strand's approach to "cross-flow" is implicitly related to a 1D flow description. It is now acknowledged that erosive burning is due to the interaction between flames and turbulence that requires a multidimensional flow description.

One can readily verify that a scaled-up motor has the same core gas flow velocity and mass flux as its geometrically identical subscale counterpart when operating at the same pressure. Thus the effects of scale cannot be related to dependencies on velocity or mass flux. Using diameter as the scale factor, the core Reynolds number varies directly with scale and the mass flow rate varies directly with the square of scale. Thus the Reynolds number per se, or the mass flow rate, cannot be a basis for an effect of scale that diminishes erosive burning. On the other hand, the axial pressure gradient in the motor varies inversely with scale and is of mechanistic significance in boundary layer theory. Another relevant parameter that varies inversely with scale is combustion zone thickness as a fraction of port radius or boundary layer thickness. Strand[64] found that application of boundary layer theory confirms the experimental findings, but shows that the scale effect is itself dependent upon scale, tending to diminish with increasing motor size. The useful implication of this theoretical result is that a large subscale motor would more closely represent full-scale solid motors than a small or standard subscale motor.

In motors, gases ejected from the propellant surface must turn to flow out the nozzle. By doing so, they flow over the burning surface; depending on how fast they flow, they can influence the combustion process, likely by increasing heat transfer back to the surface. Effects on burning rate can be measured independently, but these effects are commonly present in the flow field of a specific motor grain configuration, as discussed in the next section. Furthermore, it has been shown that erosive burning characteristics themselves for a given propellant do not scale well. Erosive burning was found to diminish in severity with increasing size of motor.[64]

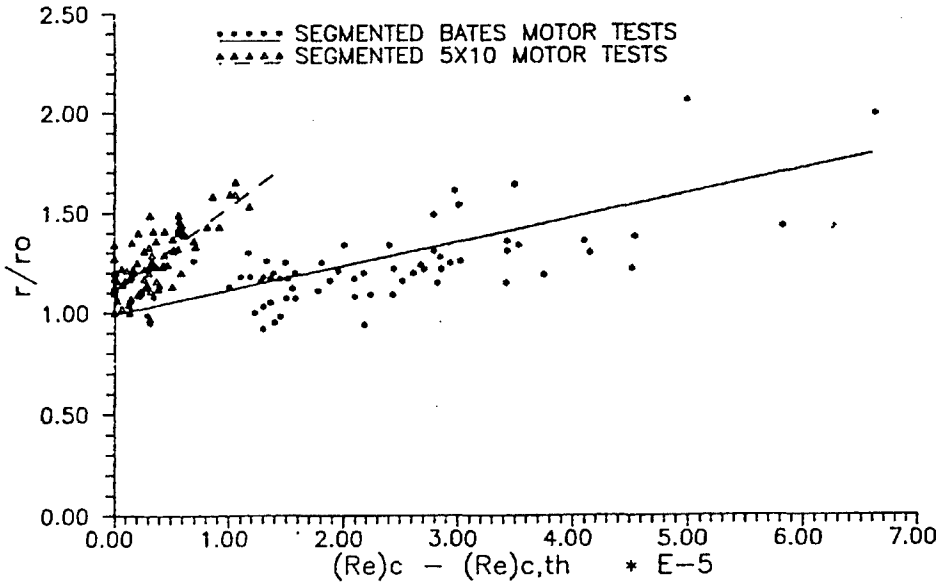

Figure 18. Burning Rate Augmentation versus {Measured Re_c – Theoretical Re_c.} for Segmented BATES and Segmented 5x10 Tests[64]

3.2.1.4 Rheology of Grain Manufacturing Process

The techniques used to manufacture a propellant grain or sample can affect its burning rate. It has been shown that solid particle orientation established during the casting process can significantly alter the burning rate[65] for cast composite propellants.

The manufacturing process is the most important contributor to the hump effect as well as being an important contributor to scale factor. Consider for example a cylindrical grain 203 mm OD X 327 mm L cast from the same HTPB propellant mix using three different manufacturing processes: plunged mandrel, rotated cast-in-place mandrel, and 3-point cast-in-place mandrel. Curves of pressure versus time and burning rate versus web thickness reveal significant influences of the grain manufacturing process, as shown in the Figure 19 and 20 below. The nozzle throat diameter and conditioning temperature were selected in order to fire the small motors at the same test conditions. The curves shown represent replicated tests to confirm the P-t behavior.

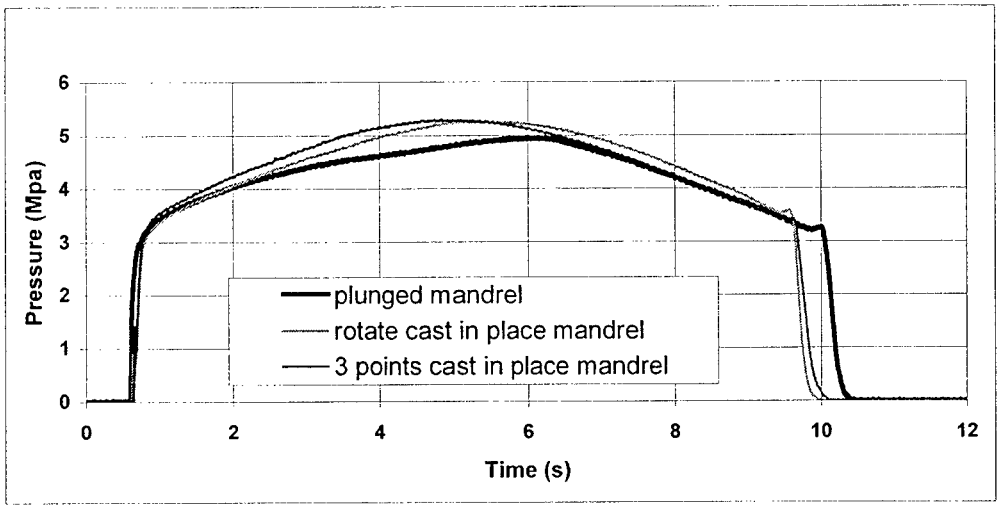

Figure 19. Influence of Grain Manufacturing Process on Motor Burning Rate on Motor P-t Behavior[62]

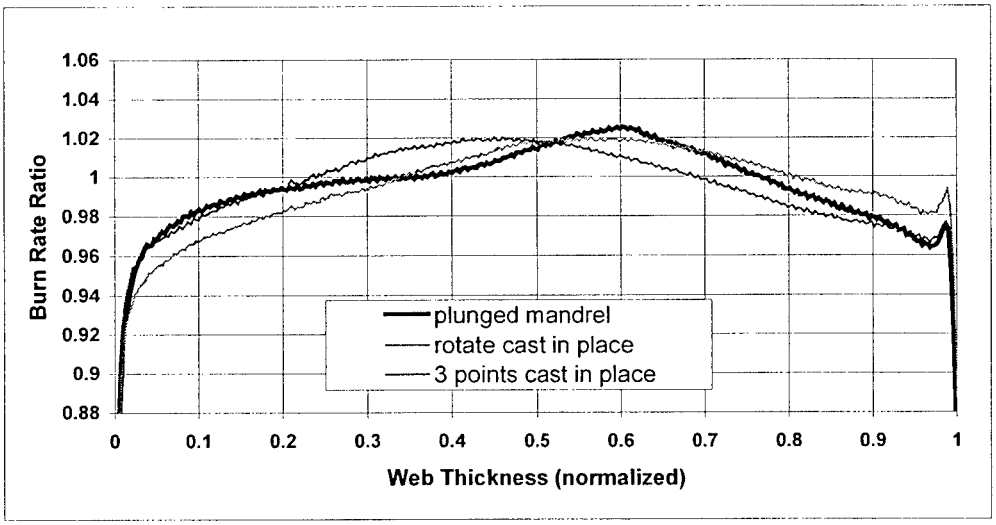

Figure 20. Influence of Grain Manufacturing Process on Motor Burning Rate Versus Web Thickness Behavior[62]

The hump behavior found in the middle of pressure-time and web thickness burn traces, as shown in these figures is commonly referred to as the "hump", "rainbow effect" or "burn rate anomaly factor" (BARF) curve[66]. The most visibly obvious features of a "hump" curve are pressure overshoot on ignition, mid-pressure trace hump or s-curve, and pressure spike near burnout commonly referred to as Friedman Curl (or Uncurl for a negative pressure spike). "Hump" is also believed by some to be influenced by the general change in trace shape due to the difference between the real deformed propellant surface area versus the undeformed area usually used in predictions, as discussed previously. This approach introduced the concept of addressing the hump issue as the ratio of the MB burning rate to the TOT burning rate, used by some in their burning rate analysis methods.[1,4]

It is generally accepted that the "hump" effect is related to the grain casting process. A hypothesis of the manufacturing process effect in cast composite propellant grains may be revealed from the arrangement of Ammonium Perchlorate crystals. Ammonium Perchlorate becomes orientated in the direction of flow during casting. This in turn introduces some anisotropy with respect to burning rate. Scale up problems arise if the flow patterns of the uncured propellant during casting are appreciably different in the large-scale motor compared to the subscale motor. Figure 21 illustrates the effects of the propellant grain manufacturing process on burning rate ratio versus web burned for 5-inch CP grains with 3-inch bore, 9-inch length.[67] Plunge casting does appear to reduce formulation gradients, reducing the midrun hump. Changing from casting in a cartridge to casting directly into a motor case also appears to reduce the hump effects.

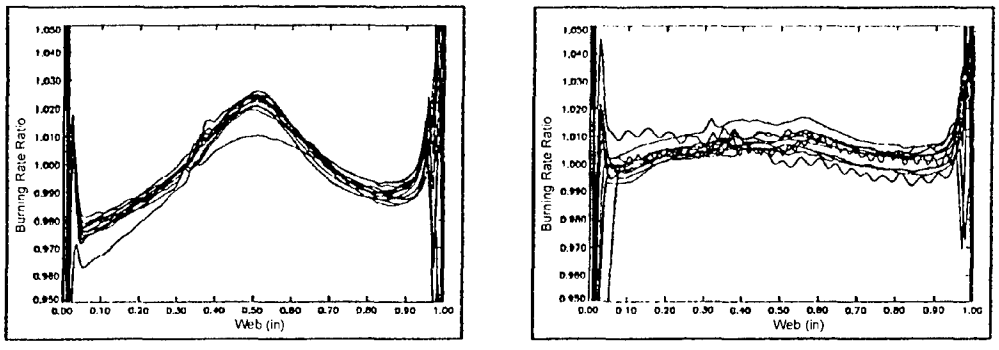

5C3-9 Plunge Cast

5C3-9 Cast with Mandrel in Place

Figure 21. "Hump" Curves for 5-inch CP Grain with 3-inch Bore, 9 inch Length[67]

Variations in grain casting methods and non-isotropic surface burn-back analysis can be used to simulate variations in the manufacturing process effect on scale factor and hump effect. Several methods can be used to calculate the manufacturing process effect on firing prediction. The most accurate method consists of modeling anisotropic burning rate behavior.[68]

Hump effect is also related to the manufacturing process and propellant formulation. It is now widely admitted that different stresses occurring during manufacturing processes, induce separation of the solid particles and changes in propellant composition which in turn leads to burning rate variations as a function of location in the grain, and relative angle of incidence between flame front and sheared lines or surfaces.[69,70,71]

In the cases illustrated in Figures 19 and 20, the difference in the calculated burning rate between the plunged mandrel grain and the cast-in-place mandrel grain is 3.2%, corresponding to 50% of observed average scale factor. Hence, it is apparent the manufacturing process can have a strong influence on scale factor and hump effect.

Motors whose grains are cast with the mandrel in place experience radial variations in burning rate across the propellant web that can influence burning rate bias on the order of 4.5% according to Watson et. al. Figure 21 shows "hump" curves produced in 12 5C3-9 motors cast with the mandrel in place compared with 12 5C3-9 motors from the same propellant batch where the mandrel was plunged into the propellant after casting. In these cases the "hump" produced a motor average burning rate bias of approximately 2.8% compared to the plunge cast grain. Atlantic Research (with 6C4-11.3) and Aerojet (with 5C3-9) have both demonstrated plunge casting can essentially eliminate the "hump" phenomenon.

The hump effect is also influenced by grain design characteristics. For example, the burning rate versus web thickness behavior can exhibit significant differences. Figures 22 and 23 show the difference between a finocyl grain design and a cylindrical port grain design.

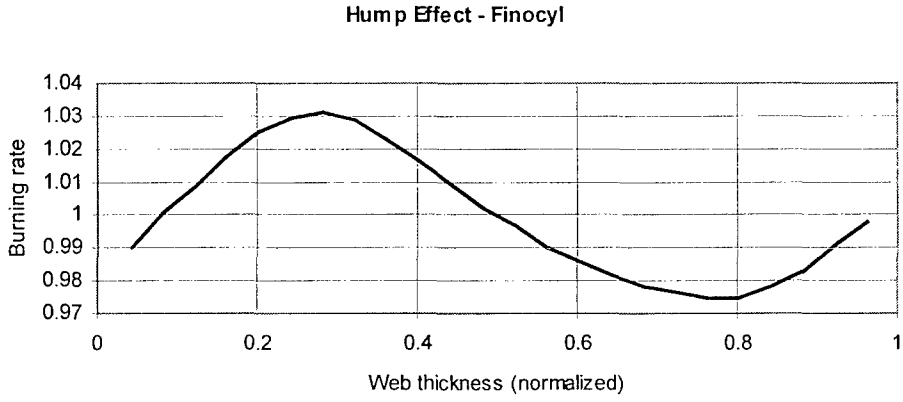

Figure 22. Burning Rate versus Web Displaying Hump Effect for an SNPE Finocyl Grain Design[62]

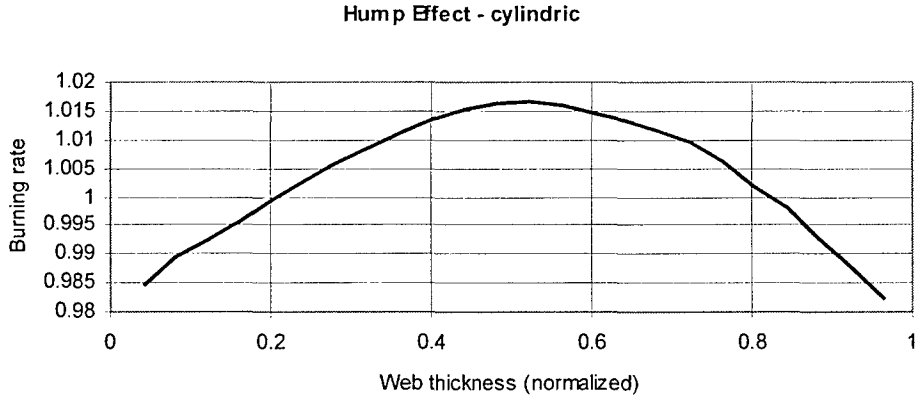

Figure 23. Burning Rate versus Web Displaying Hump Effect for an SNPE CP Grain Design[62]

3.2.2 Other Contributing Parameters

Other parameters influence the correlation of subscale and full-scale motor performance. However, industry experience suggests these parameters have a secondary effect on scaling behavior as discussed below.

3.2.2.1 Propellant Combustion Stability

Any unstable combustion (linked to acoustic or non-acoustic pressure waves that propagate up and down the motor chamber) may also increase burning rates in motors. Motor stability fundamentals and

implications to motor hardware design were discussed previously in Section 2.3.2. To improve confidence in scaling performance, experimental methods must minimize the occurrence of combustion instability and detect instability should it occur.

3.2.2.2 Radiation

Radiation plays a significant part in the energy balance at the burning surface and can affect burning rate. Principal sources of radiant energy are from the reaction of gaseous products, continuum radiation from hot particles and from hot internal linings. Blair et al.[71] showed radiation effects accounted for a portion of the observed differences in burning rates between cured strands and small motors. The effect of radiation on the propellant burning rate is not significant except for relatively small motor bore diameters. As the bore diameter is increased, the radiation gas - Al_2O_3 particle system approaches black body radiation. Figure 24 illustrates that the port diameter above which the motor cavity radiates as a black body is about 10 inches (25 cm) for a typical aluminized propellant. Increasing motor port diameter above this value should have little or no effect on propellant burning rate.

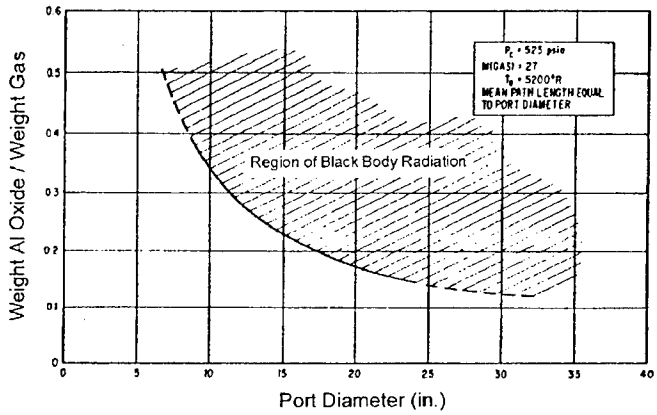

Figure 24. Path Length Required of an Al_2O_3 Particle Cloud To Produce Black Body Radiation[71]

3.2.2.3 Propellant Composition at the Propellant-Liner Interface

The propellant composition influences burning rate through the manufacturing process effect. The rheology of propellant flow near a wall creates a nonuniform distribution of propellant constituents. The effect on the propellant composition is a local composition modification at the propellant-liner interface, which generally induces a local increase in burning rate.

3.2.2.4 Propellant – Insulation Interface

Case insulation may affect burning rate by controlling heat loss at the propellant-insulation interface by local modification of the burning rate at the interface. This latter effect is controlled by the propellant stress state in some cases, by migration of chemical constituents into the insulation, or by modification of the thermal feedback to the propellant.

Differences in heat loss at the insulation interfaces may also account for some variation in burning rate when scaling up. Some of the smaller motors and devices such as strand burners are often robust in construction being designed for re-use with a minimum of refurbishment. Consequently they tend not to have high performance internal insulation, but rather thick sections to exposed metal components, which give rise to heat loss from combustion gases.

3.2.2.5 Thermoelastic Coupling

When a solid propellant undergoes rapid strain, for instance during ignition, heat is generated in the propellant, which can modify the burning rate where the local strain occurs. Propellant compressibility effects are included in this parameter.

The usual approach to the analysis of thermal effects in the burning of solid propellants involves the application of the energy equation in the general one-dimensional form. No provision is made in this form for volumetric heat release or absorption within the solid phase. It is known, however, that the rate of deformation of a material (propellant in this case) influences the energy balance.[72] The energy equation is appropriately modified for this effect for isotropic elastic solids to include a term representing thermoelastic coupling and containing a factor, ε, that represents the time rate of change of the summation of the strain rates along three orthogonal directions at the point under consideration. Because the ordinary composite propellant exhibits a high degree of incompressibility the volumetric rate of change is not very high and the magnitude of this thermoelastic coupling term is highly dependent on the local temperature, which in general is high only near the burning surface where ε will also have its highest value because of the effect of the thermal strain. The thermoelastic coupling term is insignificant under most circumstances for typical surface temperatures and burning rates. Closer examination reveals the thermoelastic coupling term may be quite significant at relatively low pressures or during transient operation when the strain rate is relatively large.[73] A 1-D analysis indicates the temperature difference (with and without the coupling term) within the heat-affected zone of a solid propellant can be approximately 1-3% as illustrated in Figure 25. Thermoelastic coupling may produce significant changes in the solid phase temperature distribution within a solid propellant during highly transient conditions of operation. The width of the heat-affected zone may also be modified slightly because of the coupling. These changes will alter the heat transfer from the combustion zone and thus change the burning rate of the propellant.

3.2.2.6 Nozzle Design

The rocket motor internal flow field velocities are dependent upon the nozzle throat cross sectional area. This is particularly so for radially burning center-perforated grains where flow velocity within the grain increases with throat area, which influences the burning rate as previously described in Section 3.2.1 relative to principal parameters.

3.2.2.7 Acceleration

Acceleration can affect the internal flow field of a rocket motor and so influence burning rate or can set up a stress state in the grain and so affect burning rate. High spin rates tend to impart a centrifugal force on particulate matter such as droplets of unburned aluminum or alumna, which tends to hold them on the burning surface of radial burners. Both axial and spin acceleration have a similar effect of burning rate augmentation, which can be influenced by motor scale.

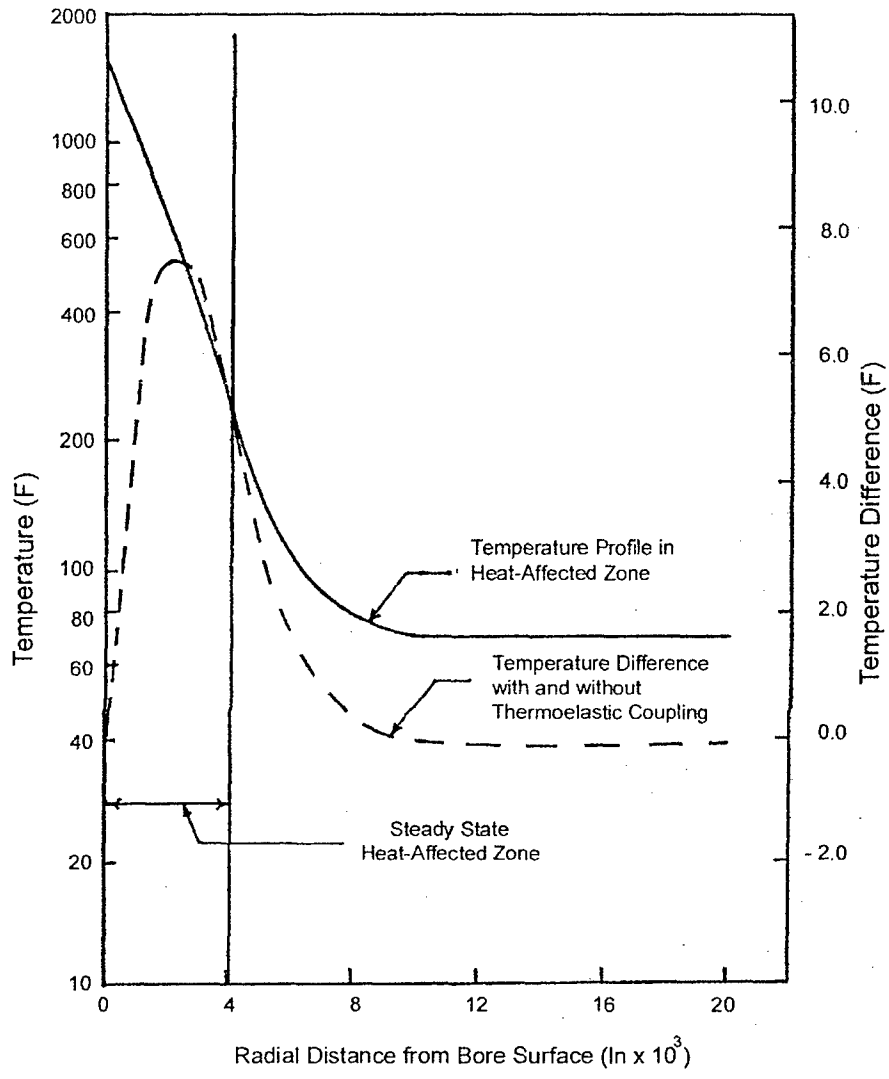

Figure 25. Influence of Thermoelastic Coupling within the Heat-Affected Zone of a Solid Propellant[73]

4.0 PRACTICAL ISSUES INFLUENCING SCALING OF MEASUREMENT METHODS

Devices and current industry practices for commonly measuring burning rate were reviewed in Section 2.4. The influence these devices have upon scaling will vary in proportion to the effect exhibited by the controlling factors previously reviewed. These influences are reviewed here for the more commonly used devices.

4.1 Strand Burner

4.1.1 Solid Strand Burning Rate

The utility of the strand burner technique for the motor designer depends on how closely it approximates propellant combustion environment in a motor, and how important any differences are. The formalization of the strand burning concept of direct propellant burning rate measurement is usually attributed to

Crawford et al as reviewed in Section 2.4.1.4. The central requirement of the strand burning method is that strands must burn one-dimensionally.

The diameter of propellant is known to influence both the burning rate and the burning stability[74]. Strands generally exhibit a critical combustion diameter (d_{cr}), below which burning will not be possible, or will not remain steady without an augmenting energy source. This is primarily a thermal effect, which for homogenous propellants is usually significant for burning near atmospheric pressure. The width of a typical strand is very small compared with the width of the propellant in a motor, so much lateral heat loss can occur in strand burning whereas heat flow from the combustion zone of a motor is essentially one-dimensional. Figure 26 illustrates these differences[75]. For most substances the critical diameter is inversely proportional to pressure. However, it was also shown that burning rates begin to decrease rapidly for values of the strand diameter below $2d_{cr}$, and can still show increases at diameters above $2d_{cr}$. As a result, the pressure dependence of the burning rate is stronger for a sample with a smaller diameter than a larger diameter. For double base compositions burning at elevated pressures, commonly used strand diameters on the order of 6 mm (0.25 inch) or larger are usually acceptable.

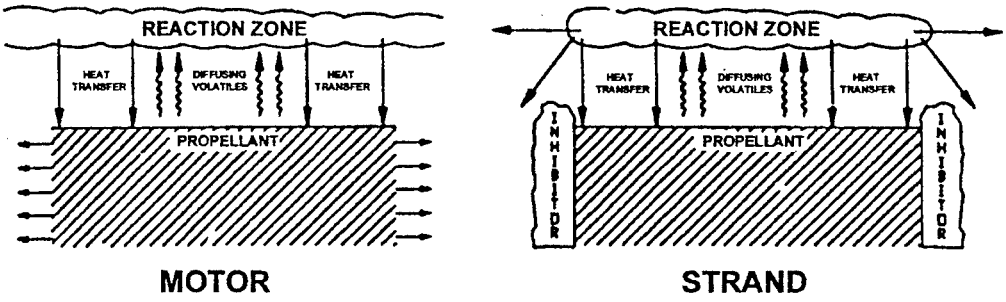

Figure 26. Comparison of Motor and Strand Combustion Environments[75]

If the lateral heat is significant in comparison with the heat transferred to the propellant surface during the burning time, the burning rate will likely be retarded. If the propellant burning rate is high compared to the lateral heat gradient this effect is minimized. In some tests this lateral heat transfer can be significant. In the case of HTPB/AP with no burning rate catalyst strands of 4 x 4 mm cross-section extinguished. Methods used to mitigate these effects include wrapping the strand with an insulating material, increasing the cross-section or size of the strand, or by raising the precombustion temperature of the propellant in the strand. This lateral heat transfer does not appear to have a significant effect with HTPB/AP propellants with burning-rate catalyst. This may be the result of a higher burning rate.

There is a related effect of strand diameter on the appearance of the secondary luminous flame. As the strand diameter is reduced, the pressure at which the luminous flame first appears increases. Therefore, any radiant heat transfer that might occur from the luminous flame is also shifted to higher pressure for smaller samples. It was also noted that flame species concentrations are affected by the reduction in strand size.[75]

Thus in research applications where solid propellant strands are burned at lower pressures, for example, in order to spatially resolve the multistage flame structure, caution must be exercised regarding the critical diameter effects on both burning rate and flame structure measurements.

Adequate characterization of strand sample burning rate should also account for a flame zone flow field that might deviate from one-dimensionality. This may be accomplished by one of two means depending upon the type of strand burner used. Additional synchronized fields of view of high-speed or rapid scanning instrumentation may be used, or alternatively, additional sensors may be used to detect optical losses and adjust the positioning controls. The latter means uses a mobile burner floor to maintain the burning surface of the strand within the field of view of the recording instruments, as discussed in Section

2.4.1.4. A key issue of this strand burner control process that appears in most studies is the manner in which optical losses within the pressure chamber affect the positioning process. A constant correction factor may be acceptable, for the case where the burning environment is reasonably stable during combustion at a fixed set of conditions.

Factors that can increase strand burning rate are generally traced to sample preparation methods. These can include non-linear burning (due to inadequate inhibition on the sides of the strand), strand damage (due to cracks or voids in the propellant surface caused by slicing), or variations in ingredient distribution (due to propellant processing). Procedures can be developed to minimize or eliminate the effects of these factors as a source of variations when comparing two strand tests.

For the purposes of scaling, the strand burner technique seeks to approximate the propellant combustion environment in a motor. The factors mentioned will have varying effects depending on the differences in the geometries of the devices being compared. Strand and motor burning rates should be different. If they are not, then either the factors that caused the combustion environments to differ are not important, or less likely, their influences just happened to offset each other.

The strand burner is a simple, fast, cost effective and accurate tool for measuring propellant burning rates. The strand burner has an advantage of decoupling measured burning rate from other phenomena present in the motor for independent study. This advantage is important during the development of new formulations or for some phases of quality and process control. Burning rate values and temperature sensitivity measured with the strand burner have been reported as nearly the same as those measured in subscale motors. The decoupling feature, while an advantage on one hand is the same source for doubt in predicting full-scale motor performance. The lack of radiative, cross-flow conditions contributes to this assessment. This method is effective for early indications of burning rate and in applications allowing a relatively wide acceptance tolerance with real motor conditions. However, a correlation between strands and subscale motors should be developed in order to determine if the controlling factors are important and at what magnitude they affect burning rates. This is especially important if an attempt is made to use strand burning rates to predict full-scale motor performance.

The Parrs[76] have recently demonstrated the taut wire method, a new strand burning technique. In this technique the burning surface is held in a fixed position by a taut, refractory material fiber and a sensitive length detector (e.g., linear potentiometer, or LVDT) determines its motion (driven by a constant force spring). This robust and inexpensive servo-positioner technique provides three new functions: (i) continuous burning rate measurement, (ii) opportunity for concurrent direct burning rate difference measurements (reference motion to other strand), and (iii) concurrent burning surface temperature measurement (make the taut fiber a resistance thermometer or thermocouple). It should be noted that all three functions can be executed simultaneously.

4.1.2 Uncured Strand Burning Rate

Early in the development of large solid propellant motors it became apparent that multi-batch motors would require a method of determining burning rate before the propellant was cast in the motor. Since the test was to be conducted rapidly, a method of casting uncured propellant into long slender tubes was devised. As increases in solids loading of the propellant took place, vacuum casting of strands gave way to pressure casting.

The original intent of the data obtained from uncured strands was that of process control, which has been extended to prediction of full-scale motor performance as will be discussed in Section 6.6. This has been successful to various degrees, and depends on the effort spent in developing correlation coefficients. This requires a great number of strand and subscale motor tests as well as full-scale tests be made early in a program. Additionally, a consistent effort must be maintained to keep the coefficient database current by additional test and analysis. Uncured strand test yield precise and reproducible data. However, the tests cannot be relied upon to relate accurately to motor rates for all propellant systems.

An important phenomenon to mention in uncured burning rate work is the burning rate gradient. Experimental tests establish the existence of this phenomenon in most propellant types and it is considered inherent to the strand casting process of flowing propellant through long slender tubes. The propellant that travels the greatest distance in the tube usually exhibits the highest solids loading and the highest burning rate. Factors contributing to this phenomenon include particle classification, oxidizer orientation, and attrition of the oxidizer during extrusion.

Crawford Bomb testing of uncured liquid strands creates challenges in the analysis and interpretation of a test. Figure 27 is a typical closed bomb test result plotted as dP/dT versus P, illustrating the characteristics of the particular phases of the closed bomb burning.[77] This plot combined with inflection points along the pressure-time curve seeks to provide such information as initiation of the igniter charge, propellant ignition, flame spreading along the propellant surface, flame penetration, main charge burning, and any variations in propellant composition. The process can be complex, leaving much to interpretation, contributing to experimental uncertainty.

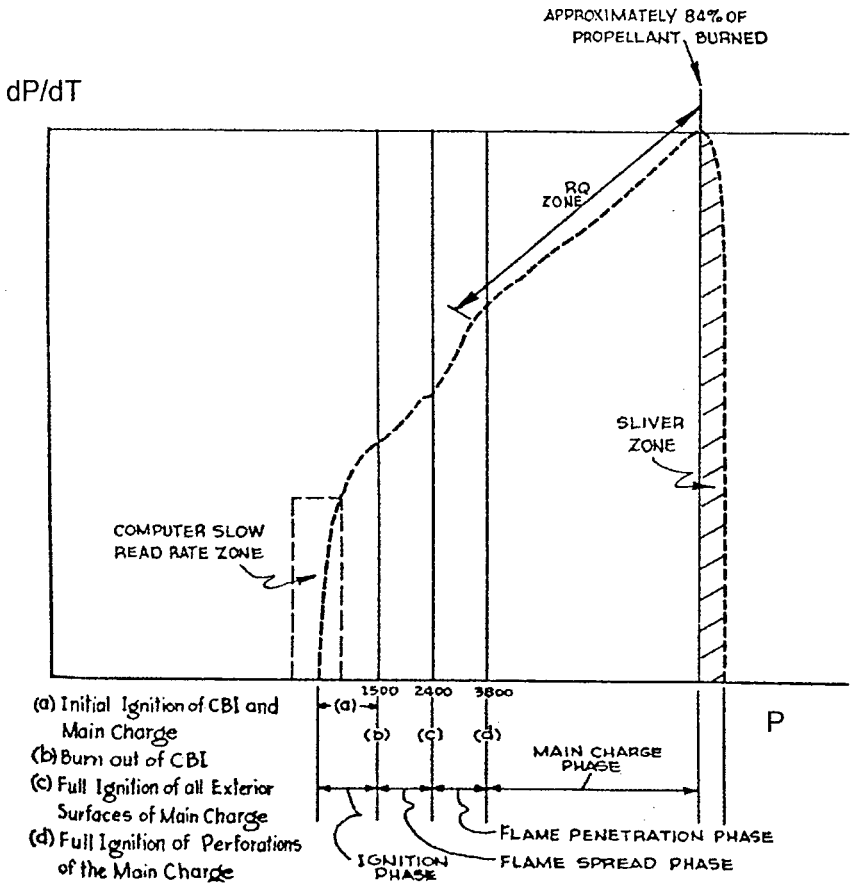

Figure 27. Typical Crawford Bomb Test Result Illustrating Phases of Propellant Burning[77]

4.2 Subscale Test Motor

The heat flow from the combustion zone of a subscale motor more closely approximates the propellant combustion environment in a full-scale motor. This contributes to the improved accuracy of the subscale motor burning rates over strand burner techniques.

Factors that can increase motor burning rate over those witnessed in strand burning include cross flow velocities, unstable combustion and cracks or voids in the grain. These factors have varying effects depending on the geometry of the motor, which can explain differences in calculated burning rates between subscale and full-scale motors.

A number of small-grain-test (<450 gm) configurations have been explored for propellant development and process control with the purpose of reducing development cost and time. Estimates of costs between strand tests, small-grain-tests, and subscale motor tests may be on the order of 1:3.4:100. This ratio may vary between facilities. Small grain test methods combined with strand and subscale motor tests provides propellant development chemists and quality assurance engineers a balanced, economical and timely approach. Some countries and facilities are using some attractive alternatives.[1,5]

Early work on burning rate scale factor was primarily concerned with the differences in burning rate between strands and small motors. With the advent of liquid strands, that permitted rapid process control, there was a great deal of effort to determine the correlation between these rates and subscale motor rates. The gross correlations were always satisfactory. However, the data dispersion about the correlation line could be relatively large, since changes in propellant composition (within propellant specifications) had different effects on the burning rate in the strands and motors. Thus, plots of motor rates versus liquid strand rates may show either very good or very poor correlation depending upon the propellant ingredient causing the burning rate shifts.

The Design of Experiments (DOE) method may be used to reduce the resources necessary to identify essential dependencies with fewer iterations of the test/design cycle.[78,79,80] These dependencies often cannot be fully predicted beforehand. This is one reason why DOE is used in these studies. Many rapid design/analysis tools exist for these applications, allowing the entire design process to be iterated in a timely manner.[81] These methods may be used to partially offset the perceived statistical advantages of strand burner test methods. The DOE method uses statistical techniques to build polynomial approximation models for the functional relationships between output responses (performance characteristics) and input design variables (propellant characteristics). The parametric model is then used to determine the effect of design variables on the output responses and to predict the best design variable values to optimize the performance characteristics. It is also assumed that the fitted surface is an adequate representation of the true response function within the range of the variables examined. Statistical confidence decreases rapidly outside these limits.

4.3 Full-Scale Test Motor

Deducing a burning rate from a full-scale motor test presents challenges that contribute to measurement uncertainties. Major events occurring during a typical ballistic motor firing are shown in Figure 28.[82] The overall observation is that the general "haystack" trace shape makes it difficult to define a meaningful web burning time or representative average pressure. These observations suggest that one must deduce a rate versus pressure relationship rather than an average burning rate from each test. Furthermore, instantaneous (dynamic) burning rate may be significantly different from the steady-state burning rate at each pressure. Therefore, to deduce burning rate it is obvious that one must understand the interaction phenomena occurring during motor operation. In addition, the complexity of the problem suggests that an iterative procedure is necessary for burning rate determination.

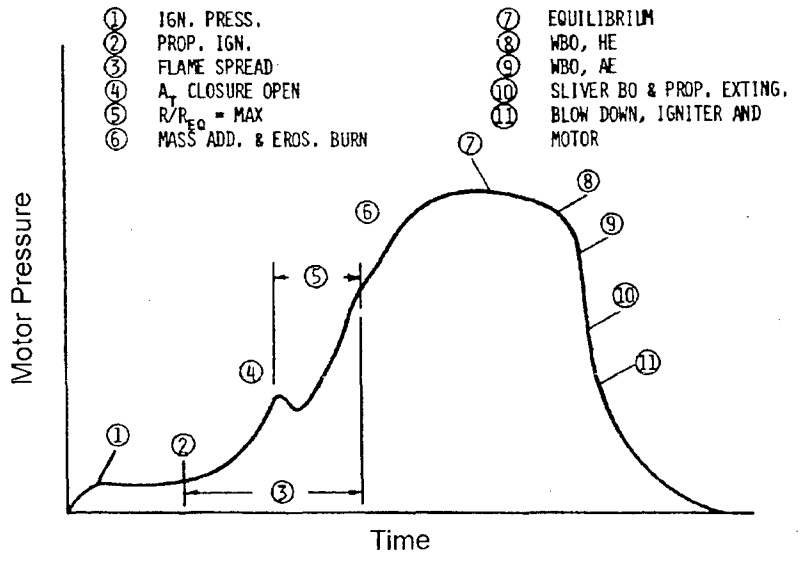

Figure 28. Events During a Typical Test Motor Operation[82]

Eleven distinct events may occur during motor operation beginning with igniter pressurization (1), heating exposure and spot propellant ignition (2), flame spreading across the propellant surface (3), followed by blowout of a motor throat-area closure used for more rapid ignition (4), followed by a period of maximum dynamic burning effects (5), followed by a period of pronounced mass addition effects (total pressure loss due to the introduction of radial momentum to port flow) and erosive burning effects (6). If equilibrium does occur in the motor, its duration is near P_{Max} for a short period of time (7), followed by web burnout of the motor in the head- (8) and aft-end (9). The time lapse between these two events depends on the burning rate differences between the head- and aft-end (caused by mass addition pressure differential), erosive burning influences, and core misalignment (manufacturing) tolerance build-ups. Finally, sliver burnout occurs in the motor (10), followed by possible propellant extinguishments from dynamic burning associated with rapid depressurization of a low L* motor, and vented vessel blow down of the motor (11). The transient events described here typically occur to some degree in all motor tests. The significance of each event, with respect to data analysis, depends on details of the particular design.

Motors differ significantly in the ratio of burning surface to exposed inert surface. Standard subscale test motors tend to have an excessive amount of inert surface through which heat losses can occur compared to the exposed inert surface of full-scale motors. Chamber gas residence times are relatively short because of the low L* values characteristic of subscale motors. Additionally, standard subscale test motors generally contain a larger nozzle heat sink, contributing to considerable heat losses. These heat losses can be accounted for if the motor wall temperature remains relatively constant during motor operation, and if one understands the loss mechanism.

Selection of the burning rate for a large motor that is to be compared to either a subscale motor or strand data contributes to uncertainty in the scaling process, and is not always an obviously clear process. In earlier days most of the large research motors fired were unique, often did not receive detailed ballistic analysis, and thus an average burning rate was selected. Even in development programs, detailed ballistic analysis is often ceased before motor qualification and production. The best-fit ballistic analysis of the average of qualification or production motors would not necessarily result in the same burning rate constants as obtained earlier in the development program. One problem encountered because of these situations is correction of burning rates to standard pressures and temperatures is usually based on burning rate exponents, n, and temperature coefficients π_k, determined by strand or small motor data early in the program.

The average burning rate is usually calculated using tangent-bisector, thickness-time methods, which are influenced by the individual analysts experience. The design web thickness is routinely used instead of the actual web thickness because the bore is not customarily measured after cure to determine an actual distance burned. Determination of the actual burning time (web action time) is accompanied by typical uncertainty unless the ignition and tail-off are unusually distinct, as discussed in Chapter 4. The average burning rate is then related to the average head end chamber pressure, where the average is taken over the burning time (web action time) selected. One may introduce several errors in relating the average head end chamber pressure and the foregoing defined average burning rate to subscale device rate. The full-scale motor pressure-time trace is generally not neutral; consequently, average $\{P^n\}$ is not equal to $\{\text{average } P\}^n$, which introduces a small error.[83] The average full-scale motor rate is generally not corrected for erosive burning. The average head end chamber pressure is not corrected for the pressure drop along the grain. Therefore the derived burning rate-pressure relationship may be incorrect. These problems in selecting a full-scale propellant burning rate become less significant after one finds that the propellant burning rate is a function of the distance burned. Burning has been found to be significantly lower near the beginning and end of the web than in the middle. A typical example is shown in Figure 29 for a 156-inch diameter motor, which indicates the variation in burning rate scale factor that would have been required to match the observed pressure-time curve. Similar phenomena have been observed with 120-inch and 260-inch diameter motors, but to a lower magnitude on the 120-inch motor. Discussions of this phenomenon with industry indicate that it may be present in motors with webs as low as 2.5 cm (1 inch). It is clear that, if the phenomena vary appreciably from motor to motor and remain unexplained, it will be difficult to predict the burning rate of large motors very accurately.

A number of early scale factor studies have indicated the full-scale motor burning rate, aside from being influenced by the principal parameters (Section 3.2.1) of grain conditions at firing and grain processing, depends on two major effects: (1) the inherent burning rate of the propellant, and (2) a scale factor that depends on the variable used to control the burning rate. An example of the latter point based on U.S. experiences with acoustic emission methods is discussed in Section 7.1.1.

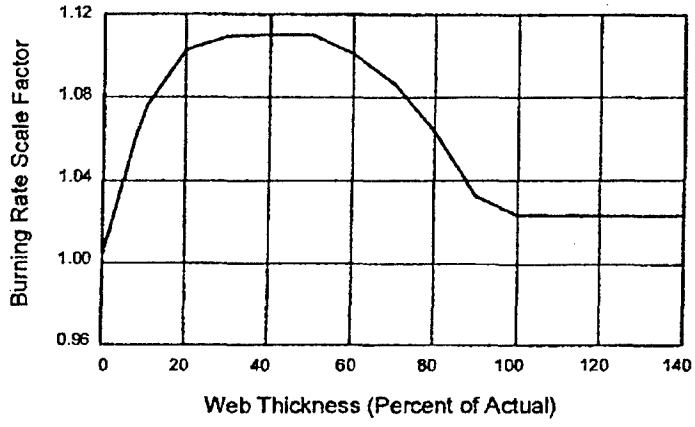

Figure 29. Burning Rate Scale Factor Variation with Web for a 156-inch Diameter Motor[82]

5.0 INDUSTRY PERFORMANCE CORRELATION PRACTICES

Accuracy of solid rocket thrust-time prediction is becoming increasingly more important in solid rocket design. One of the most significant variables in this prediction is the propellant burning rate. Accuracy of this value depends on empirical methods for calculating burning rate from subscale motor tests and for correlating this rate with predictions derived from full-scale motor tests. General methods of correlation and description of industry scaling approaches are discussed in the following paragraphs.

5.1 Propellant Burning Rate Correlation

Burning rate is a necessary input variable to solid rocket performance prediction. In most performance prediction programs this value, which represents the propellant's true reference rate, is the only input variable that cannot be calculated or estimated with significant accuracy; therefore, it must be obtained by experimental methods. Burning rate can be determined analytically using present combustion models, but in general these values are used only to indicate trends and are not intended to have the accuracy required in performance predictions. To predict thrust to an accuracy of ±3%, using SPP for example, burning rate should be known to within ±1%, because this variation will result in a thrust variation of 1.5 – 2%. A burning rate variation of > ±1% would allow little or no tolerance for other input variables.

Propellant burning rates are typically measured in subscale test devices such as small ballistic motors and strand bombs as reviewed earlier. Use of the strand bomb is perhaps more straight forward than subscale motors, but for reasons noted earlier the strand bomb is not considered the most accurate subscale test device for correlating scale effects. The subscale test device most often used is a small test motor, usually 3.8 – 13 cm (1.5 – 5 inch) in diameter. An average burning rate is evaluated using methods discussed earlier, whose accuracy depends on the neutrality of pressure-time curve and other factors discussed earlier.

Average burning rates frequently are measured in a similar manner for full-scale motors. These values of course reflect augmentation from erosive burning if present, neutrality of the pressure-time curve, analysis method used and other factors associated with full-scale motor operation as previously discussed. Figure 30 illustrates representative performance prediction methodology used to correlate subscale motor burning rate with full-scale motor behavior.[84] The input value of measured propellant burning rate used in this process is based on a definition for burn time duration. This duration is intended to mean the time interval consistent with web and total propellant consumption (for a sliverless grain).

The methods of applying the burning rate to performance prediction are important for consistent burning rate correlation. If one were, for example, trying to determine the propellant burning rate by "matching" the predicted thrust-time or pressure-time curve with the actual curve, some judgment might be involved in determining what a "good match" would be. Various combinations of C* and burning rate, for example, might produce predicted performance curves that would appear to correlate with the actual performance. Figure 30 depicts a more analytic approach to correlate burning rate through performance prediction. A unique value of input burning rate is obtained by evaluating an equal number of output and input variables. This is analogous to simultaneous solution of five equations with five unknowns. This illustration using five input variables is not intended to imply that only five variables are necessary. When burning rate is correlated in this manner, the predicted thrust-time and pressure-time curves should then be more highly correlated with the actual curves. Of course this assumes an accurate model of the grain geometry and an accurate performance prediction code. Methods of expressing subscale to full-scale correlations and examples of industry experience base are discussed in subsequent sections.

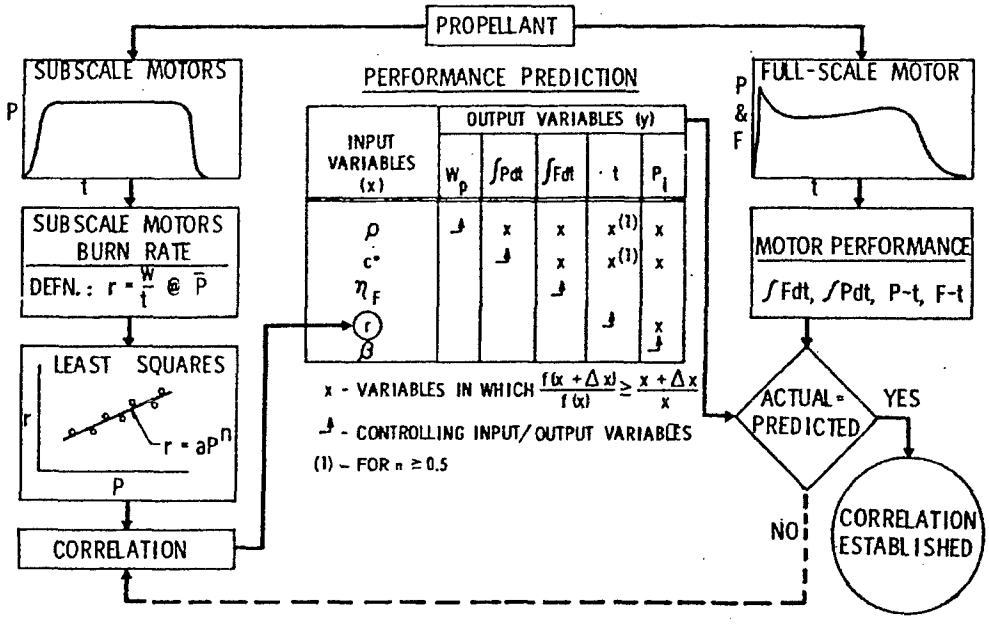

Figure 30. Typical Methodology for Propellant Burning Rate Correlation[84]

5.2 Burning Rate Scale Factor

5.2.1 Early Scale Factor Approach Basics

Scale factor is the ratio of the biased mean results for two different measurement systems (motors of different sizes or designs, or strands) containing nominally the same propellant. As a scale factor reflects error in two different measurement systems, changes in either system will affect scale factor.

What constitutes a "change" or "difference" may be very subtle. For instance, fractional percentage changes in curing agents alter propellant viscosity and bulk modulus appreciably. Viscosity affects flow processes and the resulting formulation gradients. Modulus affects grain deformation and therefore web thickness. Both changes will affect the apparent scale factor. As a result of subtle changes such as these, "scale factor" is not purely a measure of the effect of physical size (scale), but more a measure of uncertainty to define differences between two burning rate measurement systems. Hence, early applications of "scale factor" accounted for these differences in a global manner, without attempting to identify their individual sources.

Changes in scale factor between propellants tested in the same measurement systems sometimes vary on the order of 10% (0.95 to 1.05). However, scale factor is much less variable within some well defined narrow range of formulation for a particular propellant, hence its utility in predicting motors. Scale factor is generally considered a property of the ballistic test motor (BTM) or other subscale test device. Scale factor is a correction that must be applied to get the "right" rate because of various errors in the subscale devices. However, the definition is referenced to the predicted ballistics of the full-scale motor, so some consideration must be given the question of the accuracy of the prediction itself.

The definition above was couched in terms of predicted ballistics because, in the first application, the preliminary designer must guess at what the scale factor will turn out to be when the first full-scale motor is fired. The designed is generally wrong by from 0.5% to as much as 2%. This error is probably a fair measure of the basic accuracy of the mean prediction, assuming the designer's expert guess is exact. Of course, the designer immediately recalculates the required scale factor and pronounces that the scale factor on burning rate (in the BTM) was slightly in error.

It is impossible to directly correlate scale factor and web thickness, without further details as suggested by Figure 31 and 32 from French and US experiences. There are a number of parameters influencing burning rate in subscale and full-scale motors. These parameters may influence scale factor differently, with some of them causing an increase, while others cause a decrease. The SNPE scale factor data shown in Figure 31 can vary on the order of 8% for the composite propellants tested in the same measurement systems.

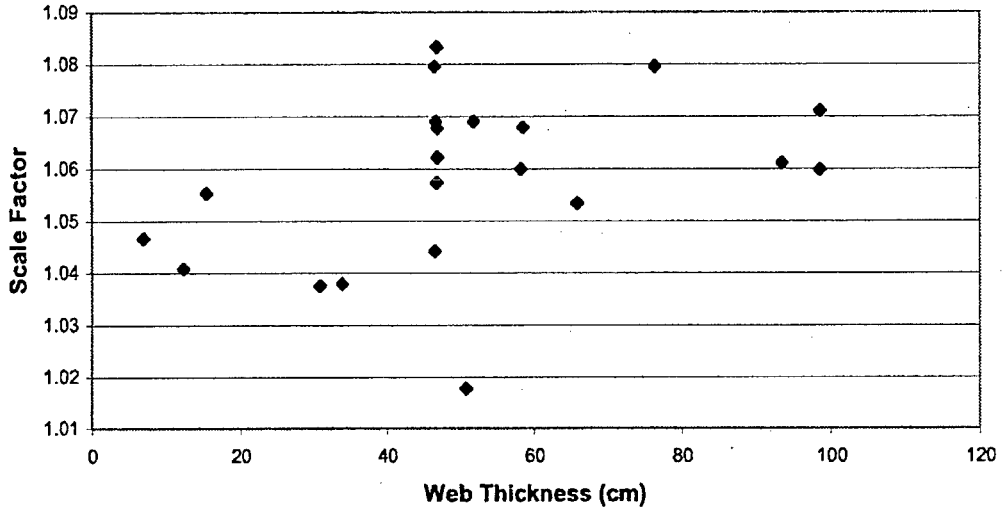

Figure 31. Scale Factor versus Web Thickness for Composite Propellant[62]

Scale-up data is presented in Figure 32 for a number of US solid rocket motors ranging in diameter from 20 inch to 260 inch. The data supporting this figure is discussed further in Section 7.2, Table 5.0. Scale factors shown in Table 5.0 range from 0.996 to 1.128, a variation of 13% for many different motors, development programs and test methods.

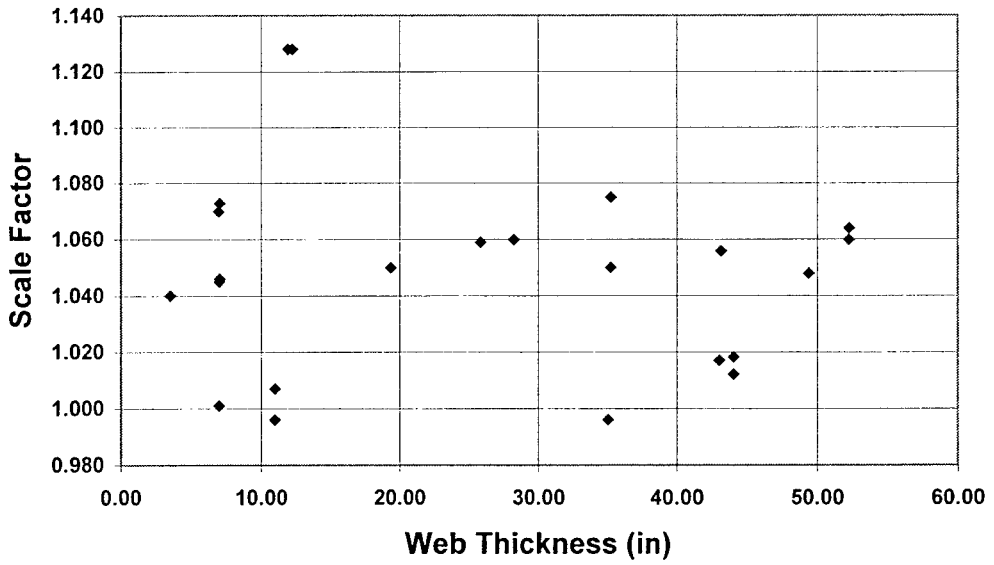

Figure 32. Scale Factor versus Web Thickness for US AP/PBAA and AP/PBAN Propellants and Motor Diameters from 20 inch to 260 inch[82]

5.2.2 Modern Refinements to the Scale Factor Approach

Historically "scale factor" has been a measure of the uncertainty to define the differences in burning rate between a subscale burning rate measurement device or small motor and a larger motor. It was recognized that if the sources of some of these differences could be identified then the resultant uncertainty could be reduced, hence reducing the "scale factor" dispersion.

It is now recognized that scale factor has both steady and non-steady components. The scale factor usually discussed is the steady component, the ratio of the rate required to predict full-scale (FS) motor mean ballistics to the mean rate measured in ballistic test motors (BTM's). The non-steady component is the ratio of the instantaneous rate required to predict instantaneous FS motor ballistics to the mean rate required to predict mean FS motor ballistics. The non-steady component is usually defined, not in time, but in web thickness burned, and is probably best known as the "hump" curve, previously discussed.

While the "hump" effect is generally accepted as being due to the manufacturing process, it should be subdivided into a grain deformation effect and a transient motor effect. The ignition peak and the Curl/UnCurl (see previous discussion on grain rheology in Section 3.2) are transient motor phenomena not directly related to the grain thickness burned. The "hump" effect is both pressure- and temperature-dependent due to grain deformation and transient motor components.

Since it is difficult to anticipate a "hump" curve, predicting overall "hump" curve behavior is generally not attempted. However, selected elements of the problem may be analyzed. Every prediction technique usually has the capability to predict erosive burning and mass addition effects from an erosive burning model or a database. Additionally, an ignition pressure peak is usually predicted. When one compares the preliminary prediction to the first motor firing, it is not unusual for the instantaneous pressure to be off 5-10%, sometimes 15%. One reason is that the data in databases confound erosive rate and end effects or formulation gradients. Resolving differences of this order are worth pursuit in the future.

There are two deficiencies in SPP, and probably other predictions, which contribute a significant fraction of the general scale factor problem.

1. Predictions often do not include grain deformation from either shrinkage or pressurization strain.
2. Predictions often do not consider end effect transients.

Grain deformation must be separately modeled, since the SPP does not do it automatically.[85] Modeling the grain deformation can run from easy to almost impossible depending on the grain design. Most if not all users do not model the deformed grain. The SIG code accepts an FEM mesh so the modeling of the deformed grain is relatively easy. Large motor experience indicates this effect is on the same order as the other poorly known quantities. Rheology effects seem to be more important than deformation effects.

All versions of SPP V7 grain design and ballistics account for start up and tail off transients with questionable and limited success, using a pressure derivative approach. It would seem ballisticians have accumulated other errors in the tail off, which dominate for most motors. We suspect that end effects, while they are nominally "hump" effects, also alter the apparent mean rate, and thereby the apparent mean scale factor. Resultantly, the slivers must be right to avoid errors in both the apparent mean burning rate and the hump or tail off. In general, there are large deficiencies in the SPP family of models for burning rate. Most motor companies do not measure all of the quantities necessary to even attempt to quantify some of the inputs required for accurate modeling. Ballistic test motor measurements quite often assume the simplest of burning rate models. It is only on mature motors that all of the necessary motor information is available for modeling, and then the companies are generally reluctant to release it.[85]

5.2.3 Thorough Scaling Definition

Full scale SRM burning rate analysis is performed using burning rate deduced from ballistic specimen test firings. A thorough means of predicting full-scale experimental results from theoretical analysis includes introducing two correcting factors:

1. A constant, linear (web independent) correction often called Scale Factor, and
2. A variable, non-linear (web dependent) correction mainly resulting from the manufacturing process. This factor can be referred to as a Global Hump Effect (SNPE), which can be a source of confusion, since several other effects are combined into this factor, or Surface Burn Rate Error, SBRE curve (Thiokol) or Hump curve (Aerojet).

The variable motor scale factors are discussed further in Section 7.3 for French and US industry experiences. For clarity, the scale factor historically referred to is actually a "global scale factor", which seeks to account for the combined effects of both the constant and the variable components.

The application of these factors is illustrated by correlating the subscale motor firing of an SNPE 6300 gm, 29 cm X 16 cm BARIA motor (see Annex A for full description) with full-scale motor prediction. Figure 33 depicts the pressure-time comparison of the BARIA motor firing and full-scale motor prediction prior to making any corrections. A constant correction is the factor deduced by comparing burning time from the theoretical analysis of a full-scale motor with the burning time of subscale ballistic motor, as illustrated in Figure 34. This parameter represents a linear or steady scale effect between subscale motors used to characterize the burning rate of a full-scale motor.

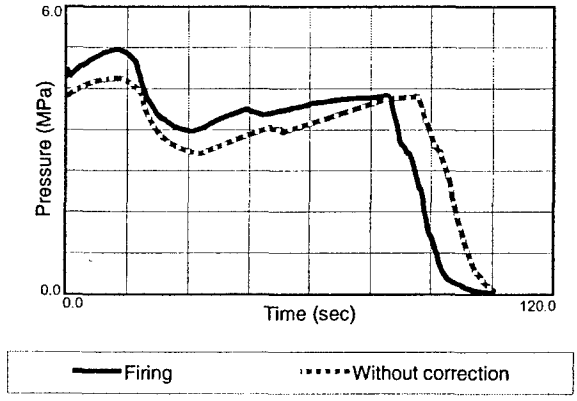

Figure 33. Pressure-Time Comparison of a 6300 gm BARIA Motor Firing and Full-Scale Motor Prediction Without Corrections[62]

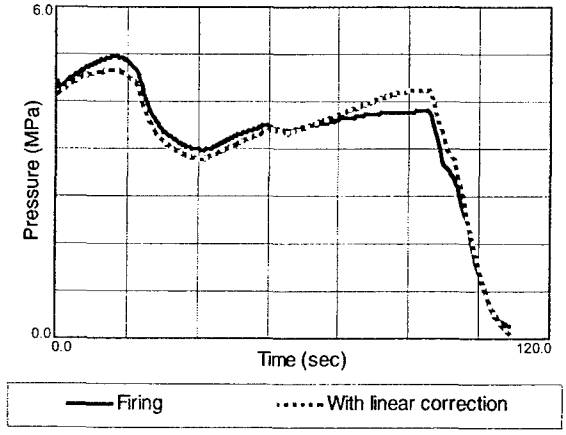

Figure 34. Pressure-Time Comparison of a 6300 gm BARIA Motor Firing and Full-Scale Motor Prediction With a Linear Burning Rate Correction[62]

The non-linear correction is the ratio of {the instantaneous rate required to predict full-scale motor} over {the mean rate of theoretical analysis with scale factor correction}. This ratio is evaluated in the SNPE approach and is a characteristic of the full-scale motor. Figure 35 depicts the pressure-time comparison of the BARIA motor firing and full-scale motor prediction after making both the linear and non-linear corrections.

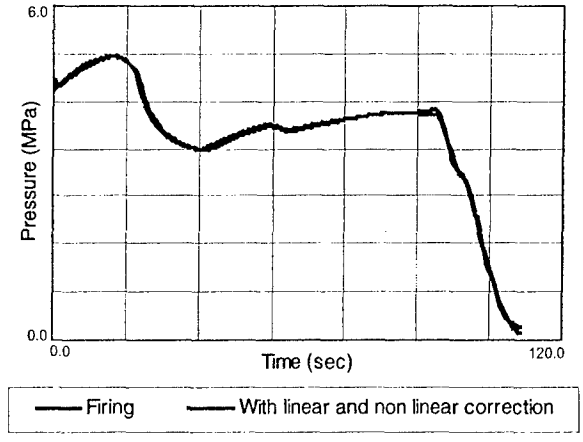

Figure 35. Pressure-Time Comparison of a 6300 gm BARIA Motor Firing and Full-Scale Motor Prediction With Linear and Non-Linear Burning Rate Corrections[62]

As previously discussed, many parameters influence both the linear and non-linear corrections. However, for grain design reasons the influence of both corrections are considered separately as scale factor and global hump effect.

The hump effect generally influences burning rate variation on the order of 10% maximum around the mean value of the burning rate. The hump effect is primarily influenced by grain design characteristics, manufacturing process and propellant formulation as discussed in Section 3.2. Other parameters that can disturb hump effect include grain deformation, thermoelastic coupling, ignition, and the tail-off phase. Some analyses consider these parameters a second order influence, while other analysts have observed stronger influences.

Figure 36 depicts the result on scale factor when important global parameters (Section 3.2) are accounted for in the performance analysis. The dispersion on scale factor is substantially reduced from 13% in Figure 32 with an average scale factor of 1.0450 to a dispersion of 2.6% and an average of 1.0149. This reduction in dispersion was effected by application of a thorough, rigorous and integrated combination of ballistic prediction and testing of full-scale and subscale motors, and cured and liquid strands (as reviewed in Section 7). The full-scale ballistic prediction included the principal effects of real grain geometry at firing (including grain deformation and erosive burning) and grain manufacturing process, as suggested in the ballistic test correlation methodology reviewed earlier in Section 5.

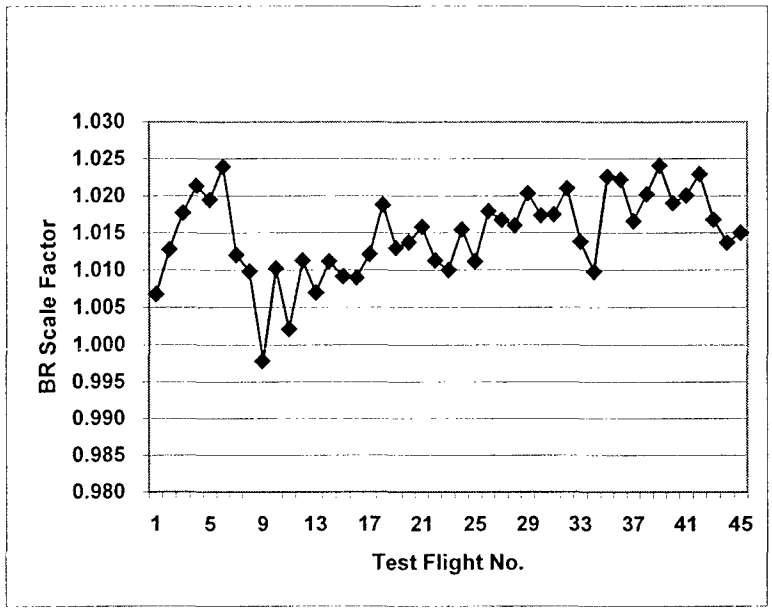

Figure 36. Scale-up Data for Shuttle SRM and RSRM Motors Illustrates Reduction in Scale Factor Possible by Accounting for Global Parameters[61]

6.0 STRAND BURNER-TO-MOTOR BURNING RATE COMPARISON

The strand burner has enjoyed widespread use as a burning rate measurement device. In recent times its use as a tool for predicting full-scale motor performance has become less frequent however. This is due in part to the fundamental problems reviewed in Section 4.1, which include thermal effects associated with sample size, propellant processing and sample preparation, and lack of radiative, cross-flow conditions representative of motor conditions.

A correlation between strands and subscale motors should be developed, as recommended in Section 4.1, in order to determine if the controlling factors are important and at what magnitude they affect burning rates. We shall review industry examples of efforts to define the differences in burning rate between a strand burner, subscale burning rate motor and a larger motor.

6.1 Scaling Challenges - Industry Examples and Results

6.1.1 United States

In the interest of economy, many researchers have relied heavily on strand burners to determine steady-state combustion properties. Considerable disparities can be found between the burning rate results found from strand burners, and those obtained in small motors. The effect of pressure on the burning rate of a typical, uncatalyzed, reduced smoke composite propellant is shown in Figure 37a. This reversed sigmoid curve differs considerably from the popular conception of "normal" response to pressure. As shown in Figure 37b, a normal $\bar{r}_b = a_b \bar{p}^n$ curve (Eqn. 1) is frequently easy to draw if few data points are available. More sophisticated investigators acquire a few more data points, plot two straight lines, and identify the point of the intersection shown in Figure 37c as a "break" in the slope or pressure exponent. The pressure of the "break" has been designated P*.

Figure 38 illustrates[82] disparities between strand burner and small motors. Small motor and strand burning rate versus pressure is plotted for a typical uncatalyzed reduced smoke propellant. The strand burner results are confusing as well as misleading with respect to rate and slope. Additionally, the strand data do not reveal clearly the pressure P* above which conventional motor operation is impossible. Encountering many such disappointing results have encouraged many researchers to avoid the use of strand burners for measuring burning rate for many propellant applications. Developments of novel hardware and test methods have on occasion reduced the cost of testing 2x4-inch motors almost to that of strand testing.

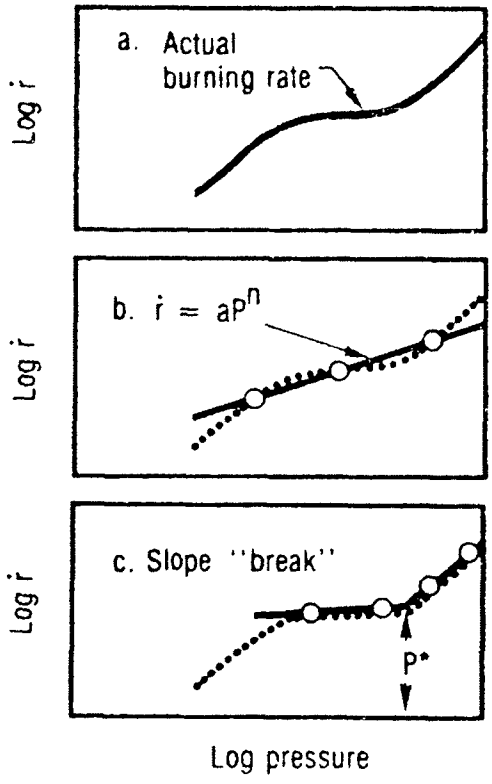

Figure 37. Potential Errors in Defining Burning Rate and Slope[82]

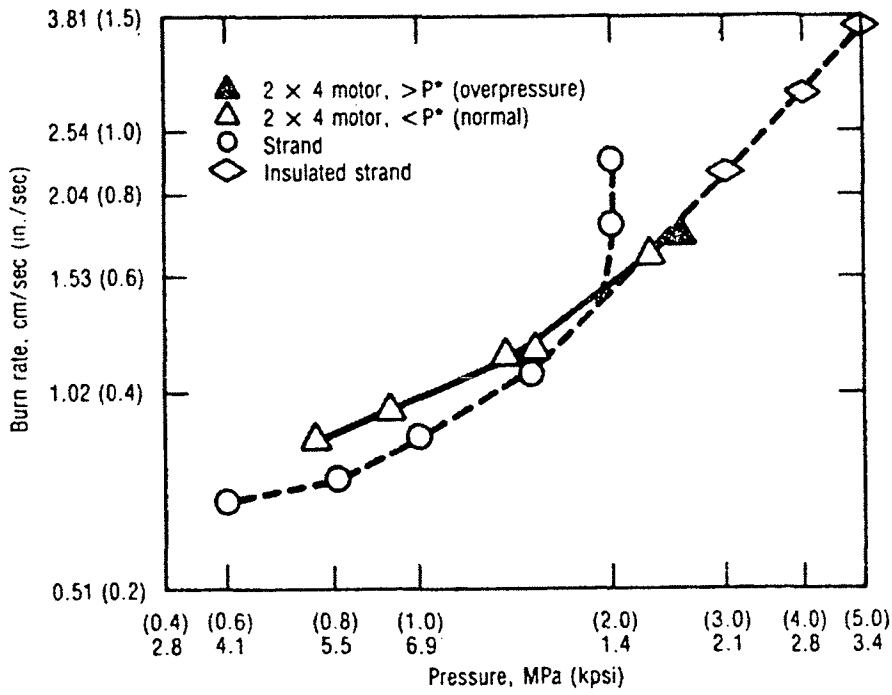

Figure 38. Disagreement of Strand and Small Motor Burning Rates[82]

A review of models and mechanisms for pressure exponent breaks in composite solid propellants must rely heavily upon experimental strand data. Figure 39 is a composite plot of burning rate data from various facilities employing several experimental strand methods. J. Martin and C. Henderson of Atlantic Research developed an empirical correlation of critical r* and P* from pre-1970 data called the "barrier theory" to characterize the pressure exponent break in the deflagration of AP. The pressed strands of AP (solid line and open circles, Figure 39) indicate the break occurs in the deflagration of AP at a critical pressure of about 34 MPa (5000 psia). The pressed strands of AP contained small amounts of fuel material for cohesion and inhibition. Glick[86] expanded this correlation by saying it is not so much a burning rate barrier as it is a region where the AP rate contribution to the overall burning rate becomes dominant over the Summerfield burning rate for solid propellants. Post-1970 data have shed additional light upon the barrier and Glick theories. Glaskova and Bobolev[87] acquired data (solid triangle, Figure 39) using pressed strands without any fuel material present. Boggs[88] acquired data (solid circle, Figure 39) using large single crystals of pure AP. Also, Graham & Larimer[89] acquired additional bare and insulated strand data (solid square and diamond, Figure 39).

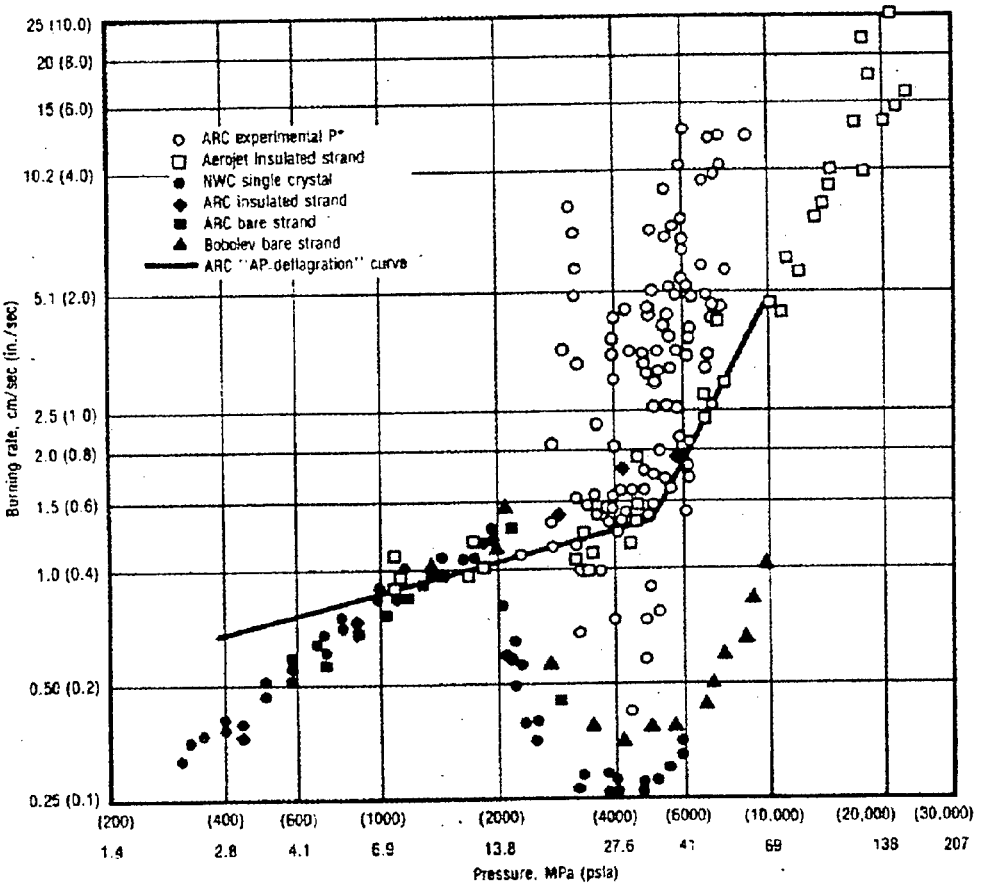

Figure 39. Comparison of Pressure Exponent Break Points for AP Burning Rates Using Different Strand Methods from Various Facilities (Data pre-1970 to 1985)[82]

Using pure AP it was observed that burning rate undergoes a sharp decrease with increasing pressure above 13.8 MPa (2000 psi) before turning upward again above 34 MPa. Glaskova[90] attributed this to a change in the pressure-dependent chemistry. It is interesting that such a small amount of fuel present in the older strands could have made such a difference in the combustion of AP at pressures above 13.8 MPa. The additional post-1970 r*-P* data shown in Figure 38 are further evidence against a definitive relationship between exponent breaks in propellant burning rate and AP deflagration. Subsequent developments suggested the mechanism most directly responsible for the P* pressure exponent break in composite propellants is the change in multiple flame structure from diffusion flame control to AP flame control.[82] This appears to be well described by modern composite propellant combustion models. This effect was masked for years by the strand preparation and test methods used in earlier developments. Care must be exercised in the application of strand techniques, as they can contribute considerable uncertainty to properly characterizing the phenomena of interest.

Comparisons of measured strand burning rates with small motor rates for formulation development of HTPB/AP non-aluminized propellants are illustrated in Figure 40.[82] Illustrated is a comparison of calculated and measured burning rates independent of pressure or composition. It is evident that with a few exceptions the strand rates here are within 95% confidence limits of the model calculation and compared within 2% of the 4500 gm (10 lbm) motor data (with a motor/strand burn rate ratio variation from 0.977 to 1.122). Strand and motor measured temperature sensitivity of burning rate, σ_p, also agreed

well. There were however, unexplained observed differences in the effect of temperature on pressure sensitivity, π_k, between the strand predictions and motor measurements. Strands are not suitable for determining π_k. The temperature coefficient of pressure, π_k, is more easily measured in motors as it is the effect of initial propellant temperature upon motor operating pressure as *Kn* is kept constant. On the other hand, temperature sensitivity, σ_p, a propellant property, is easily measured in a strand burner and therefore can be compared among propellants without the influence of motor geometry. Temperature sensitivity, σ_p, is very difficult to measure with motors because of the difficulty of doing different tests at the same chamber pressure while varying initial propellant temperature. Fortunately, both σ_p and π_k are related through Equation 14 in Section 2.2, but to measure each directly, both strand and motor techniques are needed.

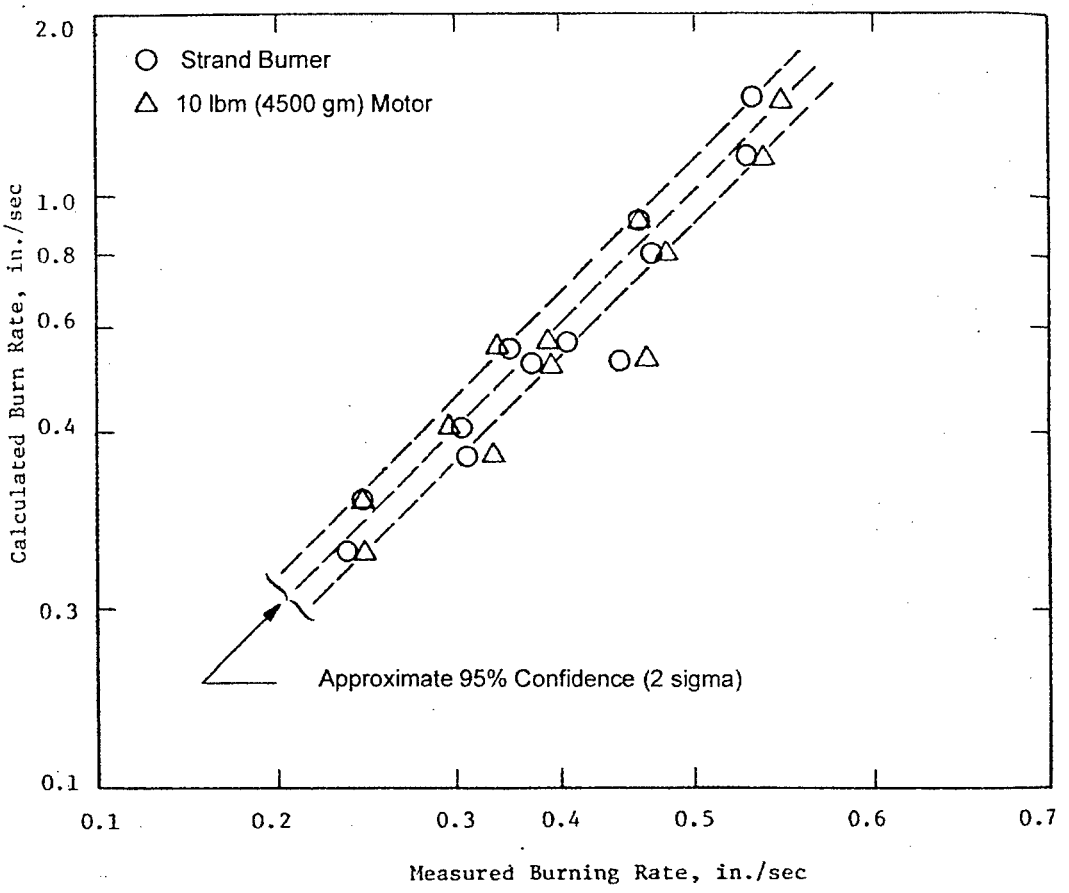

Figure 40. Comparison of Measured and Calculated Strand and Small Motor Burning Rates for Fundamental Studies of HTPB/AP Smokeless Propellants[82]

6.2 Strand Burner-to-Motor Scaling Successes - Industry Examples and Results

6.2.1 Canada

An example of work conducted to successfully measure propellant burning rate for non-aluminized HTPB/AP propellant comes from Canada.[75] They indicate the strand burner is a better tool for measuring the effects of small formulation changes for quality control work. Motor and strand results are displayed in Figure 41. The burning rates at 6.895 MPa (1000 psia) are shown indicating they were within 1.6% of

each other. A statistical analysis was performed to see if the regression lines for motors and strands, below the slope break where viable motors would operate, were significantly different. First, an *F*-test verified that the motor and strand variances were not significantly different at 95% confidence. A first *t*-test verified that the slopes of the motor and strand regression lines were not significantly different, but a second *t*-test failed to show that they were coincident.

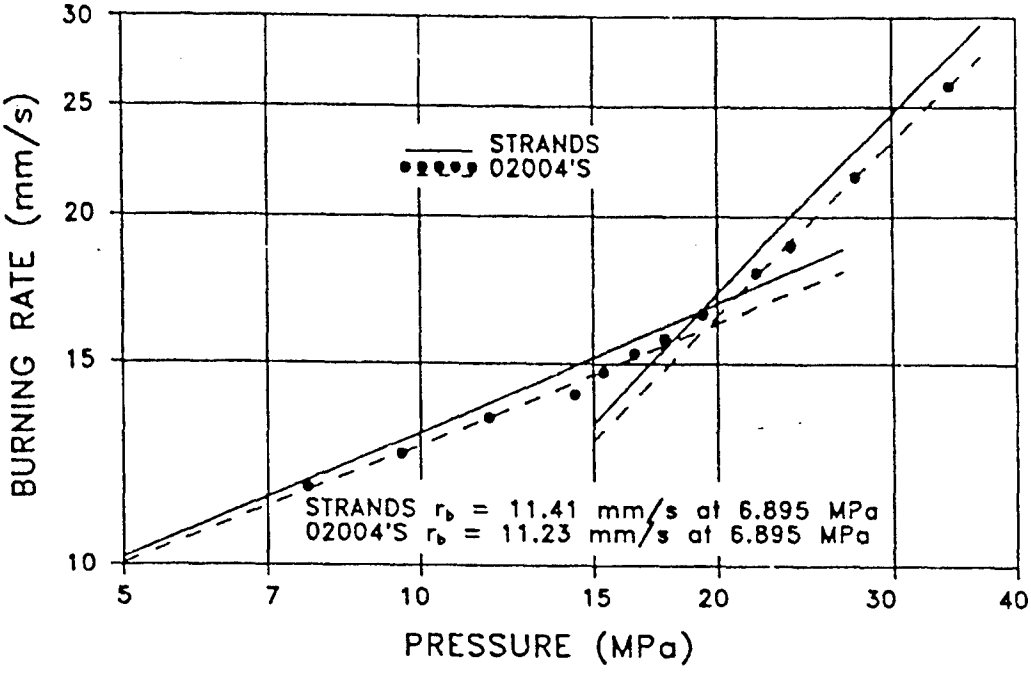

Figure 41. Agreement Between 2x4 Motor and Strand Burning Rate Data for Non-aluminized HTPB/AP Propellant[75]

6.2.2 United States

Limited success using cured propellant strands to measure burning rate by Thiokol prompted the development of alternative methods in the late 1970's. Several variables contribute to reducing the accuracy of cured strand burning rates. Conventional nitrogen methods produce an increase in pressure and temperature inside the combustion chamber during testing. Timing wires and strand inhibitors must also be used.

Koury[91] developed a method for testing strands under water by measuring the burning rate using an acoustic pickup. The acoustic emission (AE) method measures the acoustic emissions in the 100,000 to 300,000 Hz range generated as the propellant strand burns. Figure 42 illustrates the improved discrimination capability of the AE method over traditional strand pressure-time behavior. The AE signal in Figure 42 displays greater sensitivity to burning variances than the pressure signal, superimposed on the same time scale. The strand is burned in a conventional strand combustion bomb, which is filled with a liquid medium. The burning propellant transmits the acoustic signal to sonic pickup mounts on the side of the bomb. The AE work was originally conducted under a NASA contract to determine if the AE method could be used to replace the subscale batch check motors made on each propellant mix cast into the SRM as part of the Space Shuttle Program. Additionally it was of interest to evaluate the effects of sample orientation, position in the propellant loaf, size of propellant strands and uncured (liquid) strands for process control.

The full-scale rocket motor, subscale motor, liquid strand, or cured strands do not generally have the same burning rate at the same pressure. The AE liquid strand was found to have the largest response to changes in iron oxide for instance (Figure 43) as compared to other test devices.[82] This was desirable for process control when iron oxide was one of the weighted ingredients. The reasons for the different burning rates at the same pressures were traced to variables associated with the different methods and different burning rate pressure exponents. It was found possible to obtain a correlation between the AE cured strand, batch check motor and the SRM. The AE liquid strand was used in process control and studies showed that 1,500 psia pressure provided a greater sensitivity to changes in propellant formulations.

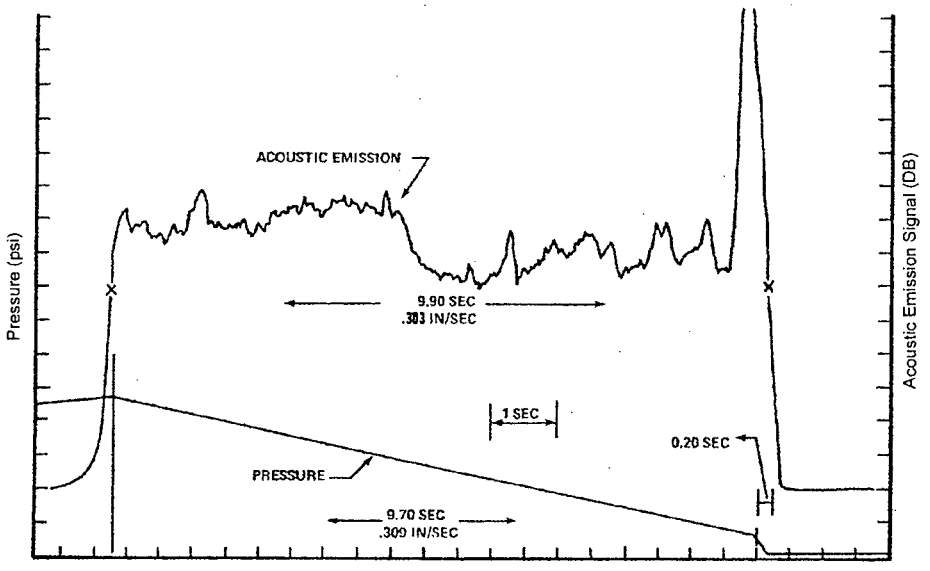

Figure 42. Comparison of Acoustic Emission and Pressure-Time Response[91]

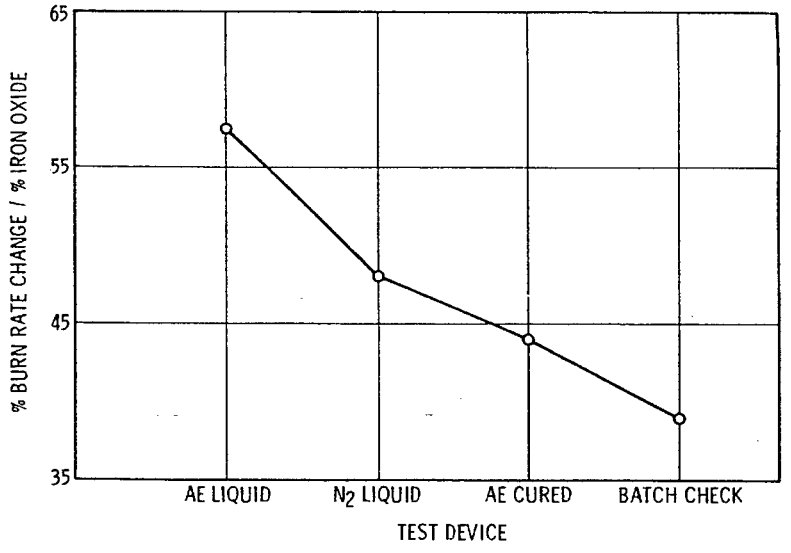

Figure 43. SRM Propellant Burning Rate Response, Ratio of % Average Burning Rate / % Iron Oxide for Different Test Techniques[82]

The oxidizer grind ratio was changed to obtain the desired Shuttle SRM burning rate for DM-1 and DM-2 motor standardizations. The statistical analysis of the AE cured strands and the 5-inch batch check motor versus the change in oxidizer grind ratio for these standardizations is illustrated in Figures 44 and 45. The data illustrates differences between strand and motor, yet it can be seen that the AE cured strands correlated better with percent ground oxidizer. Other data substantiated that the AE cured strand data correlated better statistically than the 5-inch motor data and equal to the AE liquid strand burning rate data. The precision of both cured and liquid strand data was 0.5%.

Herrington[92] studied the correlation of subscale motors and uncured strands for a number of propellant formulations and was able to correlate best by plotting P/r_{Motor} against $P/r_{Liquid\ Strand}$ over a range of pressures. Results indicated the scale factor between liquid strands and subscale motors is affected by burning rate catalyst, but not by the ratio of ground to unground oxidizer, differing from production motor experience.

The acoustic emission method has many advantages over the conventional nitrogen strand burning system. It is a rapid and precise method for measuring burning rates of uncured and cured propellant. The test results correlate well with batch check motors and the AE method can accurately measure the differences in propellant formulations. The cost of testing AE strands is small when compared with other methods.

7.0 COMPARISON OF SUBSCALE DEVICE WITH FULL-SCALE MOTOR BURNING RATE

7.1 Strand Burner Correlations – Industry Examples and Results

7.1.1 Acoustic Emission Method – United States

Solid rocket motor performance predictions are possible by establishing a correlation between full-scale motor performance, small ballistic test motors, liquid strand burning rate tests and/or solid strand burning rate tests. The accuracy of these predictions will be maintained if the correlation between motor performance and any of the subscale test methods remains constant. A shift in the correlation between liquid strand burning rate and large motors was observed on two operational Titan 120-inch motors. Some subtle change in the propellant raw material was suspected to be the cause. An investigation was conducted to re-establish the correlation between full-scale motor performance and the liquid strand burning rate, and to determine the cause of the performance shift. The cause was traced to the AP oxidizer material in a manner similar to that discussed in the previous section related to the AP grind. The program challenge was resolved by re-establishing a constant correlation between full-scale motor performance and the liquid strand burning rate similar to that shown in Figure 43.

A correlation between liquid and solid strand burning rate is typically established if the correlation between the solid strand and ballistic motor burning rates yields a reasonable satisfactory correlation coefficient ($R > 0.7$). In some cases this does not occur and a direct correlation is established only between full-scale motor web action times and solid strand burning rates. In the following example the solid strand burning rate data exhibited good precision and thus such a correlation was established. Figure 46 shows the correlation of 24 full-scale motor web action times versus average solid strand burning rate. The solid strand rates associated with each 120-inch motor were averaged. The average solid strand burning rates were compared to the motor web action time, normalized to 80 F. The correlation (R) of 0.922 with standard error of estimate (Sy) of 0.53% was deemed statistically significant. Since the ballistic prediction program required burning rate as an input, a regression analysis with 120-inch motor burning rate was developed as is shown in Figure 47. For this regression, the web action times were converted to 120-inch motor average burning rates at 550 psi (80 F) using average web thickness, measured average chamber pressure and a burn rate exponent from solid strand data.

In this study, the burning rate reproducibility for tests of cured solid strands was greatly dependent on sample preparation, sample selection, and technique used in determining combustion ignition and burnout. The orientation of solid particles was a significant contributor to the burning rate variability within

cured cartons. Strand burning rates taken between in the horizontal and vertical directions exhibited variability.

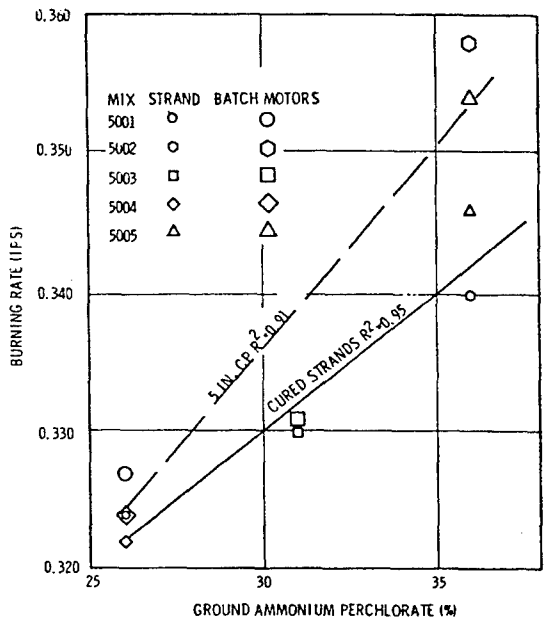

Figure 44. Comparison of Strand and 5-inch Motor Burning Rate Sensitivity to % Grind of AP, Evaluation 991[93]

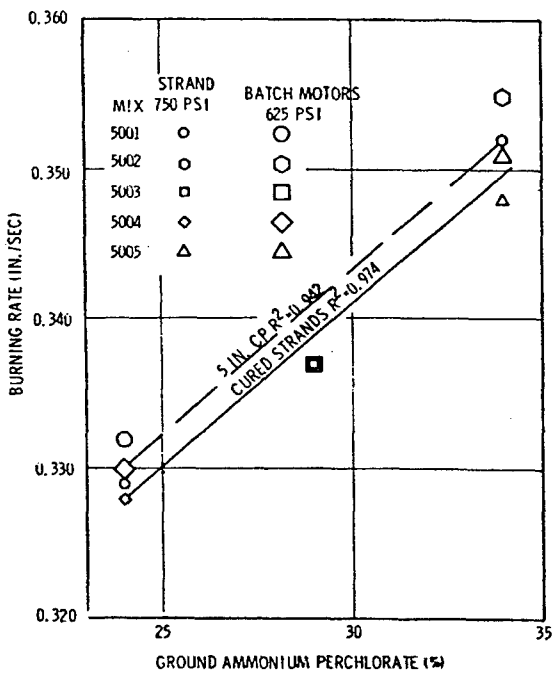

Figure 45. Comparison of Strand and 5-inch Motor Burning Rate Sensitivity to % Grind of AP, Evaluation 997[93]

The use of acoustic emission for measuring the burning rate of cured solid propellant (discussed in Section 6.2.2) was developed in support of the Titan 120-inch motor program. The evaluation between the acoustic emission and other methods showed the acoustic emission method would increase precision and accuracy. By the use of cured propellant strand, the full-scale Titan 120-inch motor could generally be predicted within 1.6%, with a subsequent cost savings over the subscale ballistic test motor on each propellant batch. The results of this study demonstrated the applicability of using the solid strand burning technique for predicting full-scale motor performance.

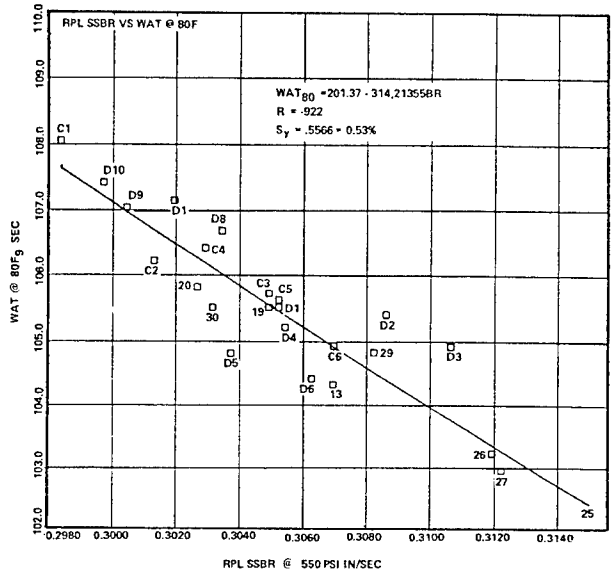

Figure 46. Full-Scale 120-inch Web Action Time versus Solid Strand Burning Rate[91]

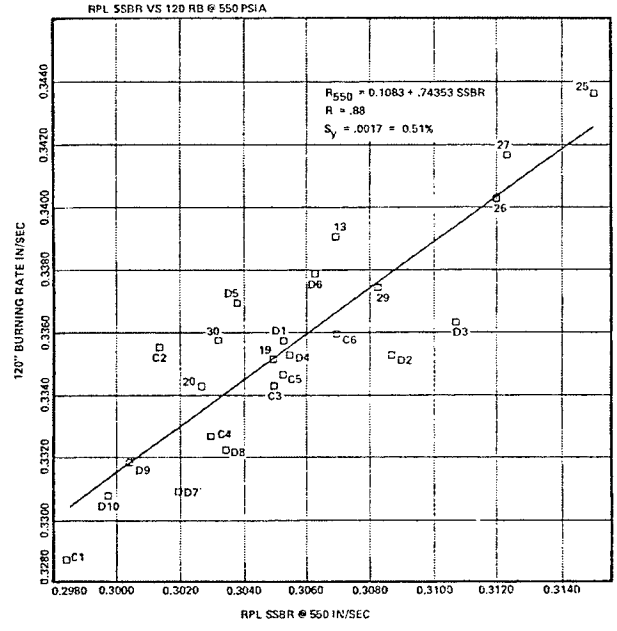

Figure 47. Full-Scale 120-inch Burning Rate versus Solid Strand Burning Rate[91]

NASA contracted Thiokol to determine if the AE strand burning rate method could be used to replace the 5-inch CP ballistic batch check motor used to predict full-scale motor performance for the Shuttle SRM. They showed it possible to obtain a correlation between the AE cured, AE liquid, batch check motor and the SRM.[93] Table 2.0 is an average of the 160 mixes cast into the DM-1 and DM-2. It can be seen that the AE cured strand predicted the SRM burning rate with the same degree of accuracy as the batch check motors. The use of AE cured strand burning rate has been applied to other propellant formulations. It was used on two Trident I (C-4) propellant standardizations, resolving questionable batch check motor data to show that the propellant was satisfactory. It was used to evaluate cross-link double base and high-energy propellants for other development programs. This procedure was also used for the Standard Missile development at high burning rates and pressures up to 31 MPa (4,500 psi). It has also been used on the Minuteman program to evaluate burning rate problems on several mixes.

Table 2. Burning Rate Data Comparison Subscale Device to Full-Scale Shuttle SRM[93]

Test Method	SRM No.	Subscale		Full-Scale SRM r_b (ips)	Scale Factor
		r_b (ips)	$\pm\sigma$ (ips)		
AE Cured r_b	DM-1	0.3443	0.0030	0.3566	1.036
AE Cured r_b	DM-2	0.3440	0.0039	0.3494	1.016
5-inch r_b	DM-1	0.3458	0.0041	0.3566	1.031
5-inch r_b	DM-2	0.3430	0.0035	0.3494	1.019

The burning rate variability within a full-scale motor may be determined by measurement of strand burning rates at known locations in the motor. This is known as burn rate mapping, and is reasonably common in the aerospace industry for full-scale motors. Mappings have been done on a wide variety of full-scale motors, from single batch castings to multiple batch castings. Acoustic emission techniques are often employed in the US for this work. In general, full-scale mappings tend to show that the burning rate is dependent on two parameters; sampling location within the motor and orientation of the sample in the motor. An example of the radial location on burning rate can be seen in Figure 48. A maximum occurs mid-web, with minima near the bore and near the case. This behavior has been seen for a variety of full-scale motors.

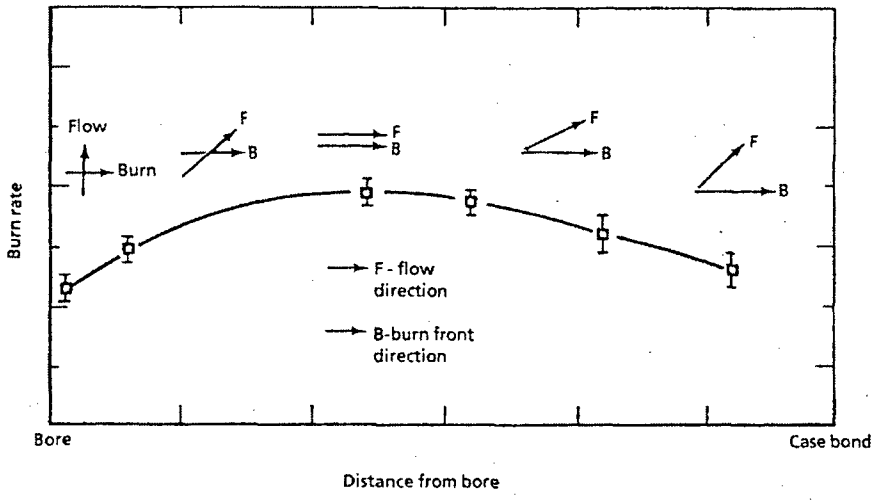

Figure 48. Burning Rate as a Function of Radial Location in a Full-Scale Motor Using Radially Oriented Cured Strands[82]

Currently, the effects of motor location, particularly web (i.e. radial) location, can be predicted by considering the orientation of the burning front with respect to the direction of propellant flow established during casting. Burning rates measured parallel to flow are frequently different from burning rates measured perpendicular to flow. This has been demonstrated at the subscale level by flowing propellant down an incline, cutting cured strands parallel and perpendicular to the flow, and comparing the measured burning rates.

In general, burning rates parallel to flow tend to be higher than burning rates perpendicular to flow. This suggests that if the burning front in a full-scale motor is parallel to flow direction, the burning rate will be higher than when the burning rate is measured perpendicular to the flow. Accounting for the behavior shown in Figure 48 only requires that burning front be perpendicular to flow at the bore, parallel at mid-web, and perpendicular again at the case. Figure 49 shows a sketch of a typical, multiple batch cast, full-scale motor with mix lines and probable flow direction drawn in corresponding to burning rate mapping shown in Figure 48.

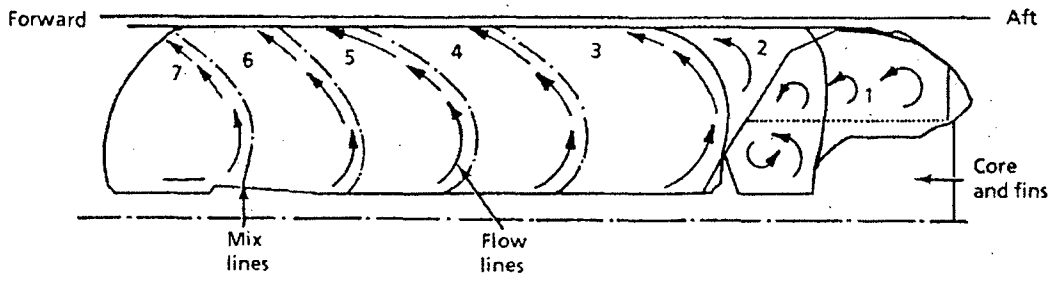

Figure 49. Sketch of Full-Scale Motor with Mix Lines and Probable Flow Lines[82]

This dependence can also be used to explain the second inhomogeneity commonly found in full-scale motor mappings; the dependence of burning rate on sample orientation. The effect of sample orientation is shown very clearly in Figure 50.[94] If at some spot in the motor, a radially oriented burning strand is parallel to flow, then an axially oriented burning strand taken from the same location must necessarily be perpendicular to the flow. This implies that different strand sample orientations will produce different burning rates, even when the motor location is kept constant.

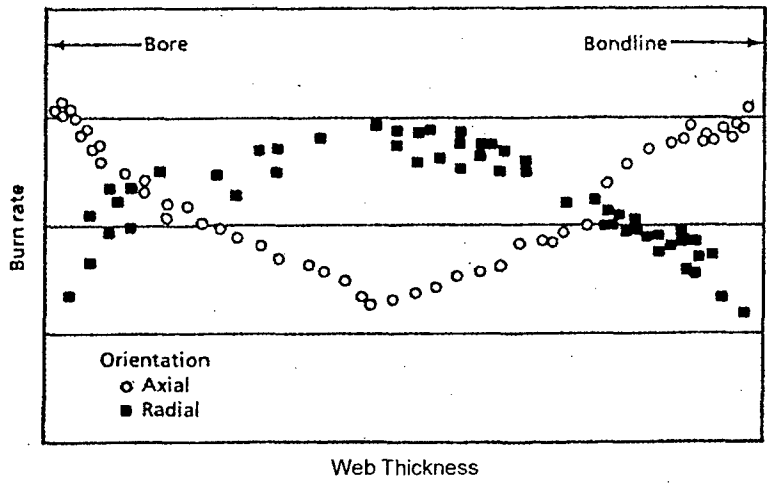

Figure 50. Effects of Radial and Axial Sample Orientation on the Burning Rate, Taken Across the Web of a Full-Scale Motor[94]

Although extensive studies show that burning rate anisotropy can be attributed to propellant flow direction, the actual details of such mechanisms are very unclear. Generally, the propellant is assumed to form 'flow lines', as a result of the casting process. Usually, these flow lines are believed to be the result of particle orientation, e.g. small particles lining up behind bigger particles during shear. Sometimes they are thought to consist of thin streaks of polymer/plasticizer that have demixed and are oriented with the flow as a result of casting. In either case, the current mechanism implies a microstructural inhomogeneity that occurs as the propellant experiences shear flow, particularly down the core.

Representative burning rate variability was characterized for a small ICBM third stage motor with a finocyl design with seven fins. Full-scale firings exhibited a reproducible deviation from predicted ballistic behavior attributed to a burning rate during fin burnout that was about 10-12% above normal. It was determined from mapping that a substantial portion of the burn surface yielded burning in the tangential direction. When the mean difference between radial and tangential burning was added to the highest mean rates observed in the tangential direction, regions were identified in the tangential direction that were 12-13% faster than the radial direction. Thus, the ballistic behavior of the motor was consistent with the measured strand data. The variations were attributed to local variations in propellant composition correlated with the geometry of the casting process.

Full-scale motors are manufactured using a wide variety of casting configurations, such as casting on or off the core, casting on or between fin molds. Casting aft end up or aft end down, single or multiple batch castings, slit plate designs, and so on. A particular configuration is selected for many reasons, including minimizing burning rate anisotropies that result from propellant flow. Burning rate mappings are valuable to means to assess anisotropies caused during casting. In conjunction with a consistent mechanism, burning rate mappings can be used to redesign a casting process, if necessary, to reduce burning rate variations to their lowest possible level.

These effects expand upon the rheology of grain manufacturing as a global parameter influencing scaling as introduced in Section 3.2. Accounting for these effects is sought with the use of a variable scale factor as reviewed in Section 7.3.

7.1.2 Ultrasonic Method – France

SNPE France currently uses the ultrasonic technique for screening and development of propellants for tactical applications. Excellent comparison has been obtained between ultrasonic measurements in strands and pressure-time data for small and large motor firings as presented in Figures 51 and 52. Uncured propellant is tested in Figure 51. The plots illustrate continuous burning rate response to monotonically increasing pressure. The data also suggests a difference in response exists between testing with either increasing or decreasing pressure. The unique advantage of the ultrasonic method is linked to the fact that the number of tests is low (usually two) and that it yields a continuous burning rate, which can be used in ballistic codes.

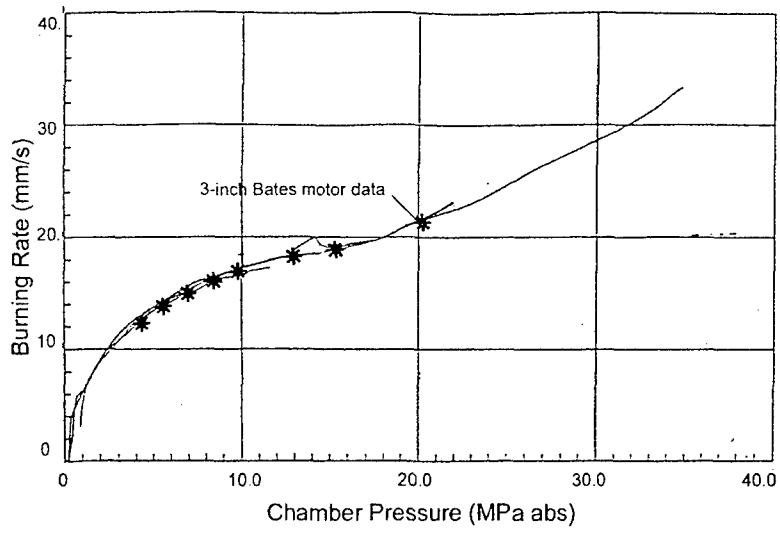

Figure 51. Comparison Between Results Obtained with Ultrasonic Method and Standard Subscale 3-inch Bates Motor Firing[62]

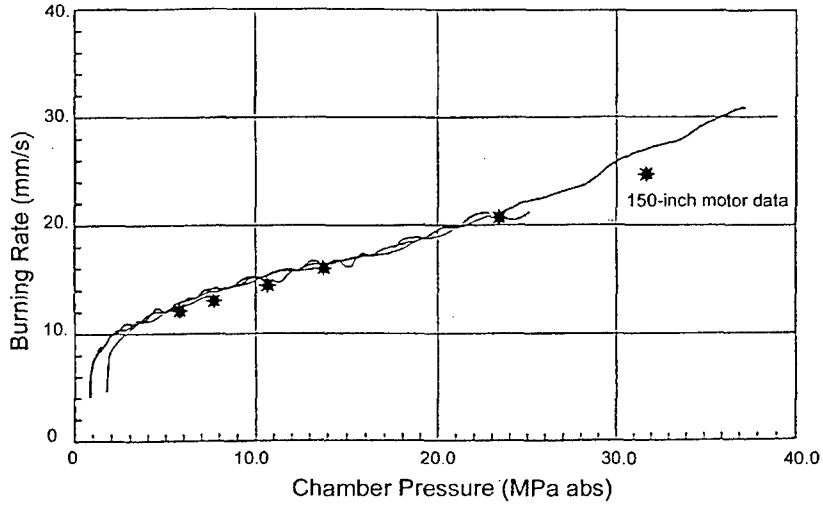

Figure 52. Comparison Between Results Obtained with Ultrasonic Method and Standard Campanule 150-inch Large Scale Motor Firing[62]

7.2 Constant Motor Scale Factor – Industry Examples and Results

7.2.1 Germany

The following Table 3.0 provided by Bayern-Chemie, Germany[95] compares large motor burning rate data with 2-inch SSTM (subscale test motor) data. Motors contain finocyl, wagon wheel, star center perforated and tube-and-rod grain configurations.

Table 3. Scale-up Data Bayern-Chemie, Germany[95]

Motor No.	Motor L / D	Propellant Mass (kg)	Motor r_b (mm/s)	2-inch SSTM r_b (mm/s)	Delta r_b Motor (%)	Scale Factor - Full-Scale /SSTM
1	2	8	40.5	38.4	+ 5.5	1.055
2	10	15	9.8	9.33	+ 5.0	1.050
3	11.5	22	10.5	10.1	+ 3.7	1.040
4	1	24	36.4	34.1	+ 6.7	1.067
5	7	> 300	11.67	11.20	+ 4.2	1.042
6	8	40	42.5	40	+ 6.3	1.063

Data Courtesy of Bayern-Chemie

Bayern-Chemie performs the following steps for the design of a rocket motor:

1. Selection of a propellant
2. Determination of the burning rate of the selected propellant by means of 2-inch subscale test motors (SSTM's)
3. Increase of the burning rate r_b by 5% (r_b + 0.05 r_b)
4. First approximated design of the rocket motor grain
5. Test firing of rocket and 2-inch SSTM's from the same batch. Determination of scaling factor.
6. Final design of the grain using the actual scaling factor.

7.2.2 Italy

The burning rate scale factor is a ballistic parameter considered constant along the web and it is derived (for a given propellant type) from the ratio of the measured burn rate in standard small scale motor and the full-scale motor value obtained by test results analysis code. This discussion and accompanying plots are provided courtesy FIAT AVIO.

The burning rate of the standard small-scale motors (under defined operating conditions) can be calculated using typical methods based on web over time or mass balance, while the burning rate at motor level (under the same defined operating conditions) is extracted by comparing theoretical and experimental pressure-time traces and imposing that a minimum error occurs during tail-off phase.

Applying this approach to Ariane 5 solid boosters, the scale factor of the central and aft segments can be calculated. The results are reported in Figure 53 and Figure 54 and they have been found to correlate well with the reference burning rate (nominally 7 mm/s) under standard small-scale motor tests.
Some observations can be made:

1. All data are obtained with reference to the same motor grain configuration. The grain configuration used in the ballistic code is referred to the "as cast" condition.

2. The scale factor seems to correlate well with the reference burn rate from standard small-scale motors both for the central and aft segments. Data dispersion seems higher for aft segments than the central one.

3. For the central segment, four different motor configurations have been tested: **a)** datum comes from Ariane 5 boosters with a heavy wall case (steel). All remain data are obtained with light wall case (steel). The first group of 5 data named **b)** are obtained considering a first value of burn rate target (at BARIA level). The second group of 13 data named **c)** are obtained increasing the burn rate target by means of ferric oxide. The datum **d)** comes from an Ariane 5 booster having the propellant loaded with HTPB binder by a different supplier.

4. For the aft segment, only three motor configurations have been tested: i.e. **a)**, **b)**, and **c)**.

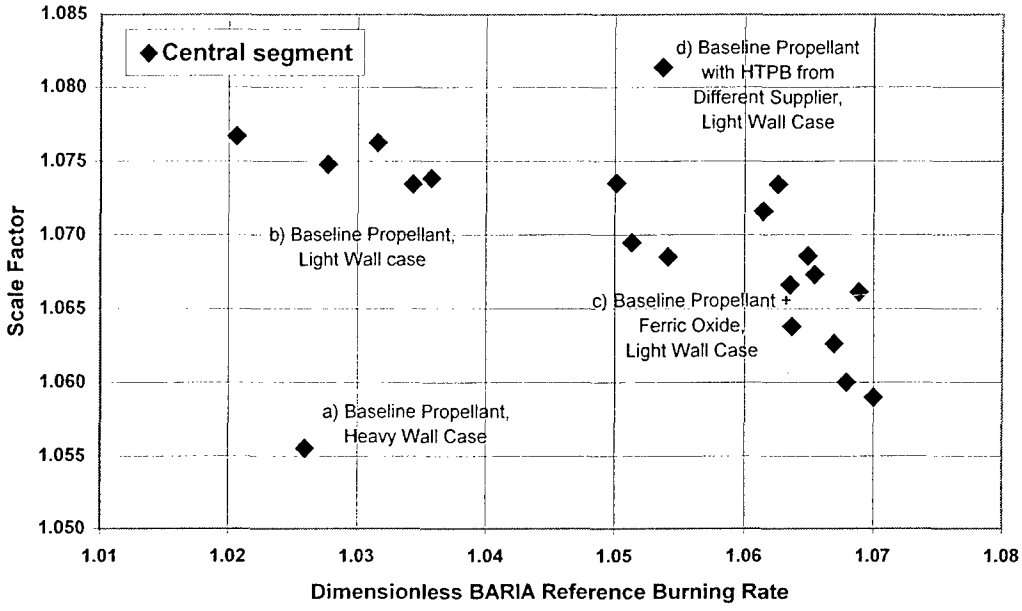

Figure 53. Ariane 5 SRB Test Results Analysis, Central Grain Segment[96]

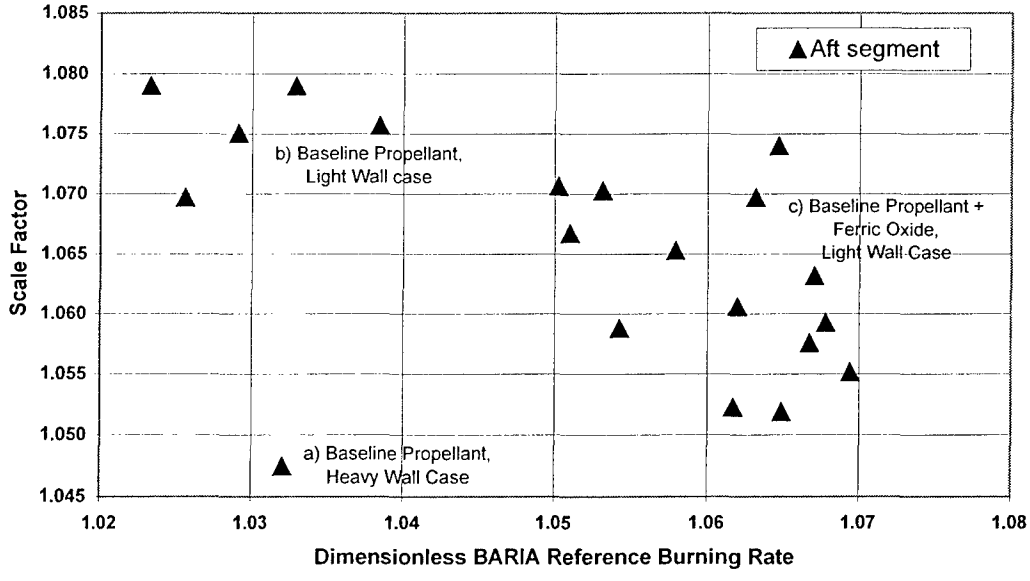

Figure 54. Ariane 5 SRB Test Results Analysis, Aft Grain Segment[96]

7.2.3 United Kingdom

The following Table 4.0 provided by Royal Ordnance Defence Rocket Motors, UK[97] compares 5, 10 and 15 cm diameter motor burning rate data. Motors include uninhibited tubular grains, rectangular uninhibited 61 mm x 20.3 mm x 10.15 mm slab grains, and slotted radial grain designs.

Table 4. Scale-up Data Royal Ordnance Defence Rocket Motors, UK[97]

			Subscale				Large Scale				
Propellant	**Temp (C)**	**Pressure (MPa)**	**Grain**	**Dia (mm)**	**Length (mm)**	**r_b (mm/s)**	**Grain**	**Dia (mm)**	**Length (mm)**	**r_b (mm/s)**	**Scale Factor - BR Ratio**
ADV/19	+20	11.2	T	50	76.2	12.9	SR	152.4	482.6	13.7	1.06
OIO/10	+20	7.23	T	50	76.2	6.8	SR	152.4	462.6	6.93	1.02
ADT/27	+20	4.1	T	50	76.2	5.66	SR	152.4	462.6	6.09	1.08
RIGA	+60	7.0	Slab	10x20	61.0	6.6	SR	97	426	7.0	1.06
RIGA	-30	6.1	Slab	10x20	61.0	6.0	SR	97	426	6.25	1.04

Data Courtesy of Royal Ordnance Defence Rocket Motors

T = uninhibited tubular grain
Slab = rectangular uninhibited slab 61 mm x 20.3 mm x 10.15 mm
SR = slotted radial grain

Initial internal ballistic predictions at RO Defence Rocket Motors are performed using a 1D uncoupled code. The burning rate input to this code is taken from the 2-inch K-round for composite propellants and from slab, disc or small motor firings for double base propellant. Where burning rate scale factor data is available from similar motors this is generally used in the first prediction. Otherwise, an assumed scale-up factor of 5% is typically used in the first instance. Once the first full scale firings have been performed across the operational temperature range, then a more accurate scale factor can be determined and used for subsequent development iterations and for setting propellant acceptance limits. Hence, a constant motor scaling factor is used. While it is not regular practice in motor design to account for grain deformation or 3D flow effects, codes in existence and in development will accommodate these effects. For small tactical motors RO Defence generally finds it sufficient to use simple 1D codes and to allow for grain refinement in development firings.

7.2.4 United States

Scale-up data is presented in Table 5.0 (see Figure 32) for a number of US solid rocket motors ranging from 20 inch to 260 inch in diameter. Summarized in Table 5.0 are motor and grain dimensions, grain design, propellant composition, full-scale motor burning rate, and scale factor referenced to batch or subscale motors. Two primary propellants are shown AP/PBAA/Al and AP/PBAN/Al. Scale factors shown in the table range from 0.996 to 1.128, a variation of 13% for many different motors, development programs and test methods. Experimental uncertainty is not reported, but was generally observed to decrease with newer motor designs and with increase in number of motors fired in each size class.

Sensitivity of scale factor to grain web thickness does not reveal a clear dependency as illustrated in Figures 31 and 32 for a large range of motors or propellants, without considering further contributing factors. However, less data dispersion is revealed in Figure 55 when only data for AP/PBAN/Al propellant motors is examined. Careful consideration of contributing factors can lead to defining statistically significant trends in selected parameters of interest as suggested by Figure 56. Generalized trends for sensitivity of scale factor with web to aluminum type are revealed as derived from NATO/RTO WG 016 discussions.[98]

Motor Dimensions		Grain	Grain Dimensions				Propellant	Full Scale	Scale Factor
Dia	Length	Design	OD	Port ID	Length	Web_{EFF}	Composition	Motor BR	BR_{Full}/BR_{Scale}
(in)	(in)		(in)	(in)	(in)	(in)		(in/sec)	
20.0	79.3	CP 6-pt star	19.9	5.98	55.0	6.96	AP/PBAN/Al	-	1.001
36.1	183.6	CP 6-pt star	35.8	21.90	137.6	6.94	AP/PBAA/Al	-	1.070
36.1	184.0	CP 6-pt star	35.8	21.80	137.6	7.00	AP/PBAA/Al	0.236	1.063
36.1	184.0	CP 6-pt star	35.8	21.80	137.6	7.00	AP/PBAA/Al	0.230	1.045
36.1	184.0	CP 6-pt star	35.8	21.80	137.6	7.00	AP/PBAA/Al	0.723	1.046
40.0	102.6	CP w/fwd slot	39.7	15.84	79.2	11.95	AP/PBAA/Al	-	1.128
40.0	97.1	CP w/fwd slot	39.8	15.24	63.3	12.28	AP/PBAA/Al	-	1.128
43.1	203.1	10-pt dendrite	42.8	-	158.0	3.50	AP/PBAA/Al	-	1.040
44.0	146.0	CP 3-pt star	43.4	22.00	108.0	11.00	AP/PBAA/Al	0.444	0.996
44.0	146.0	CP 3-pt star	43.4	22.00	108.0	11.00	AP/PBAA/Al	0.443	1.007
44.0	146.0	CP 3-pt star	43.4	22.00	108.0	11.00	AP/PBAN/Al	0.455	1.007
44.4	155.6	CP 4-pt star	44.0	18.00	117.3	19.35	AP/PU/Al	-	1.050
100.0	501.6	Segmented CP	99.3	29.0	413.0	35.20	AP/PU/Al	0.263	1.075
120.0	1016.0	Segmented CP	119.5	49.50	780.0	35.00	AP/PBAN/Al	0.445	0.996
120.1	1015.8	5-seg CP	120.0	49.60	777.0	35.20	AP/PBAN/Al	-	1.050
146.0	1503.0	Segmented CP	144.6	56.60	1282.0	44.00	AP/PBAN/Al	0.368	1.012
146.0	1513.0	Segmented CP	144.6	56.60	1282.0	44.00	AP/PBAN/Al	0.368	1.018
156.0	400.7	Segmented CP	152.0	55.40	310.3	49.40	AP/PBAN/Al	0.738	1.048
156.0	901.7	Segmented CP	152.0	68.80	780.7	43.10	AP/PBAN/Al	0.769	1.056
156.0	849.0	Segmented CP	151.6	102.4	696.00	25.80	AP/PBAA/Al	0.234	1.059
156.0	849.0	Segmented CP	153.2	68.6	709.00	43.00	AP/PBAA/Al	0.295	1.017
260.0	969.3	3-spoke CP	259.4	154.90	729.0	52.25	AP/PBAN/Al	0.464	1.064
260.0	969.6	3-spoke CP	259.4	154.90	729.0	52.25	AP/PBAN/Al	0.460	1.060

Data Courtesy of JHU/CPIA Archives

Table 5. Scale-up Data for Various Size Motors and Propellants, United States

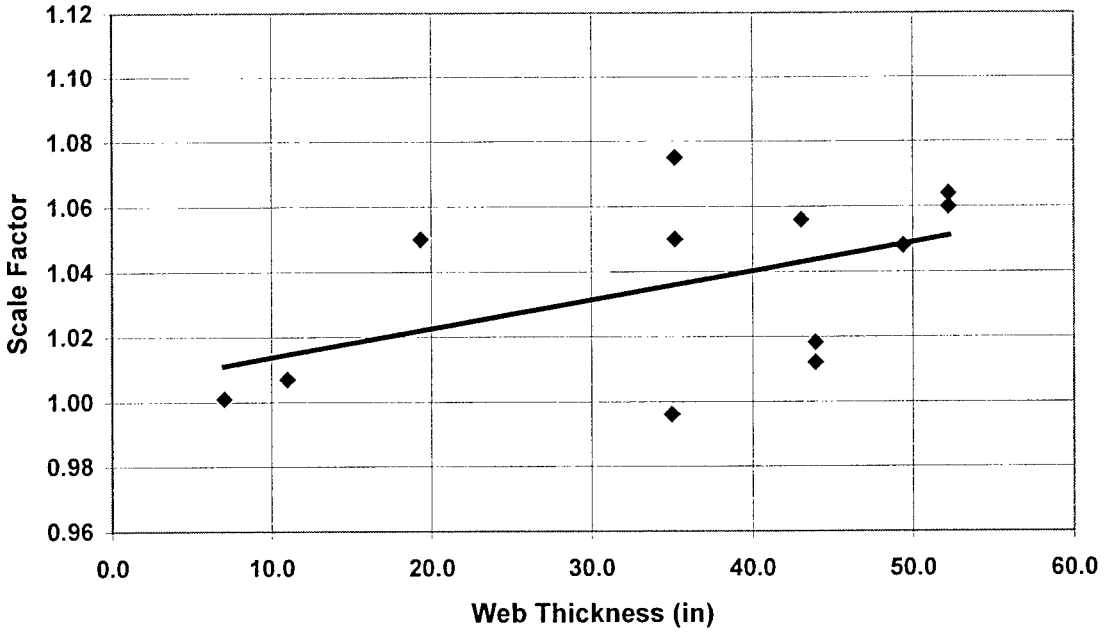

Figure 55. Scale Factor versus Web Thickness for AP/PBAN/Al Propellant Motors (Table 6.4)

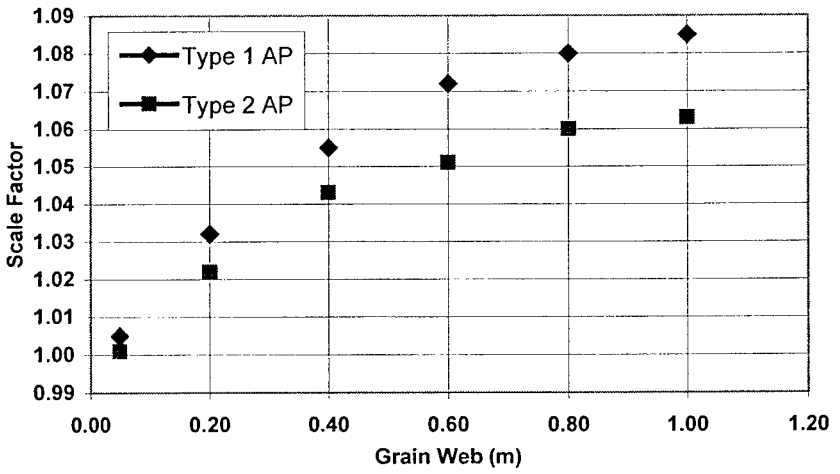

Figure 56. Generalized Trends Discussed in NATO/RTO WG 016[98]

The key elements of early methods used to scale burning rate for the Space Shuttle booster motors are reviewed below.

Motor Casting - The process began with the casting of motors in 4 segments; each segment involved 40 mixes. For the flight motors, a 5-inch center-perforated (CP) motor was also cast out of every third mix for subscale testing. For full-scale ground testing, a 5-inch CP motor was cast out of every mix. This was to generate a more complete statistical database and to obtain propellant pressure exponent.

Subscale Motor Testing & Analysis - The motors were fired at expected flight motor conditions 60 °F and 625 psia. The RSRM burning rate was based on a web thickness-over-web time method. The classical burning rate expression $r_b = aP^n$ was used. The RSRM program used the design drawing value for web thickness. This thickness was not corrected for any real motor effects. The tangent-bisector method of analysis was used to obtain web burn time. All calculated 5-inch CP motor BR values were averaged. The same procedure was followed for the left and right booster motors.

Scale Factor Calculation -

$$\text{Predicted } r_b = \text{Average 5-inch CP } r_b \text{ X Scale Factor}_n \text{ (SF}_n\text{)} \quad (18)$$

Typically predicted r_b = 0.368 in/sec at 625 psia and 60 °F

$$SF_i = \{\text{Firing Derived average } r_b\}_i / \{\text{average } r_{b\ \text{subscale}}\}_i \quad (19)$$

$$\text{Average } SF_n \left((_{i=1} \{SF_i / n_{\text{firings}}\} \text{, where } SF_n = 1.0149 \right. \quad (20)$$

$$\{\text{Average } r_{b\ \text{predicted motor}}\}_i = \text{Average } SF_n \text{ x } \{\text{Average } r_{b\ \text{subscale}}\}_{n+1} \quad (21)$$

The observed SF historically ranged between 1.000 and 1.0225. A nominal average value of 1.0149 was typically used to predict flight RSRM {Average $r_{b\ \text{predicted motor}}$}.

Following a Shuttle flight, the actual RSRM burning rates were deduced and compared with the predicted values. This information was archived and used in the fine-tuning of the scale factor used on subsequent flights. Based on many flights, typically scale factor was found to oscillate about a nominal value 1.0149. Two significant influences on scale factor were observed causing actual web thickness to vary from the drawing web thickness and subsequently accounted for as discussed in the next section on variable motor scale factor, pressure deformation, and thermal shrinkage of cast grain.

7.3 Variable Motor Scale Factor – Industry Examples and Results

7.3.1 France

The following Table 6.0 is provided by SNPE, France and compares Mimosa (11.35 cm diameter), Campanule (86 cm diameter) with conventional strand burner and ultrasonic burner data. The scaling factors are evaluated following the methods reviewed earlier in Section 5.2.3.

SNPE performs full-scale SRM burning rate analysis using burning rate deduced from ballistic specimen test firing. They use two correction factors to predict full-scale experimental results from theoretical analysis, as discussed previously (Section 5.2.3):

1. A constant, linear (web independent) correction called Scale Factor, and
2. A variable, non-linear (web dependent) correction called Global Hump Effect.

The source and magnitude of these factors are discussed below.

Table 6. Scale-up Data SNPE, France[62]

Full-Size Grain Type	Propellant	Subscale Method	Subscale r_b (mm/s)	Pressure (MPa)	BR Ratio Full-Scale/ Subscale
Finocyl	Aluminized Composite	Mimosa Motor	27.6	10.5	0.96
Finocyl	Aluminized Composite	Campanule Motor	22	12	0.93
Circular Radial	Aluminized Composite	Campanule Motor	44	11	0.95
Star Shaped Radial	Aluminized Composite	Campanule Motor	11.6	12.5	0.94
Star Shaped Radial	Double Base	Strand Burner	15.9	19	1
Star Shaped Radial	Double Base	Ultrasonic	15.9	19	1

Data Courtesy of SNPE

7.3.1.1 Real Grain Geometry – Combined Grain Deformation & Erosive Burning Effects

SNPE confirmed grain deformation as one of the more significant factors influencing the correlation of subscale and full-scale motor performance. Their correction for these effects includes the combined influence of both the grain and case design, and gas flow and pressure distribution within the rocket motor.

The grain design influences the extent of cross flow velocities and enhanced variations in static and total pressure distributions over the burning surface. The gas cross flow conditions may even be sufficient to promote erosive burning.

Generally, the grain deformation, illustrated previously in Figures 13, 14 and 15 for SNPE grain designs, reduces the effective web thickness producing a reduction in average scale factor. Thus, accounting for the real grain geometry has the effect of reducing the dispersion in average scale factor. SNPE estimated real solid grain geometry to contribute as much as 30% of observed average scale factor of 8% for large motors illustrated in Figure 31. The exact value depends on the details of the grain design, case design and type of manufacturing process.

7.3.1.2 Rheology of Grain Manufacturing Process

SNPE confirmed the manufacturing process to be the most important contributor to the hump effect as well as being an important contributor to scale factor. Figure 21 illustrated previously the effect of three different manufacturing processes: plunged mandrel, rotated cast-in-place mandrel, and 3-point cast-in-place mandrel on burn rate ratio versus web behavior for a cylindrical grain.

SNPE found the "hump" is related to the grain casting process and the arrangement of Ammonium Perchlorate crystals relative to the direction of flow during casting. This in turn introduces some anisotropy with respect to burning rate as illustrated in Figure 57. SNPE found the hump effect corresponds to burning rate variations as a function of location in the grain, and relative angle of incidence between flame front and sheared lines or surfaces. Scale up problems will arise if the flow patterns of the uncured propellant during casting are appreciably different in the large-scale motor compared to the subscale motor.

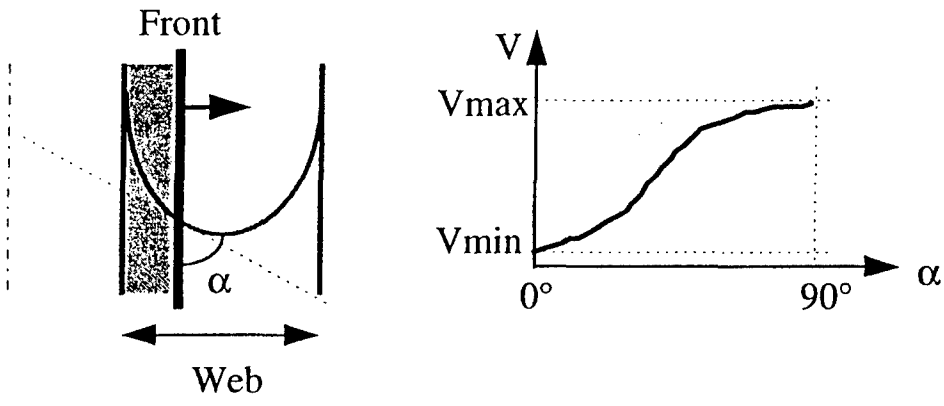

Figure 57. Hump Effect Corresponds to Burning Rate Variations as a Function of Location in the Grain and Relative Angle of Incidence between Flame Front and Sheared Lines[62]

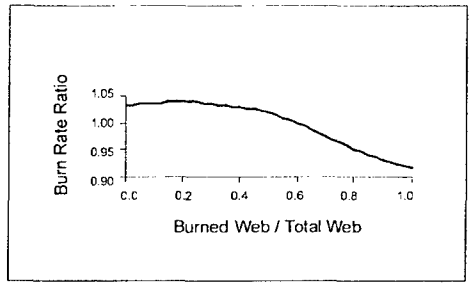

Figure 58. Representative Variable Motor Scale Factor of Burn Rate Ratio versus Fraction of Web Burned[62]

Figure 58 illustrates burn rate ratio versus fraction of web burned behavior used to characterize the Global Hump Effect SNPE uses in accounting for scale.

In the cases illustrated previously in Figures 20 and 21, the difference in the calculated burning rate between the plunged mandrel grain and the cast-in-place mandrel grain is 3.2%, corresponding to almost 50% of observed average scale factor of 8% illustrated in Figure 31. Hence, it is apparent the manufacturing process can have a strong influence on scale factor and hump effect.

7.3.2 United States

7.3.2.1 Early Scaling/Modeling Efforts

The Space Shuttle Redesigned (now called Reusable) Solid Rocket Motor (RSRM) is a four-segment motor that contains over a million pounds of PBAN propellant. The forward segment has eleven fins in the head end that transforms into a center perforated (CP) grain about halfway down the segment. The two center segments, which are interchangeable, and the aft segment have multiple tapered CP grain designs. Figure 59 illustrates the RSRM grain design and pressure-time behavior. The case is made of D6AC steel with a diameter of 146 inches and a total length of about 1400 inches. During a typical

launch there are several loads applied to the propellant that deforms the grain geometry, which changes the exposed surface area. A change in surface area results in a change in performance.

Grain deformation of a solid rocket motor is an important factor in accurately modeling its performance. Deformation can affect maximum pressure and thrust, burn time, performance trace shape and tailoff. Motor parameters such as propellant web thickness, case strength and diameter, propellant mechanical properties, and grain geometry will determine the extent of the effects that deformation will have on performance.

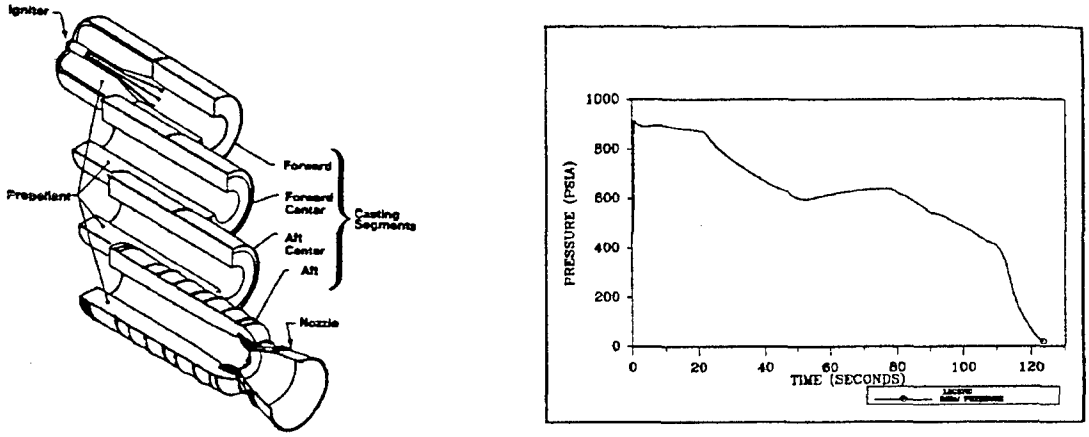

RSRM Grain Design

RSRM Pressure vs Time

Figure 59. RSRM Grain Design and Pressure-Time Behavior[99]

Early in the Space Shuttle program the performance of the solid booster was predicted based on as-cast grain geometry, grain deformation was not modeled. Adjustment factors were estimated based on historical large motor data. A target burn rate was selected and an estimated scale factor was applied to the subscale burn rate data to predict the full-scale motor burn rate. An adjustment factor called Surface Burn Rate Error (SBRE) was applied to the predicted performance trace based on Titan and Minuteman historical data. The SBRE factor included unknown contributions from the burn rate augmentation and grain geometry modeling error. After each motor firing, the SBRE was calculated and the predicted SBRE for the next motor was updated using the historical SBRE. Also the burning rate was determined based on the burn time and the as-cast web thickness. The delivered burning rate was compared with the subscale predicted burning rate and a historical scale factor was established. After several SRM test firings, a good indication of the average SBRE curve and the burning rate scale factor was determined. Thus after these firings two factors, the SBRE and scale factor were used to help predict the performance of the motor for future firings. SBRE is applied to the instantaneous burning rate, while the scale factor is applied to the reference burning rate. These two factors and the burning rate were consistent and therefore the ballistic predictions were accurate. Figure 6.47 shows a typical RSRM pressure trace with the peak head end pressure occurring at about 0.6 seconds.

Figure 60 shows the comparison of the as-cast SBRE and the deformed SBRE. The shape of the curve changed, but the magnitude of the as-cast and the deformed data are roughly the same. This indicates the bumps and blips are due to the geometry model, but the primary driver of the SBRE curve is directional burn rate bias. Directional burn rate bias causes the burning rate to change from the bore to the insulation. Directional burn rate testing done on the PBAN propellant used in the RSRM shows the bias can be as high as 8.2%.[99]

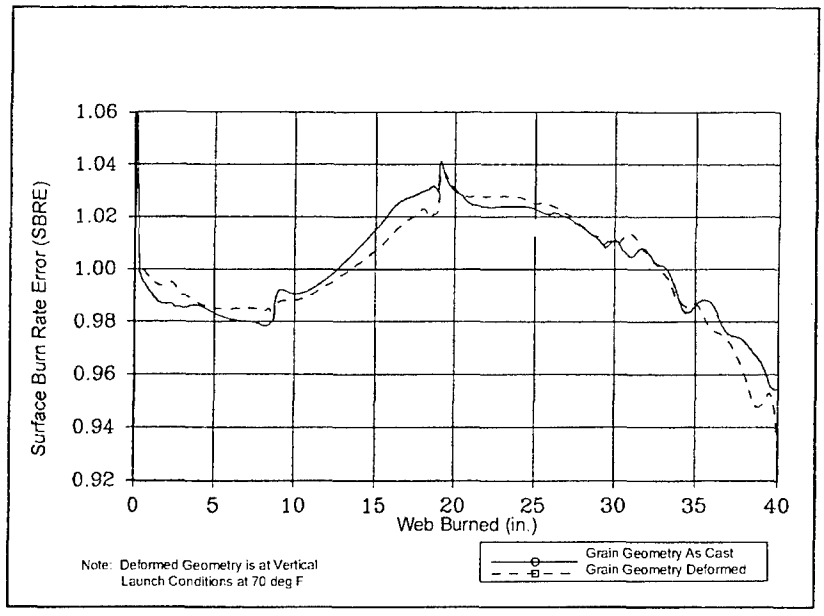

Figure 60. Representative RSRM SBRE Comparison for As-Cast and Deformed Grain Geometry[99]

7.3.2.2 Later Scaling/Modeling Efforts

Application of state-of-the-art ballistic modeling techniques addresses the design challenges reviewed earlier (Section 3). Advanced ballistic modeling techniques include ballistic/structural/CFD flowfield-grain interaction, deformed grain structural response, erosive burning response characterization, and 2-D spatial burning rate mapping due to propellant rheology effects. Modeling fidelity is further improved by using extensive large motor experience base for validation purposes.

In addition to improved ballistic models, efforts should be made to identify potential design modifications to accommodate remaining uncertainties. This can be accomplished by conducting sensitivity studies to characterize the motor design envelope, followed by performing uncertainty analyses to generate estimates of predicted uncertainties in ballistic parameters and their impact on performance.

Improved Motor Internal Flowfield Modeling – Analysis of RSRM test experience shows that the traditional 1-D ballistic model predicts motor internal pressure distribution reasonably well except during the first five seconds of burn. The 1-D model over-predicts aft end pressure early in the burn. 2-D and 3-D flow effects must be considered during this period. Application of this approach provides improved flowfield modeling, nozzle mass flow rate predictions and thrust-time predictions without resorting to empirical correlations. Improved loads predictions for case/nozzle component design, and improved grain structural assessment are also the result of this analysis approach.

Grain Deformation Analysis – Due to ambient pressure cure of large SRM propellant grain, the propellant experiences a thermal shrinkage load under firing conditions. This is further complicated by long term storage, motor pressurization and launch acceleration loads on the grain. The total impact of these loads on the RSRM web thickness is on the order of 2.5 – 38 cm (1 – 1.5 inches) at ignition. Modeling the as-cast geometry would introduce unnecessary uncertainty in the ballistic prediction if these effects were ignored. A deformed grain geometry model accounts for these effects to generate the best estimate of the motor internal geometry under actual firing conditions. Coupled CFD/structural/ballistic internal flow

calculations are performed to account for any possible grain/flowfield coupling of the propellant, and to get to the final grain configuration under firing conditions at the rollover pressure. The effect of grain deformation on surface area versus burn distance for each segment of the RSRM as well as the overall motor was illustrated previously in Figure 16.

Advantages of using the deformed geometry description include improved correlation with measured data (reduced empirical matching required), improved resolution on the tail-off, and more accurate flowfield predictions due to modeling of actual geometry under firing conditions. This improves the accuracy of both the pressure drop prediction and the erosive burning model. In addition, a coupled structural/CFD analysis identifies potential failure modes associated with structural/flowfield interactions, and assures a stable design.

Erosive Burning – Erosive burning effects can be significant for motors with high L/D's (such as Titan and RSRM) because of the relatively high flow velocities within the motor. Erosive burning affects both the maximum pressure prediction early in the burn and the tail-off slope late in the burn, both of which are critical design parameters. Figure 61 shows the RSRM hump (SBRE) curve (Figure 60) with and without accounting for erosive burning, illustrating significant effects are present. An erosive burning model is based on the deformed geometry and accurate internal flowfield model discussed previously, and is calibrated from the large motor database.

The advantages of accounting for the potential for erosive burning effects in the motor design and predictions are:

1. Improved confidence in the maximum pressure prediction
2. Improved tail-off modeling
3. Better estimates of exposure times for insulation design
4. Improved ignition model resolution
5. Better estimates of pressure drop early in the burn

All of this again reduces the amount of empiricism in the ballistic model and improves predictive accuracy.

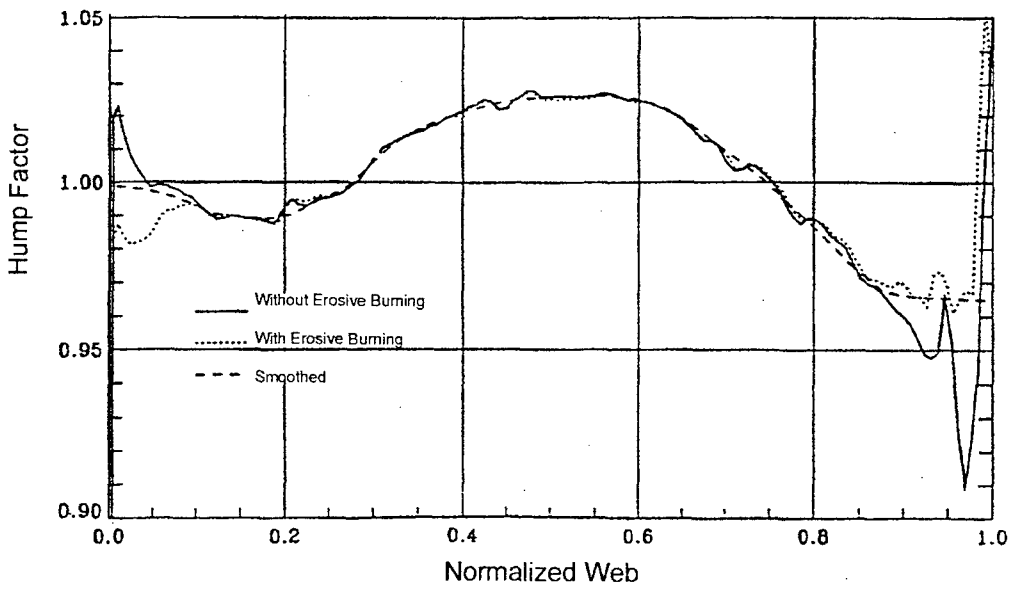

Figure 61. Erosive Burning Model Effect on RSRM Hump Curve[99]

Rheology of Grain Manufacturing Process – The largest single prediction uncertainty for a first time motor firing is the motor trace shape. Variations in this motor trace shape from predicted to measured are attributed to special burn rate variations within the motor. These variations are referred to as "hump" effect because of the characteristic low-high-low burn rate variation during the burn, as discussed earlier (Section 3). The ballistic model includes spatial burn rate mapping based on flow analysis of the propellant cast process, because of the demonstrated effect of propellant flow during cast on variations in propellant burn rate. The propellant flow model has been correlated with casting hardware (i.e. slit plate location) and subscale test motors (i.e. propellant sensitivity to rheology). Figure 62 demonstrates the influence of slit plate location and flow line orientation on the burning rate variation within the motor. Figure 63 shows RSRM predicted versus measured pressure data, as well as the characteristic hump (SBRE) curve derived from these two pressure traces. Application of this correlation to the RSRM geometry and process produces an improved correlation with measured data.

Application of spatial burn rate mapping provides the potential of eliminating the "hump" effect and its attendant uncertainty from the full-scale motor prediction. There is also the potential to eliminate subscale to full-scale burning rate scaling if this approach is also applied to subscale motor ballistic analysis. This reduces the amount of empiricism in the predictive model and improves the accuracy of the prediction.

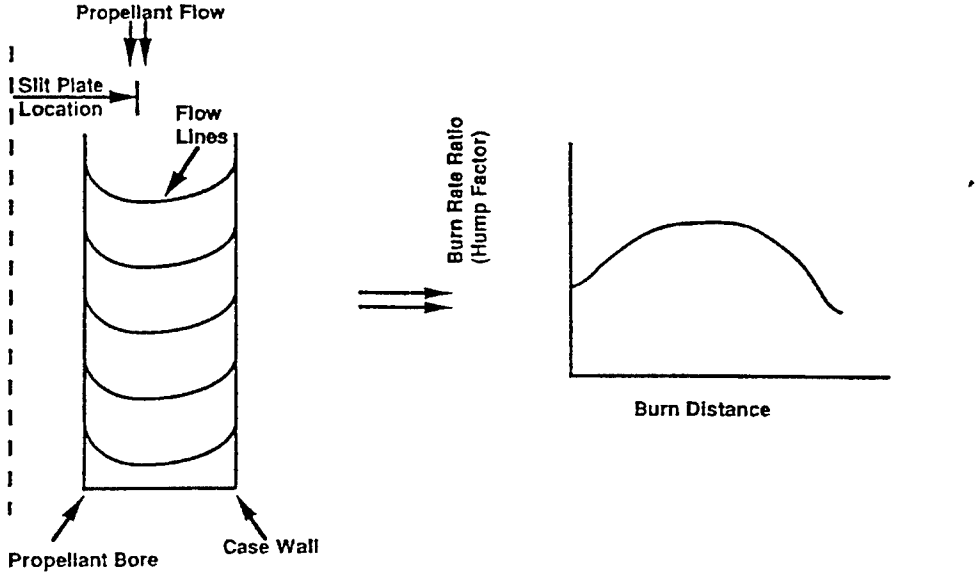

Figure 62. Slit Plate Location Effect on Radial Burn Rate Variation[99]

Figure 36 previously depicted the result on scale factor when important global parameters (Section 3.2) are accounted for in the Shuttle SRM and RSRM performance analysis. The dispersion on scale factor is substantially reduced from 13% in Figure 32 with an average scale factor of 1.0450 to a dispersion of 2.6% and an average of 1.0149. This reduction in dispersion was effected by application of a thorough, rigorous and integrated combination of ballistic prediction and testing of full-scale and subscale motors, and cured and liquid strands, as reviewed previously. The full-scale ballistic prediction included the principal effects of real grain geometry at firing (including grain deformation and erosive burning) and grain manufacturing process, as suggested earlier in the ballistic test correlation methodology reviewed in Section 5.2.3.

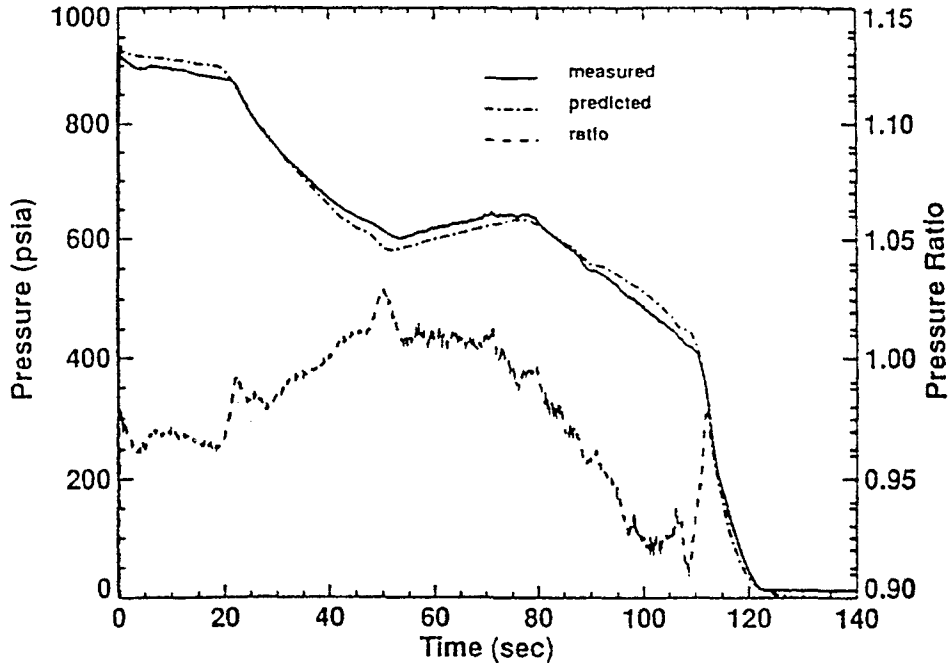

Figure 63. RSRM Measured Pressure versus Theoretical Prediction[99]

8.0 SCALING RECOMMENDATIONS

8.1 Background / Objectives

Accurate prediction of internal ballistics for the first full-scale solid propellant motor of a new design becomes increasingly important as motor size increases and fewer development motor firings are called for with success-oriented programs.

The rocket motor designer must have a good understanding of the variation of propellant burning rate in order to produce an efficient design and minimize design iterations during development. The fundamental factors influencing scaling and historical approaches are reviewed to correlating subscale and full-scale motor burning rate. Survey results from the participants of AVT Working Group 16 are presented as a historical basis for accounting for scale effects.

Solid propellant burning is not a steady process, but rather an intrinsically unsteady and multidimensional process. The flame structure in solid propellant burning is complex and flame models and empirical burning rate laws are used to seek its understanding. Different measurement techniques are approximate means to define the "real" burning rate. This makes experimental uncertainty and error analysis an important element of this process. Each propellant exhibits an "intrinsic" burning rate, which an ideal experiment, with non-idealities eliminated, seeks to measure.

Knowledge of burning rate of solid propellants, whether steady or unsteady, under a variety of operating conditions, is of critical importance for applications (due to their sensible influence on performances and cost of propulsive devices) and also for fundamental reasons (understanding of combustion processes). Furthermore, since no available theory/model is capable of predicting burning rates with accuracies within 1% while including the effects of rate modifiers, they must be measured experimentally. However, while experiments measuring steady burning rates are reasonably robust, those measuring unsteady values

are fragile and still a matter of research. Since a variety of experimental hardware and methods are in use today, even for the common steady-state operations, the need arises to understand and perhaps standardize the different approaches developed among the NATO countries.

The fundamental physics, features, empirical laws and analytical models, stability measurement methods, and scaling of burning rate are reviewed in the report. Analysis results in this study are expressed in terms of the simple power law rate equation, often referred to as the St. Robert's, St. Venant's or Vielle's law, $r = ap^n$. Two fundamental classes of empirical burning rate definitions are in use for motor applications: the thickness/time method and the mass conservation or mass balance method.

8.2 Fundamental Factors Influencing Scaling of Burning Rate

The underlying reasons for the differences observed in burning rate between large-scale motors, subscale motors, strands and non-intrusive methods are summarized and reviewed in detail. Some are evident from a consideration of burning rate physics and can be identified independently in the laboratory. Some are derived from a consideration of the engineering design of the motor and its operating environment. The degree of scaling exhibited by a strand burner, subscale or full-scale motor will vary in proportion to the effect exhibited by the influencing parameters. Understanding and accounting for these parameters, in subscale hardware design serves to mitigate the scaling effects. Factors are summarized that should be avoided in subscale hardware that typically contribute to modeling complexity and confounding test results.

8.3 Practical Issues Influencing Scaling of Measurement Methods

The combustion zone of a subscale motor more closely than a strand approximates the propellant combustion environment in a full-scale motor. This contributes to the improved accuracy of the subscale motor burning rates over other subscale measurement techniques.

Subscale motors are used to simulate the ballistic flow conditions expected in full-scale motors and to evaluate how the motor conditions influence the "intrinsic burning rate" of the propellant. Furthermore, subscale motors are used because strand burner techniques have historically proven inadequate for predicting full-scale motor burning rate and ballistic behavior on their own.

A wide array of motors, with different design features, exists for measuring burning rate within the 23 facilities in 7 countries surveyed. Complete details of test hardware used by the facilities surveyed are provided elsewhere.[5] Subscale motor sizes used vary from <250g to over 10,000g. The predominant configuration encountered is the circular, center-perforated grain in the weight classes under 5000g. While the 5x10 cm (2x4 inch) motor is the most widely used tool, this motor is also not standardized with respect to dimensions and propellant mass, which varies between 120g - 450g. The WG recommends standardizing this motor by increasing the web of the propellant grain to nominally 13mm, resulting in a propellant weight of approximately 300-400g. This would cover the majority of propulsion applications and allow greater international cooperation in correlating burning rate data.

The WG created a summary of the use of burning rate measurement hardware in relation to the life cycle of the propellant versus its application. The smaller motor sizes (<200g to 5,000g) are used in the research/technology, screening and development phases for both tactical and space/strategic propulsion. Large subscale test motors (5,000g to over 10,000g) are mainly used in the screening through performance verification phases for space/strategic applications. WG 016 findings suggest 2000g-5000g motors provide satisfactory scale-up for smaller full-scale motors ($D \leq 76$ cm). The largest motors with grain weights from 22kg up to 60 kg permit satisfactory scaling for very large boost motors for space or strategic applications.

Recommended burning rate measurement practices, including test hardware, instrumentation, and data reduction are summarized elsewhere.[4,5] Further attention to refining experimental methods in order to reduce motor test data variability is warranted.

The Design of Experiments (DOE) method may be used to reduce the resources necessary to identify essential dependencies with fewer iterations of the test/design cycle. These methods may be used to partially offset the perceived statistical advantages of strand burner test methods.

Deducing a burning rate from a full-scale motor test presents challenges that can contribute to measurement uncertainties. These observations suggest that one must deduce a rate versus pressure relationship rather than an average burning rate from each test. Furthermore, instantaneous (dynamic) burning rate may be significantly different from the steady-state burning rate at each pressure.

Accurate burning rate predictions of a new solid rocket motor are made difficult by apparent effects of processing and geometry variations on propellant burning rate. Differences exist between subscale and full-scale motor internal ballistics and often in the methods used to analyze them, which are influenced by the individual analysts experience. Burning rate correlations between subscale devices and large motors are somewhat limited by the availability of accurate data. Quantitatively, the scaling experiences of a particular motor manufacturer are not generally applicable industry-wide.

8.4 Industry Performance Correlation Practices

Propellant burning rate is one of the most significant variables influencing the accuracy of solid rocket thrust-time prediction. An analytic methodology is recommended for correlating burning rate through this performance prediction. A thorough means of predicting full-scale experimental results from theoretical analysis should include two correcting factors, a constant scale factor correction and a variable correction resulting mainly from the grain manufacturing process.

Historically, "scale factor" has been a measure of the uncertainty to define the differences in burning rate between a subscale burning rate measurement device or subscale motor and a larger motor. Current thorough industrial practices seek to identify the sources of the differences in order to reduce uncertainty (or "scale factor" dispersion) in burning rate between scales.

8.5 Strand Burner-to-Motor Burning Rate Comparison

Industry challenges and successes in strand burner-to-motor and subscale-to-full-scale burning rate comparisons are reviewed. The strand burner, while enjoying widespread use as a burning rate measurement device, has in recent times become less used as a tool for predicting full-scale motor performance. This is due in part to the fundamental problems reviewed in Section 3. Correlations between strands and subscale motors are recommended in order to determine the influence of the controlling factors. The strand burner is a better tool for measuring statistically significant effects of small formulation changes for quality control work, given proper test design and conduct. Solid rocket motor performance predictions are possible by establishing a correlation between full-scale motor performance, subscale test motors, and liquid and solid strand burning rate tests. The confidence and accuracy of these predictions will be maintained if the correlation between motor performance and any of the subscale test methods remains constant.

Limited success of cured propellant strands led to the development of the acoustic emission (AE) method using liquid strands for improved discrimination capability over traditional strand pressure-time behavior. The full-scale rocket motor, subscale motor, liquid strand, or cured strands do not generally have the same burning rate at the same pressure, but it is possible to obtain a correlation between them. The acoustic emission method has many advantages over conventional the nitrogen strand burning system.

The ultrasonic technique is currently used in France and the US for screening and development of propellants for tactical applications. Excellent comparison has been obtained between ultrasonic measurements in strands and pressure-time data for small and large motor firings. The unique advantage of the ultrasonic method is the numbers of tests are low (usually two) and that it yields a continuous burning rate, which can be used in ballistic codes.

8.6 Comparison of Subscale Device with Full-Scale Motor Burning Rate

Selected facilities and countries were surveyed to identify industrial scaling practices. Relatively few facilities and countries develop and field large solid rocket motors. This is reflected in the fact that only a portion of the propulsion community surveyed have established test motor scaling practices. Many countries and facilities use only a constant scale factor correction. Methods of evaluating scale factor may or may not attempt to account for some of the fundamental factors influencing scaling. This emphasizes the scaling experience of a particular motor manufacturer may not generally be applicable to another because of industry-wide differences in subscale devices, test methods and analysis methods. Various companies in the U.S. and France include the recommended variable motor scale factor correction, but seek different means of accounting for the principle parameters that contribute to differences in real motor internal geometry with scale. An effort to agree on consistent scaling methods would contribute to success in international cooperative programs.

8.7 Future Developments

Factors crucial to industrial acceptance are cost effectiveness and robustness. Until recently, ballistic test motors were focused on burning rate characterization. However, passive motor stability diagnostics provide concurrent modal frequency and stability margin estimates from low-level pressure oscillations present. Therefore, the cost effectiveness of the ballistic test motor *as a propellant charactizer* can be increased by nothing more than increasing the sensitivity of the pressure measurements.

New measurement techniques will require a re-examination of propellant characterization techniques and hardware, as well as test technique development. For example, ballistic test motors having characteristic frequencies in regimes of interest will be desirable; this will necessitate new geometric configurations. In a similar way, the ability of measurement techniques to enhance the accuracy of sensitivity measurements, the key to empirical formulation development, will instigate the development of instantaneous, multiple, simultaneous rate difference measurements in a variable-pressure environment. Lastly, concurrent measurement of burning rate, sensitivities, and stability-related information offer potentially valuable interactions. The ZN methodology, for example, connects steady and nonsteady behavior. Therefore, with both steady and nonsteady information in hand, other information can be accessed.

Refinement of current techniques, development of innovative techniques and necessary theoretical accessories will provide excitement and improved solid rockets in the future. Detailed solid rocket simulations in progress will assist these potential developments. A fully-coupled ballistic test motor simulation, for example, would demonstrate the effects of cure shrinkage and grain temperature on the web; the effect of ordered particle distributions near the case and bore; combustion efficiency dependence upon heterogeneity, etc.; and, connection between low-level pressure oscillations and physical processes.

The NATO RTO AVT WG 016 activities have acted as a catalyst for efforts to improve burning rate measurement and analysis methods within the solid propulsion community. The WG recommends, as a minimum, that members of the propulsion community review these findings as a means of advancing their own burning rate measurement and analysis methods.

9.0 References

[1] "Evaluation of Methods for Solid Propellant Burning Rate Measurements," NATO RTO Advisory Report, NATO RTO AVT Working Group 016, Chaired & Edited by R. S. Fry, Johns Hopkins University/CPIA, August 2001.

[2] Brooks, W.T., "Burn Rate Considerations in Solid Rocket Motor Performance Prediction," AIAA Paper 76-601, presented at AIAA/SAE 12th Propulsion Conference, Palo Alto, CA, July 1976.

[3] Fry, R. S., "Solid Rocket Motor Test and Test Techniques, Component Testing & Verification, Solid Propellant Burning Rate," AIAA Solid Rocket Technical Committee Lecture Series, 36th Aerospace Sciences Meeting, January 1998.

[4] Fry, R.S., "Solid Propellant Subscale Burning Rate Analysis Methods for U.S. and Selected NATO Facilities," JHU/CPIA CPTR 74, July 2001.

[5] Fry, R.S., "Solid Propellant Subscale Burning Rate Test Techniques and Hardware for U.S. and Selected NATO Facilities," JHU/CPIA CPTR 75, July 2001.

[6] DeLuca, L.T., "Burning Rate Fundamentals," Chapter 2 of "Evaluation of Methods for Solid Propellant Burning Rate Measurements," NATO RTO Advisory Report, NATO RTO AVT Working Group 016, Chaired & Edited by R. S. Fry, Johns Hopkins University/CPIA, August 2001.

[7] F.A. Williams, M. Barrère, and N.C. Huang. Fundamental Aspects of Solid Propellant Rockets. Technivision Services Slough, UK, 1969. AGARDograph 116.

[8] F.A. Williams. Combustion Theory. The Benjamin/Cummings Publishing Company, Menlo Park, CA, 2nd edition, 1985. pp.

[9] G.P. Sutton, Rocket Propulsion Elements. Wiley, New York, NY, USA, 6th edition, 1992.

[10] R.T. Holzmann, Chemical Rockets, Marcel Dekker, New York, NY, USA 1969.

[11] A. Davenas., Solid Rocket Motor Design, volume 170, AIAA Progress in Astronautics and Aeronautics, "Tactical Missile Propulsion", edited by G.E. Jensen and D.W. Netzer, chapter 4, pages 57-113. AIAA, Reston, VA, USA, 1996.

[12] K. Klager, and G.A. Zimmerman. Steady Burning Rate and Affecting Factors: Experimental Results, volume 143, AIAA Progress in Astronautics and Aeronautics, "Nonsteady Burning and Combustion Stability of Solid Propellants", edited by L.T. DeLuca, E.W. Price, and M. Summerfield, chapter 3, pages 59-109. AIAA, Washington, DC, USA, 1992.

[13] C. Huggett, C.E. Bartley, and M.M. Mills, Solid Propellant Rockets. Number 2 in Princeton Aeronautical Paperbacks. Princeton University, Princeton, NJ, USA, 1960

[14] Y.M. Timnat. Advanced Chemical Rocket Propulsion. Academic Press, London, UK, 1987

[15] V.E. Zarko and K.K. Kuo. Critical Review of Methods for Regression Rate Measurements of Condensed Phase Systems, pages 600-623. Special Topics in Chemical Propulsion, "Non-Intrusive Combustion Diagnostics", edited by K.K. Kuo and T.P. Parr. Begell House, Inc., New York, NY, USA, 1994.

[16] M. Barrère, A. Jaumotte, B. Fraeijs De Veubeke, and J. Vandenkerckhove. Rocket Propulsion. Elsevier Publishing Company, Amsterdam, Netherlands, 1960.

[17] B.L. Jr. Crawford, C. Huggett, and F. Daniels, and R.E. Wilfong. Direct Determination of Burning Rates of Propellant Powders. Analytical Chemistry, 19(9): 630-633, 1947.

[18] M. Summerfield, G.S. Sutherland, M.J. Webb, H.J. Taback, and K.P. Hall, Burining Mechanism of Ammonium Perchorate Propellants, Volume 1 of AIAA Progress in Astronautics and Aeronautics, "Solid Propellant Rocket Research", edited by M. Summerfield, pages 141-182. Academic Press, New York, NY, USA, 1960.

[19] J.A. Steinz, and M. Summerfield, Low Pressure Burning of Composite Solid Propellants. Volume 88 of Advances in Chemistry Series, chapter 9, pages 244-295. American Chemical Society, Washington, DC, USA, 1969.

[20] J.A. Steinz, P.L. Stang, and M. Summerfield. The Burning Mechanism of Ammonium Perchlorate Based Composite Solid Propellants. Technical Report AMS-830, Princeton University, Princeton, NJ, USA, 1969. PhD Thesis, Aerospace and Mechanical Sciences Department.

[21] A. Davenas et Collaborateurs, Technologie des Propergols Solides. Masson, Paris, France, 1989.

[22] J.W. Cornelisse,H.F.R. Schöyer, and Wakker K.F. Rocket Propulsion and Spaceflight Dynamics. Pitman Publishing Limited, London, UK, 1979.

[23] Ya.B. Zeldovich. On the Combustion Theory of Powder and Explosive. Journal of Experimental and Theoretical Physics, 12:498-510, 1942.

[24] Ya.B. Zeldovich, O.I. Leypunskii, and V.B. Librovich. The Theory of the Unsteady Combustion of Powder. Nauka, Moscow, Russia. 1975.

[25] B.V. Novozhilov. Nonstationary Combustion of Solid Rocket Fuels. Nauka, Moscow, Russia, 1973. Translation AFSC FTD-MT-24-317-74.

[26] A.A. Zenin. Thermophysics of Steady Combustion Waves of Solid Propellants, volume 143, AIAA Progress in Astronautics and Aeronautics, "Non steady Burning And Combustion Stability of Solid Propellants" edited by L. DeLuca, E.W. Price, and M. Summerfield, chapter 6, pages 197-231. AIAA, Washington, DC, USA, ,1992.

[27] W.H. Miller and Barrington. A Review of Contemporary Solid Rocket Motor Performance Prediction Techniques. Journal of Spacecraft and Rockets, 7 (3), 1970.

[28] N. Kubota. Survey of Rocket Propellants and Their Combustion Characteristics, volume 90, of AIAA Progress in Astronautics and Aeronautics, Fundamentals of Solid Propellant Combustion, edited by K.K. Kuo and M. Summerfield, chapter 1, pages 1-52. AIAA, Washington, DC, USA, 1984.

[29] N. Kubota. Temperature Sensitivity of Solid Propellants and Affecting Factors: Experimental Results, volume 143 of AIAA Progress in Astronautics and Aeronautics, Nonsteady Burning and Combustion Stability of Solid Propellants, edited by L. DeLuca, E.W. Price, and M. Summerfield, chapter 4, pages 111-143. AIAA, Washington, DC, USA, 1992.

[30] O.K. Rice and R. Ginell. The Theory of the Burning of Double-Base Rocket Powder. Journal of Physical and Colloid Chemistry, 54 (6): 885-917, 1950.

[31] R.G. Parr and B.L. Jr. Craford. A Physical Theory of burning of Double-Base Rocket Propellants. Journal of Physical and Colloid Chemistry, 54 (6): 929-954, 1950

[32] M.W. Beckstead, R.L. Derr, and C.F. Price. A model of composite solid-propellant combustion based on multiple flames. AIAA Journal, 8(12): 2200-2207, 1970.

[33] M.R. Denison and E. Baum. A Simplified Model of Unstable Burning in Solid Propellants. ARS Journal, 31:1112-1122, 1961.

[34] B.V. Novozhilov. Stability Criterion for Steady-State Burning of Powders. Journal of Applied Mechanics and Technical Physics, 6(4): 157-160, 1965.

[35] B.V. Novozhilov. Theory of Nonsteady Burning and Combustion Stability of Solid Propellants by the ZN Method, volume 143 of AIAA Progress in Astronautics and Aeronautics, 'Nonsteady Burning and Combustion Stability of Solid Propellants' edited by L. DeLuca, E.W. Price, and M. Summerfield, chapter 15, pages 601-641. AIAA, Washington, DC, USA, 1992

[36] L.T. DeLuca, R. DiSilvestro, F. Cozzi. Intrinsic Combustion Instability of Solid Energetic Materials. Journal of Propulsion and Power, 11(4):804-815, 1995. See also Comments, Journal of Propulsion and Power, 13(3):454-456,1997.

[37] L.T. DeLuca, M. Verri, F. Cozzi, A. Jalongo, and G. Colombo. A Survey of Pressure-Driven Burning of Energetic Solid with Arrhenius Surface Pyrolysis. In "Challenges in Propellants and Combustion 100 Years After Nobel" edited K.K. Kuo, pages 493-514. Begell House, New York, USA 1997.

[38] Zucro, M.J. and J.D. Hoffman, "Gas Dynamics," John Wiley & Sons, 1977, Vol II.

[39] A. Annovazzi. Burning Rate Measurement at FIAT AVIO - Comprensorio BPD. Private communication, 13 November 1997.

[40]E.W. Price. Experimental Observations of Combustion Instability, 1984, volume 90 of AIAA Progress in Astronautics and Aeronautics, Fundamentals of Solid Propellant Combustion, edited by K.K. Kuo and M. Summerfield, chapter 13, pages 733-790. AIAA, Washington, DC, USA, 1984.

[41] E.W. Price. L' Instability, 1992, volume 143, AIAA Progress in Astronautics and Aeronautics, , Nonsteady Burning and Combustion Stability of Solid Propellants, edited by L. DeLuca, E.W. Price, and M. Summerfield, chapter 9, pages 325-361. AIAA, Washington, DC, USA, 1992.

[42] F.E.C.Culick, and V. Yang. Prediction of the Stability of Unsteady Motions in Solid-Propellant Rocket Motors, volume 143, AIAA Progress in Astronautics and Aeronautics, "Nonsteady Burning and Combustion Stability of Solid Propellants", edited by L. DeLuca, E.W. Price, and M. Summerfield, chapter 18, pages 719-779. AIAA, Washington, DC, USA, 1992.

[43] H.B. Mathes. Applications of Combustion Stability Technology to Solid Propellant Rocket Motors, volume 143, AIAA Progress in Astronautics and Aeronautics, "Nonsteady Burning and Combustion Stability of Solid Propellants" edited by L. DeLuca, E.W. Price, and M. Summerfield, chapter 19, pages 781-804. AIAA, Washington, DC, USA, 1992.

[44] G.H.S. Young. Methods of Burning Rate Control in Solid Propellants, pages 285-302. AGARD Combustion and Propulsion Panel. Pergamon Press, 1960.

[45] S.F. Sarner. Propellant Chemistry. Reinhold Publishing Corporation, New York, NY, USA, 1966.

[46] R.O.Hessler. Private communication, 15 December 1997.

[47] A.A. Juhasz, and C.F. Price. The Closed Bomb Technique for Burning Rate Measurement at High Pressure, volume 63 of AIAA Progress in Astronautics and Aeronautics, "Experimental Diagnostics in

Combustion of Solids", edited by T.L. Boggs and B.T. Zinn, pages 129-151. AIAA, Washington, DC, USA, 1992.

[48] C. Zanotti, A. Volpi, M. Bianchessi, and L.T. DeLuca. Measuring Thermodynamic Proprieties of Burning Propellants, volume 143, AIAA Progress in Astronautics and Aeronautics 'Nonsteady Burning and Combustion Stability of Solid Propellants', edited by DeLuca, L.T., E.W. Price, and M. Summerfield, chapter 5, pages 145-196. AIAA, Washington, DC, USA, 1992.

[49] N. Eisenreich, H.P. Kugler, and F. Sinn. An Optical System for Measuring Burning Rates of Solid Propellants. Propellants, Explosive, Pyrotechnics, 12:781-80, 1987.

[50] J.M. Tauzia and P. Lamarque. Solid Rocket Propellant Behaviour During Static Firing Test Using Real Time X-Ray Radioscopy. In AGARD PEP 90th Symposium on Advanced Non-Intrusive Instrumentation for Propulsion Engines, Paper 35. AGARD, Paris, France, 1998.

[51] L.D. Strand, A.L. Schultz, and G.K. Reedy. Microwave Measurement of Solid Propellant Pressure Coupled Response Function. Journal of Spacecraft and Rockets, 17(6): 483-488, 1980.

[52] P.Kuentzmann, J.C. Demarais, and F. Cauty. Mesure de la Vitesse de Combustion des Propergols Solides par Ultrasons. La Recherche Aérospatiale, (1):55-79, 1979.

[53] L.H. Caveny, A.J. Saber, and M. Summerfield. Propellant Combustion and Burning Rate Uniformity Identified by Ultrasonic Acoustic Emissions. AIAA, Washington, DC, USA, 1976. AIAA Paper 76-696.

[54] C.M. Mihlfeith, A.D. Baer, N.W. Ryan. The Response of Burning Rate Propellant Surface to Thermal Radiation. AIAA Journal, 10(10):1280-1285, 1972.

[55] L.C. Yang, Miner, E.L., and Ramanos, "Application of Plasma Capacitance Gage (PCG) for Real Time Measurements of Solid Rocket Motor Internal Insulation Erosion", AIAA Paper 90-2327, July 1990.

[56] S. Rampichini, D. Ruspa, and L.T. DeLuca. The Acoustic Emission of Underwater Burning Solid Rocket Propellants. In: Special Topics in Chemical Propulsion "Combustion of Energetic Materials", edited by K.K. Kuo and L.T. DeLuca. Begell House, New York, NY, USA, 2001.

[57] R.O.Hessler. An Analysis of Burning Rate Round-Robin Data. Technical Report, JANNAF Combustion Meeting, West Palm Beach, FL, 27-31 October 1997.

[58] R.O. Hessler, and R.L. Glick. Comparison of Burning Rate Calculation Methods. Technical report, JANNAF Combustion Meeting, West Palm Beach, FL, 27-31 October 1997, 1997.

[59] Miller, W.H. and Barrington, D.K., "A Review of Contemporary Solid Rocket Motor Performance Prediction Techniques," Journal of Spacecraft and Rockets, 7 (3): 225-237, 1970.

[60] Egar, M.A., F.W. Jordan, and L.W. Stockham, "A Robust Ballistic Design Approach for the Space Shuttle Advanced Solid Rocket Motor," AIAA 93-2058, 29th Joint Propulsion Conference, June 1993.

[61] "Solid Rocket Motor Performance Analysis and Prediction," NASA Space Vehicle Design Criteria (Chemical Propulsion) NASA SP-8039, May 1971.

[62] NATO/RTO France SNPE contribution

[63] Cosstephens, S.D., "An Efficient Model for Coupling Solid Rocket Internal Flows with Grain Deformation," AIAA 95-2875, 31st Joint Propulsion Conference, July 1995.

[64] Strand, L.D., "Erosive Augmentation of Solid Propellant Burning Rate: Motor Size Scaling Effect," CPIA Publication 557, Vol III, pp379-391, November 1990.

[65] Friedlander, M.P., Jordan, F.W., "Radial Variation of Burning Rate in Center Perforated Grains," AIAA-84-1442, June 1984.

[66] Hessler, R.O., and Glick, R.L., "Comments on Burning Rate Measurement in Rocket Motors," Communication to the NATO/RTO WG 016, December 1997.

[67] Watson, T.J., F.W. Jordan and L.W. Stockham, "Accurate Burn Rate Measurement for Sub-Scale Test Motors," AIAA-93-2060, 29th AIAA Joint Propulsion Conference, June 1993.

[68] Le Breton, P., D. Ribéreau, F. Godfroy, "SRM Performance Analysis by Coupling Bidimensional Surface Burnback and Pressure Field Computations," AIAA 98-3968, July 13-15, 1998, Cleveland, OH

[69] Uhrig, G., D. Ribéreau, A. Hiss, C.M. Brauner, G. Namah, O. Suys," Processing Effects on Ballistic Response of Composite Solid Propellant Grains," AIAA 95-2585, July 10-12, 1995, San Diego, CA.

[70] Heister, S.D.," Influence of Propellant Rheology on Ballistic Response of Solid Rocket Motor," AIAA 91-3394, June 24-26, 199, Sacramento, CA.

[71] Blair, D.W., et al. "Some Research Problems in the Steady State Burning of Composite Solid Propellants," in M. Summerfield, ed., "Solid Propellant Rocket Research," p 183-206, Academic Press, N.Y., 1960.

[72] Fung, Y.C., Foundations of Solid Mechanics, Prentice-Hall, Englewood Cliffs, New Jersey, 1965.

[73] Sforzini, R.H. and Foster, W.A., "Solid-Propellant Rocket Motor Ballistic Performance Variation Analysis," NASA CR-144264, October 1975.

[74] Field, Richard, "Observations of Surface Structure and Regression Behavior of Solid Propellant Strands Burning Under Narrow Gap Conditions," PhD Thesis, Mechanical Engineering Department, Pennsylvania State University, December 1993

[75] Stowe, R.A., "Strand Burning rate of Solid Rocket Propellant," DREV R-4675, Defense Research Establishment, Quebec, Canada, June 1992

[76] Parr, T.P., and Hanson-Parr, D., "HMX Ignition and Combustion Flame Structure," CPIA Pub 662, Vol I, pp. 481-490, Oct 1997.

[77] Periman, E.A., Pierce, J.W., and Bolleter, W.T., "Propellant Ballistic Performance as Measured in a Computerized Closed Bomb," 2nd International Symposium on Ballistics, October 1978.

[78] Hicks, C.R., "Fundamental Concepts in the Design of Experiments", John Wiley & Sons, New York, 1982

[79] Montgomery, D.C., "Design and Analysis of Experiments," John Wiley & Sons, New York, 1991

[80] Wadsworth, H. M. Jr., Stephens, K.S. and Godfrey, A.B., "Modern Methods for Quality Control and Improvement", John Wiley & Sons, New York, 3rd Edition, 1986

[81] Stat-Ease, Inc., Design-Expert Software, Version 5.0, Minneapolis, MN, 1999.

[82] Archives of The Johns Hopkins University / Chemical Propulsion Information Agency.

[83] Brock, F.H., "Relationship Between Average Burning Rate and Average Pressure in Solid Rockets," E.N. Journal of Spacecraft and Rockets, December 1966.

[84] Brooks, W.T., "Burn Rate Considerations in Solid Rocket Motor Performance Prediction," AIAA Paper 76-601, presented at AIAA/SAE 12th Propulsion Conference, Palo Alto, CA, July 1976.

[85] Doug Coates, SEA Private communication.

[86] Glick, R.L., "Exponent Breaks in Composite Solid Propellants," J. Spacecraft and Rockets, Vol 12, March 1975, pp 185-187.

[87] Glaskova, A.P. and Bobolev, V.K., "Influence of the Initial Temperature on the Combustion of Ammonium Perchlorate," Doklady Akademii Nauk SSSR, Vol. 185, No. 2, 1969, pp 346-348.

[88] Boggs, T.L., Netzer, D.W. and Zurn, D.E., "Ammonium Perchlorate Combustion: Effects of Sample Preparation; Ingredient Type; and Pressure, Temperature and Acceleration Environments," J. Combustion Science and Technology, Vol. 7, 1973, pp 177-183.

[89] Graham, P.H. and Larimer, M.W., "Systematic Investigation of High Pressure Propellant Ballistics,"AFRPL-TR-72-28, Atlantic Research Corporation, Alexandria, VA, January 1972.
REPLACE WITH REF 20.

[90] Glaskova, A.P. Catalysis of Explosive Combustion, Nauka, Moscow, 1976.

[91] Koury, J.L., "Solid Strand Burn Rate Technique for Predicting Fullscale Motor Performance," AFRPL-TR-73-49, October 1973.

[92] Herrington, L.E., "Correlation of Motor and Strand Composite Propellant Burning Rate," AIAA Journal, Vol. 2, No. 9, pp1671-1673, September 1964

[93] Christensen, W.N., "Rocket Motor Burning Rate Prediction Using An Acoustic Emission Strand Burning Rate Technique," CPIA Publication 297, Vol II, pp 389-401, Feb 1979

[94] Svob, G.J., Veit, P.W., Landuk, L.G., "Experimental Evaluation of As-Processed Propellant Grains," CPIA Pub 388, Nov 1983, pp 227-234.

[95] NATO/RTO Bayern-Chemie contribution

[96] NATO/RTO FIAT AVIO contribution

[97] NATO/RTO RO Defence Rocket Motors contribution

[98] NATO/RTO RO WG 016 Meeting discussions

[99] Hutchison, B.J., P.J. Downey, "Effects of the RSRM Grain Deformation on Ballistic Performance," CPIA Publication 580, Vol I, pp 419-426, February 1992

APPENDIX A

NATO PROPULSION INDUSTRY CONTRIBUTORS

COUNTRY	FACILITY	REPRESENTATIVE(S)[1]
CANADA	DEFENSE RESEARCH ESTABLISHMENT VALCARTIER (DREV)	R.A. Stowe
FRANCE	SNPE	V. Bodard
	ONERA	F. Cauty
GERMANY	DYNAMIT NOBEL	R. Mackowiak
	WIWEB (formerly BICT)	Dr. Nicklas
ITALY	FIAT AVIO / BPD	R. DeAmicis, A. Annovazzi
	POLITECNICO di MILANO	A. DeNigris, C. Morandi, F. Pace, A. Ratti, M. Servieri
	CNR – TeMPE	U. Carretta
NETHERLANDS	DELFT UNIVERSITY	F. Dijkstra
NORWAY	NORDIC AMMUNITION COMPANY	St. Haugen
SPAIN	INSTITUTO NACIONAL DE TECNICA AEROSPACIAL (INTA)	M. Mulero
UNITED STATES	ARNOLD ENGINEERING DEVLOPMENT CTR	J. Seeley
	AEROJET SACRAMENTO OPERATIONS	M. Eagar, K. Smith, D. Eckley
	AIR FORCE RESEARCH LAB (AFRL/PRS)	C. Merrill
	ALLIANT TECH SYSTEMS	M. Harsh, C. Shanholtz
	AMCOM / STONE ENGINEERING	M. Lyon, S. Mustaikis II
	ATLANTIC RESEARCH CORPORATION	B. Waltz, P. Graham, K. Graham, N. Rotchford
	BF GOODRICH / UNIVERSAL PROPULSION COMPANY	H. McSpadden
	CONSULTANT	R. Glick
	GD / ARMAMENT SYSTEMS / PCRL	N. Messina
	GD / ORDNANCE & TACTICAL SYSTEMS	J. McAvinew
	JET PROPULSION LABORATORY	L. Strand
	LOCKHEED MARTIN	J. Leahy
	ORBITAL TECHNOLOGIES	M. Chiaverini
	NAVAL AIR WARFARE CTR / WPNS DIV CHINA LAKE, CA	J. Hitner
	NAVAL SURFACE WARFARE CENTER INDIAN HEAD, MD	S. Craven
	NIMIC	B. Stokes
	PENN STATE UNIV/ DEPT MECH ENGIN	K. Kuo
	PRATT & WHITNEY CHEMICAL SYSTEMS DIVISION	R. Hammond, G. Jensen, M.Emanual, G. Hawkins
	SCIENCE ENGINEERING APPLICATIONS	D. Coats
	SNAP TECHNOLOGY	F. Jordan, N. Trudell
	STONE ENGINEERING	W. Stone, B. McDonald
	THIOKOL PROPULSION	K. Wanlass, J. Furfaro, S. Palopoli, J. Edwards, A. Neunzert
	TALLEY DEFENSE SYSTEMS	F. Davis
	UNIVERSITY ALABAMA AT HUNTSVILLE	M. Moser, F. Dauch
	UNIVERSITY OF ILLINOIS	Q. Brewster
	UIUC	J. Murphey
	VIRGINIA POLYTINIC INSTITUTE	W. O'Brien

[1] In addition to the NATO RTO AVT WG 016 Members Country/Facility/Representatives

APPENDIX B

CHEMICAL PROPULSION TECHNOLOGY REVIEWS ISSUED BY JHU/CPIA

CHEMICAL PROPULSION TECHNOLOGY REVIEWS (CPTR)

CPTR 74	SOLID PROPELLANT SUBSCALE BURNING RATE TEST TECHNIQUES AND HARDWARE FOR U.S. AND SELECTED NATO FACILITIES (U-A)
CPTR 72	SUBSCALE FAST COOKOFF TESTING AND MODELING FOR THE HAZARD ASSESSMENT OF LARGE ROCKET MOTORS (U-A)
CPTR 70	OVERVIEW OF PULSE DETONATION PROPULSION TECHNOLOGY (U-A)
PUB. 688	INSENSITIVE EXPLOSIVES FOR FRAGMENTATION WARHEADS (U-E)
CPTR 99-69	BURNING RATES OF STANDARD SOLID PROPELLANTS FOR GUN APPLICATIONS (U-C)
CPTR 98-68	REUSABLE LAUNCH VEHICLE PROPULSION SYSTEMS (U-C)
CPTR 98-67	NOT ASSIGNED
PUB. 664	PROVEN GEL PROPULSION SYSTEM CAPABILITIES TO MEET ADVANCED TACTICAL AND INTERCEPTOR END-GAME MISSILE REQUIREMENTS - RESPONSE TO CPIA REPORT NO. CPTR 96-63, MAY 1996 (U-B)
PUB. 661	FIRE AND EXPLOSION HAZARDS OF LIQUID PROPELLANTS AND RELATED MATERIALS - AN ACCIDENT REVIEW (U-B)
CPTR 97-66	EXPENDABLE LAUNCH VEHICLE PROPULSION TECHNOLOGY (U-C)
CPTR 97-65	ELECTRIC THRUSTER SYSTEMS (U-A)
CPTR 96-64	ELECTRIC PROPULSION FOR SPACECRAFT (U-A)
CPTR 96-63	REVIEW OF PROPELLANT CANDIDATES FOR NEAR-TERM THEATER DEFENSE DIVERT ATTITUDE CONTROL SYSTEMS (U-B)
CPTR 96-62	NATIONAL ASSETS FOR HYPERSONIC FLOW & PROPULSION SYSTEM TESTING (U-E)
CPTR 95-60	PULSE MOTOR TECHNOLOGY (U-D)
CPTR 95-58	ENVIRONMENTALLY BENIGN CLEANING AND DEGREASING METHODS FOR THE SOLID ROCKET MOTOR INDUSTRY (U-A)
CPTR 95-57	COMBUSTION STABILITY OF INTERCEPTOR ROCKET MOTORS: A PRACTICAL APPROACH TO MANAGING INSTABILITY PROBLEMS (U-C) (This publication has a Confidential Appendix-not automatically mailed out)
CPTR 94-56	ROCKET MOTOR SERVICE LIFE PREDICTION METHODOLOGY (U-B)
CPTR 94-55	VARIABLE FLOW DUCTED ROCKET TECHNOLOGY (U) (C-E)
CPTR 94-54	EARTH-STORABLE GELLED BIPROPELLANT TECHNOLOGY (U-C)
CPTR 93-53	SOLID ROCKET MOTOR COMPONENTS FOR INSENSITIVE MUNITIONS (U-D)
CPTR 93-52	NEW HIGH-ENERGY OXIDIZERS (U-C)
CPTR 92-50	LO_2/LH_2 LIQUID ROCKET ENGINE CYCLES (U-C)

CPTR 91-48	AMMONIUM NITRATE PROPELLANTS (U-C)
CPTR 91-47	NEW SOLID PROPELLANT PROCESSING TECHNIQUES (U-C)
CPTR 89-46	STANDARD EXHAUST PLUME MODELS (U-C)
CPTR 89-45	DISPOSAL OF SOLID ROCKET MOTOR PROPELLANTS (U-C)
CPTR 88-44	GAP MINIMUM-/REDUCED-SMOKE PROPELLANTS (U) (C-C)
CPTR 88-43	ELECTROSTATIC DISCHARGE TEST METHODOLOGIES FOR SOLID ROCKET PROPELLANTS (U-C)
CPTR 87-42	NEW SOLID ROCKET PROPELLANT POLYMER BINDER MATERIALS (U-D)
CPTR 87-41	COMBUSTION INSTABILITY: INSTRUMENTATION AND DATA ANALYSIS METHODS FOR MOTORS AND LABORATORY DEVICES (U-C)
CPTR 87-40	ANALYSIS OF TRANSPORTATION-INDUCED STRESSES IN SOLID ROCKET MOTORS (U-B)
CPTR 86-39	DISPOSAL AND RECLAMATION OF PEP MATERIALS (U-B)
CPTR 86-38	CANTED AND SCARFED NOZZLES (U-C)
CPTR 86-37	CONSOLIDATED CHARGES FOR LARGE-CALIBER GUNS (U-D)
CPTR 86-36	LABORATORY METHODS FOR MEASURING COMBUSTION RESPONSE FUNCTIONS (U-A)
CPTR 85-35	STRIP LAMINATE ROCKET MOTOR CASES (U-D)
CPTR 85-34	MOISTURE AND DAMAGE EFFECTS ON COMPOSITE MOTOR CASES (U-C)
CPTR 85-33	THERMAL REACTIVITY OF TACTICAL ORDNANCE (U-D)
CPTR 85-32	HYDRAZINE COMPATIBILITY (U-C)
CPTR 85-31	COMPUTER PROGRAMS FOR PROPULSION SYSTEM COST ESTIMATION (U-D)
CPTR 85-30	BURNING RATE ENHANCEMENT BY PHYSICAL METHODS (U) (C-B)
CPTR 84-29	MOISTURE EFFECTS ON MECHANICAL PROPERTIES OF SOLID PROPELLANTS (U-C)
CPTR 84-28	INFORMATION SOURCES FOR COMPOSITE ROCKET MOTOR CASES (U-C)
CPTR 84-27	VULNERABILITY OF LOVA PROPELLANTS (U)(C-B)
CPTR 84-26	GLYCIDYL AZIDE POLYMER (GAP) (U-B)
CPTR 84-25	PLUME ELECTROMAGNETIC EFFECTS (U) (C--B)
CPTR 83-24	NOZZLELESS MOTOR TECHNOLOGY (U) (C-D)
CPTR 83-23	SOLID PROPELLANT ROCKET MOTOR THRUST TERMINATION (U-B)
CPTR 83-22	BURN RATE ENHANCEMENT OF HMX/RDX HIGH-ENERGY MINIMUM SMOKE PROPELLANTS (U) (C-B)

CPTR 83-21 KEVLAR ROCKET MOTOR CASES (U-B)

CPTR 83-20 UNDERWATER PROPULSION (U) (C-B)

CPTR 83-19 SURVEY ON PULSE MOTORS (U) (C-B)

CPTR 82-18 TEMPERATURE SENSITIVITY OF GUN PROPELLING CHARGES (U-B)

CPTR 82-17 EFFECT OF MOISTURE ON IGNITABILITY (U-B)

CPTR 82-16 MUZZLE VELOCITY IMPROVEMENT (U-B)

CPTR 82-15 RECENT DEVELOPMENTS IN THE TOXICOLOGY OF PROPELLANT HYDRAZINES (U-B)

CPTR 82-14 ULTRAHIGH BURN RATE ROCKET PROPELLANTS (U) (C-B)
CPTR 82-13 LOW VISIBILITY PROPULSION TECHNOLOGY (U) (C-B)

CPTR 82-12 HTPB PROPELLANT AGING (U-B)

CPTR 81-11 SOLID PROPELLANTS FOR DUCTED ROCKET APPLICATIONS (U) (C-B)

CPTR 81-10 MECHANICAL PROPERTIES OF MINIMUM-SMOKE PROPELLANTS (U) (C-B)

CPTR 81-9 HYPERGOLIC VAPOR DETECTOR TECHNOLOGY (U-B)

CPTR 81-8 ALUMINUM AGGLOMERATION IN BURN RATE HTPB PROPELLANTS (U-B)

CPTR 81-7 RADAR ATTENUATION BY ROCKET PLUMES (U-B)

CPTR-6 CPIA PUB. 334 (C-B)
- MECHANICAL PROPERTIES OF REDUCED SMOKE PROPELLANTS (U)
- VARIABLE GEOMETRY RAMJET INLETS AND NOZZLES (U)
- FREE-RADICAL HTPB PREPOLYMERS
- THE DETERMINATION OF THE PROPENSITY FOR DETONATION OF HIGH-PERFORMANCE PROPELLANTS

CPTR-5 CPIA PUB. 327 (U-B)
- HIGH SOLIDS AP-HMX/HTPB/Al PROPELLANTS
- TEMPERATURE SENSITIVITY OF AP/POLYBUTADIENE COMPOSITE PROPELLANTS
- GUN BARREL EROSION

CPTR-4 CPIA PUB. 316 (C-B)
- HTPB BONDING AGENTS (U)
- REDUCED SMOKE MOTOR INSTABILITY (U)
- SLURRY FUELED RAMJET COMBUSTORS (U)
- ROCKET MOTOR INSTRUMENTATION FOR STRUCTURAL ANALYSIS: IN SITU DEVICES
- LOW ALTITUDE PLUME MODELS
- SPACE SHUTTLE PLUME EFFECTS
- EXHAUST PLUME IMPINGEMENT EFFECTS

CPTR-3 CPIA PUB. 307 (C-B)
- RAMJET SLURRY FUELS (U)
- UNDERWATER ROCKET PROPULSION (U)
- SOME RECENT DEVELOPMENTS IN LIQUID PROPULSION GUN TECHNOLOGY (U)
- HIGH DENSITY SOLID ROCKET PROPELLANTS (U)
- MISSILES AND SPACE PROPULSION TECHNOLOGY
- ELECTROMAGNETIC PROPULSION
- MUZZLE FLASH SUPPRESSION
- EXTENDIBLE EXIT CONES

PARTICLE SIZE ANALYSIS
ARMY MISSILE PROPULSION TECHNOLOGY

CPTR-2 CPIA PUB. 305 (C-B)
BURN RATE CONTROL OF HMX/RDX MINIMUM SMOKE PROPELLANTS (U)
LOW SMOKE MOTOR DEVELOPMENT (U)
GUN BARREL EROSION REDUCTION
LIQUID ENGINE PERFORMANCE PREDICTION TECHNOLOGY
HYDRAZINE COMPATIBILITY
THE SPACE SHUTTLE ORBITER PROPULSION UNITS

CPTR-1 CPIA PUB. 301 (C-B)
HIGH ENERGY TOUGH PROPELLANTS (U)
SYNTHESIS OF ENERGETIC PLASTICIZERS (U)
CONTROL OF BURN RATE PRESSURE EXPONENT IN AP/HTPB COMPOSITE PROPELLANTS (U)
REVIEW OF THRUST VECTOR CONTROL FOR HIGHLY MANEUVERABLE TACTICAL MISSILES (U)
INTEGRAL ROCKET RAMJET COMBUSTOR DEVELOPMENT PROGRAMS (U)
EXHAUST PLUME SMOKE PREDICTION AND MEASUREMENT
CPIA INFORMATION STORAGE AND RETRIEVAL

INITIAL DISTRIBUTION

- ARMY -

ARMY AVIATION AND MISSILE COMD/REDSTONE ARSENAL
- 1 BEN F. WILSON
- 1 DOCUMENTS, AMSMI-RD-CS-R
- 1 DR. JAMES G. CARVER
- 1 DR. WILLIAM MELVIN
- 1 MR. J. MICHAEL LYON
- 1 TERRY L. VANDIVER

ARMY RESEARCH LAB/ABERDEEN
- 1 LOUISE LETENDRE

ARMY TANK AUTOMOTIVE & ARMAMENT COMD/PICATINNY
- 1 PATRICIA AYS

US ARMY RESEARCH OFFICE/RSCH TRIANGLE PK
- 1 D. M. MANN

- NAVY -

NAVAL AIR WARFARE CTR/CHINA LAKE
- 1 CHRIS TOFTNER
- 1 DR. FRED S. BLOMSHIELD
- 1 DR. GEOFFREY A. LINDSAY
- 1 DR. JAMES HOOVER
- 1 DR. MAY L. CHAN
- 1 HOWARD BOWMAN
- 1 JACK M. PAKULAK
- 1 JAMES A. GROSS
- 1 JAMES A. LOUNDAGIN
- 1 JAMES C. BALDWIN
- 1 MARY S. PAKULAK
- 1 STUART R. BLASHILL
- 1 TECH LIB/P. BACKES
- 1 THERESE ATIENZAMOORE
- 1 THOMAS L. BOGGS

NAVAL SURFACE WARFARE CTR/INDIAN HEAD
- 1 MICHAEL P. SIKORA

- AIR FORCE

AFRL/EDWARDS AFB
- 1 DR. LAWRENCE P. QUINN
- 1 JEANNIE PATON
- 1 JOHN H. CLARK
- 1 ROBERT C. CORLEY

AFRL/WPAFB
- 1 W. LEE BAIN

NATL AIR INTEL CTR/WPAFB
- 1 BEVERLY BRINK

- NASA

NASA AEROSPACE INFO CTR/HANOVER
- 1 ACQUISITIONS DEPT

NASA GLENN RSCH CTR/CLEVELAND
- 1 SCOTT MEYER
- 1 WOODROW WHITLOW

NASA JOHNSON SPACE CTR/HOUSTON
- 1 BARRY WITTSCHEN
- 1 GERALD SANDERS

NASA JSC WSTF/LAS CRUCES
- 1 LURLENE FORD/ET.AL.

NASA LANGLEY/HAMPTON
- 1 MR. MELVIN LUCY
- 1 S. MILLER/MS-185 TECH LIB

NASA/MARSHALL SPACE FLIGHT CTR
- 1 CN22/LIBRARY
- 1 DR. TERRY F. GREENWOOD

NASA/WASHINGTON, DC
- 1 DAVID STONE
- 1 W. R. FRAZIER, CODE QS

- OTHER GOV'T. -

DEF TECH INFO CTR/FT BELVOIR
- 2 DTIC-OCC

DTRA/ARLINGTON
- 1 FRANK TRACESKI

- NON-GOV'T. -

AEROJET/SACRAMENTO
- 1 AEROJET-TIC

AEROSPACE/LOS ANGELES
- 1 BENITA CAMPBELL, M1-199

ALLIANT AEROSPACE COMPANY/MAGNA
- 1 LIBRARY, M/S H

ATK TACTICAL SYSTEMS COMPANY LLC//ROCKET CENTER
- 1 DOTTIE LYON

ATLANTIC RESEARCH CORP/GAINESVILLE
- 1 TECHNICAL INF CTR

BOEING COMPANY/CANOGA PARK
- 1 H. E. SNELL, TIC BA29

BOEING/SEATTLE
- 1 LIB ACQ

GENERAL DYNAMICS OTS (AEROSPACE) INC/REDMOND
- 1 JAMES GURLEY

LLNL/LIVERMORE
- 1 BETTE MOORE

PACIFIC SCIENTIFIC ENERGETIC MATERIALS CO/CHANDLER
- 1 SMALLWOOD/KORCSMAROS

PENNSYLVANIA STATE UNIV/STATE COLLEGE
- 1 DR. DANIEL KIELY

RAYTHEON COMPANY/TUCSON
- 1 SHANNON MACK

SANDIA NATIONAL LABS/ALBUQUERQUE
- 1 DIV 2554/M. GRUBELICH
- 1 O-4916/S. LANDENBERGER

TALLEY/MESA
- 1 SECURITY OFFICE

THIOKOL PROPULSION/ELKTON
- 1 THOMAS HOLMAN

THIOKOL/BRIGHAM CITY
- 1 ELLEN WAGSTAFF

UNITED TECHNOLOGIES/SAN JOSE
- 1 TECHNICAL LIBRARY

UNIVERSAL PROPULSION COMPANY INC/PHOENIX
- 1 JAMES J. BAKER

Total No. 65